Closed-Loop Extrudate Thickness Control in Twin-Sheet Extrusion Blow Molding

Mostafa Darabi

Department of Electrical and Computer Engineering
McGill University
Montreal, Canada

February 7, 2021

A thesis submitted to McGill University in partial fulfilment of the requirements for the degree of Doctor of Philosophy.

Abstract

Extrusion Blow Molding (EBM) is a polymer forming technique used in manufacturing processes which produce hollow plastic parts such as fuel tanks for the automotive industry. Mathematical models built using the Finite Element Method (FEM) and simulations of the extrusion process are studied extensively in the literature. Moreover, optimization techniques have been developed in the past to improve the quality of the final parts as well as to minimize material usage. Such optimization techniques are open-loop tasks that obtain the optimal die gap setpoints for the next cycles of the EBM process. The die gap is changed during the extrusion process to obtain the desired thickness profile for the final parts and to compensate for uneven stretching in the molding stage. When new feed material is introduced or an unexpected machine drift occurs, a trial and error method is used to retune the die gap setpoints, which is time consuming and costly. Therefore, in this work, the feasibility of using a closed-loop control approach in the EBM process is studied to compensate for machine drift and disturbances in real time.

An automatic control system for regulating the extrusion process in EBM is proposed. The controller aims to increase the consistency of the manufacturing process and minimize machine drift. The thickness of the extrudate is measured online and any unexpected drift is compensated for by changing the die gap instantly. A low-order model is proposed for the controller design based on the FEM model developed in previous work. The model has a transport partial differential equation/ nonlinear ordinary differential equation cascade structure model. Moreover, the controller has a Smith predictor configuration to compensate for the die gap dependent delay generated by the transport partial differential equation. In addition, the H_∞ control theory is used to design an optimal controller in order to maintain the desired extrudate thickness in this work in the presence of disturbances or machine drift. Furthermore, a robust controller is proposed and evaluated against the nominal H_∞ controller by comparing the thickness error between the disturbed

open-loop and closed-loop systems. This new control technique may reduce useless scrapped parts and improve product quality.

Finally, the feasibility of using a laser sensor in the EBM process is studied to monitor the extrudate thickness for an in-cycle control design. In addition, an ultrasonic sensor is used to measure the thickness of the final part. Ultimately, sensor placement is addressed in this work to locate the sensors in order to obtain final parts with better quality and less material usage.

Résumé

Le moulage par extrusion-soufflage (EBM) est une technique de formage de polymère utilisée dans les processus de fabrication qui produisent des pièces en plastique creuses telles que les réservoirs de carburant pour l'industrie automobile. Les modèles mathématiques construits à l'aide de la méthode des éléments finis (FEM) et les simulations du processus d'extrusion sont largement étudiés dans la littérature. De plus, des techniques d'optimisation ont été développées dans le passé pour améliorer la qualité des pièces finales ainsi que pour minimiser l'utilisation des matériaux. De telles techniques d'optimisation sont des tâches en boucle ouverte qui permettent d'obtenir les points de consigne d'espacement de filière optimaux pour les prochains cycles du processus EBM. L'écart de filière est modifié pendant le processus d'extrusion pour obtenir le profil d'épaisseur souhaité pour les pièces finales et pour compenser l'étirement inégal dans la phase de moulage. Lorsqu'un nouveau matériau brut est introduit ou qu'une dérive inattendue de la machine se produit, une méthode d'essai et d'erreur est utilisée pour régler à nouveau les points de consigne de l'espace de filière, ce qui prend du temps et est coûteux. Par conséquent, dans ce travail, la faisabilité de l'utilisation d'une approche en boucle fermée dans le processus EBM est étudiée pour compenser les dérives et les perturbations de la machine en temps réel.

Un système de contrôle automatique pour réguler le processus d'extrusion dans l'extrusion soufflage est proposé. Le contrôleur vise à augmenter la cohérence du processus de fabrication et à minimiser la dérive de la machine. L'épaisseur de l'extrudat est mesurée en ligne et toute dérive inattendue est compensée en modifiant instantanément l'espace de la filière. Un modèle d'ordre bas est proposé pour la conception du contrôleur basé sur le modèle FEM développé dans les travaux précédents. Le modèle a un modèle de structure en cascade d'équation différentielle partielle / équation différentielle ordinaire non linéaire. De plus, le contrôleur a une configuration de prédicteur Smith pour compenser le retard dépendant de l'espace de filière généré par l'équation

différentielle partielle de transport. De plus, la théorie du contrôle H_∞ est utilisée pour concevoir un contrôleur optimal afin de maintenir l'épaisseur d'extrudat souhaitée dans ce travail en présence de perturbation ou de dérive de la machine. De plus, un contrôleur robuste est proposé et évalué par rapport au contrôleur H_∞ nominal en comparant l'erreur d'épaisseur entre les systèmes en boucle ouverte et en boucle fermée perturbés. Cette nouvelle technique de contrôle peut entraîner moins de pièces mises au rebut et une meilleure qualité du produit.

Enfin, la faisabilité de l'utilisation d'un capteur laser dans le procédé EBM est étudiée pour surveiller l'épaisseur de l'extrudat pour une conception de contrôle en cycle. De plus, un capteur à ultrasons est utilisé pour mesurer l'épaisseur de la pièce finale. En fin de compte, le placement des capteurs est abordé dans ce travail pour localiser les capteurs afin d'obtenir des pièces finales avec une meilleure qualité et une utilisation moindre du matériau.

Acknowledgements

First and foremost, I would like to thank God who gave me the perseverance and privilege to pursue this program and successfully complete it despite the many challenges faced.

I would like to express my deepest appreciation to my advisor Prof. Benoit Boulet for his continuous support, patience, motivation, enthusiasm, and immense knowledge. Without his supervision and constant guidance this dissertation would not have been possible. Furthermore, I would like to thank my PhD committee Prof. Pascal Hubert and Prof. Hannah Michalska for their guidance. Moreover, I would like to thank Dr. Hossein Vahid Alizadeh and Dr. Raffi Toukhtarian who helped me to pursue this journey with their encouragement, insightful comments, and unwavering guidance. I would like to thank Dr. Mir Saman Rahimi Mousavi, Mr. Donald Pavlasek, Mr. Nick Wilson for their help during my studies.

Last but not the least, I would like to dedicate this thesis to my family. My parents for their unconditional support and love, without whom I would not have made it here. I thank my father Dr. Ghasem Darabi for always encouraging me to embark on the challenges life puts ahead of me, and for being a stalwart at all times. I thank my mother Mrs. Beigom Karimi for her tender, loving and compassionate daily encouragements and prayers. I thank my brother Maisam, his wife Hajar, his daughter Hannah, my sister Maryam and her husband Amir for their kindness and warmth throughout the years. A special thanks to my lovely wife and best friend Aida for her endless love, support, and sacrifice whose unyielding inspiration and devotion enable me to peruse my dream. Finally, I would like to thank my sweet daughter Nika who gave me motivation and showed me brightness future.

Contents

List of Figures

List of Tables

Chapter 1

Introduction

Project overview

In this thesis, a new control technique is explained for the Extrusion Blow Molding (EBM) process. One of the products made by using the EBM process is a fuel tank. A novel technology developed by Kautex Textron GmbH & Co KG called the Next Generation Fuel System (NGFS) is used to produce fuel tanks according to standard regulations. The main objective of this work is to find a way to improve the manufacturing process for NGFS. To do so, a mathematical model is proposed to represent the extrusion process. Moreover, a closed-loop system is described to improve the manufacturing process. This project was funded through the Automotive Partnership Canada program (APC). Teams from McGill University, University of British Colombia, Kautex Textron, and the National Research Council of Canada (NRC) collaborated to conduct this project. The NGFS uses a twin sheet extrusion process to produce the fuel tank instead of using a conventional blow molding machine with a cylindrical extruder. This new technology reduces the emissions, and the weight of the tank by using less material. The ultimate goal of the project is to produce the final parts with better quality, in less time, using less material.

1.1 Polymer forming and EBM

The extrusion Blow Molding (EBM) process is used in the plastic forming industries to produce hollow plastic parts such as bottles and toys from raw polymer resins. EBM is also used in automotive industry to make vehicle parts such as car bumpers, and seats. The main advantage of EBM over other plastic forming techniques such as injection blow molding, is being able to produce large hollow parts with low tooling cost. One of the most significant characteristics of the produced part is its thickness profile. The main disadvantages of EBM are machine drift and limited control over the final thickness profile [1].

1.1.1 EBM stages

EBM is constituted of three main stages: extrusion, molding, and cooling. In the beginning of the extrusion stage, the raw polymer in powder or pellet form is fed into the hopper. A rotating screw grinds the material and transports it toward a die opening as shown in Figure 1.1. The friction due to the rotating screw increases the temperature and melts the polymer. Typically, extra heaters are used to increase the temperature and aid the melting process. Afterwards, the molten material is forced to exit the die, forming a vertically suspended extrudate. During molding, the extrudate is forced into a mold by suction or blowing, acquiring the inner shape of the mold. The extrusion and molding stages are shown in Figure 1.1. Finally, in the cooling stage, the molded part is taken out of the mold and either submerged into a water bath or cooled by air. Ultimately, the extra polymer is trimmed at the edges. The extra polymer can be reground and reused for further processing.

1.1.2 NGFS

The shape of the extudate is dependent on the die geometry. Annular dies produce cylinder shaped extrudates while slit dies produces sheet shaped extrudates. Typically, a cylindrical die is used

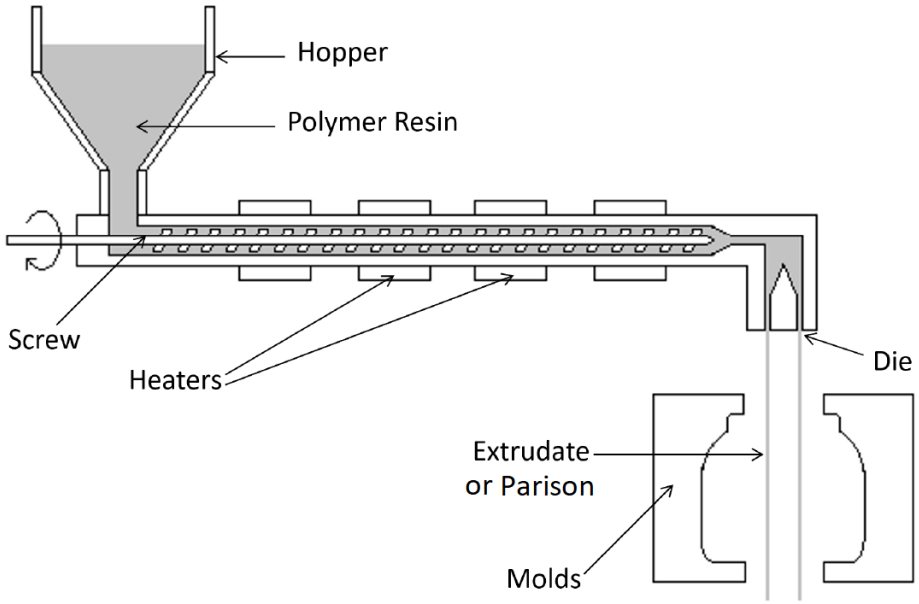

Figure 1.1: Extruder configuration

in conventional EBM machines which produces a hollow tube shaped parison as described in [3] and shown in Figure 1.2. In order to improve the manufacturing process, a slit die is used in NGFS [2, 3], where the vertically suspended twin sheet extrudates are formed during the extrusion process as shown in Figure 1.3. The overall NGFS process [3] is illustrated in Figure 1.4. In NGFS, the mold is divided into two parts. Each extrudate sheet is forced into each mold by suction, acquiring the inner shape of the mold. Then, the molds are closed to form the final part. Finally, the molded part is taken out of the mold by a robot to be cooled in the water bath or by air. In this thesis, the main focus is to design a controller for twin sheet extrudates. The cylindrical parison is not considered in this work.

Figure 1.2: Cylindrical EBM

1.2 EBM challenges

The ability to obtain a desired thickness profile along the part is challenging due to different factors effecting EBM. Once the molten polymer exits the die, the suspended extrudate may show a swelling effect, as shown in Figure 1.5. The pressure in the barrel is increased during the extrusion process and the molten material is squeezed. Therefore, the molten material travels from a high pressure region to a lower one when it exits the die. The resulting swelling effect causes the thickness of the extrudate to be larger than the die opening due to relaxation phenomena. Moreover,

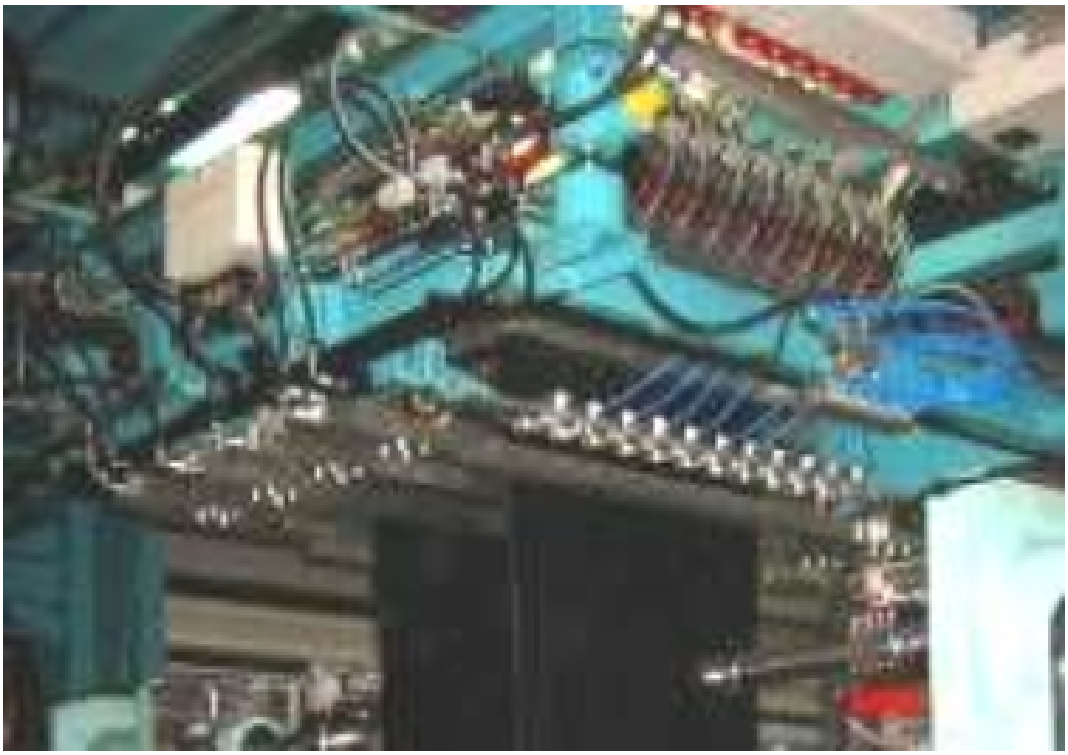

Figure 1.3: Twin sheet extruder of NGFS machine

the extrudate may sag, which causes the thickness of the extrudate to become thinner at certain locations on the extudate shown in Figure 1.5. Sagging is caused by stretching of the extrudate due to its own mass under gravity. Furthermore, different parts of the extrudate may undergo different degrees of stretching during the molding stage. Therefore, an uneven stretching will cause non-uniform thinning along the extrudate, specially for products with complex geometries such as fuel tanks [2].

1.2.1 Die gap programming

The die opening is varied during extrusion, in order to control the final thickness profile and compensate for uneven stretching, swelling, and sagging. The extrusion cycle time is divided into equal intervals in which the die gap is set to a constant value called setpoint as shown in Figure 1.6. The

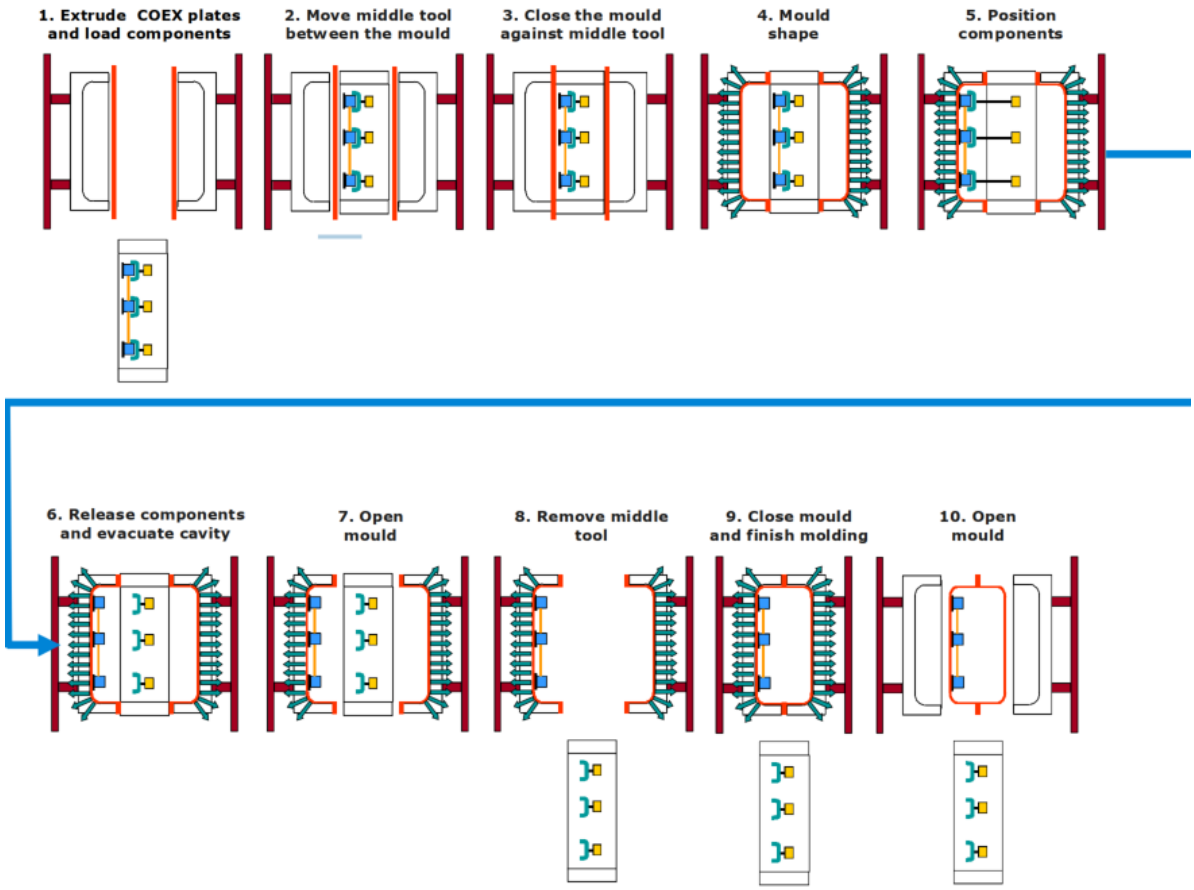

Figure 1.4: NGFS process diagram

task of assigning the setpoints to produce a desired thickness profile of the molded part is called die gap programming for twin sheet extrudates or parison programming for annular extrusion [4–8].

Typically, die gap programming is done by trial and error when a new product is introduced or machine drift is observed. Machine operators spend days to find an appropriate set of setpoints that results in a convenient part thickness profile. In addition, given that EBM is sensitive to uncontrollable factors such as new raw material and temperature, the setpoints are retuned when machine drift is observed. Moreover, die gap programming is an expensive task due to defective parts produced during trial and error in addition to manpower and time needed to obtain the desired

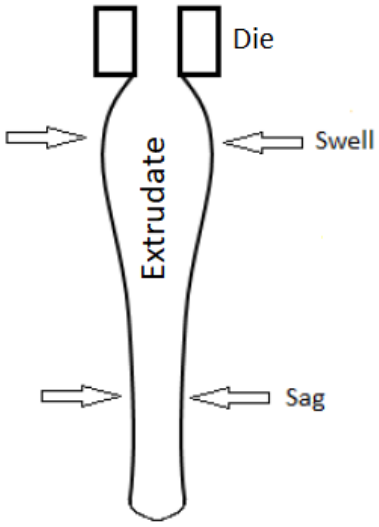

Figure 1.5: Swelling and sagging effects

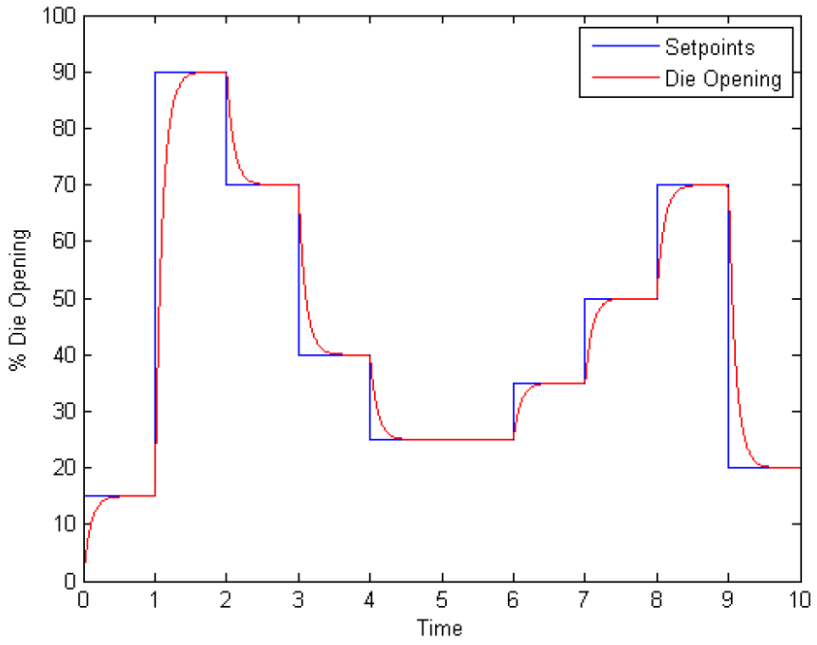

Figure 1.6: Setpoints versus time

thickness profile. In addition, physical uncertainties may affect the extrusion process. Physical uncertainty arises from various sources in the EBM process, such as barrel temperature and poly-

mer flow rate. Extrudate curl occurs during extrusion when the melt temperature of the resin is too cold [9, 10]. In addition, a variation in temperature may result in misalignment of the die or mandrel, changing the extrudate thickness. The density and flow rate of the molten resin are considered in forming the wall thickness. Moreover, excessive shrinkage of the wall thickness may occur when the resin density is too high [9].

1.3 Monitoring and control of EBM

As mentioned above, die gap programming is typically done by trial and error when a new product is introduced. This task is time consuming and expensive. Therefore, optimization methods are developed to automate the die gap programming in simulation setups [11, 12]. The optimization technique is an iterating scheme in which the desired extrudate thickness profile is obtained. Therefore, any disturbance or machine drift is compensated for in upcoming cycles. On the other hand, by using an in-cycle control scheme, the compensation occurs immediately in the current cycle.

1.3.1 State of the technology

Using automatic control in EBM can help the process overcome unexpected disturbances, uncertainties, and machine drifts. Moreover, using closed-loop control minimizes the effect of process sensor noise. In addition, on-line monitoring of thickness distribution may result in shorter cycle time and lower resin usage. Having a consistent manufacturing process enables a lower tolerance level. In the literature, in-cycle controllers regulating extrudate thickness are limited [13]. Most EBM in-cycle control reports address controlling process parameters such as temperature [14, 15]. Moreover, the feasibility of on-line monitoring of the parison thickness profile during extrusion is introduced in [16–18]. In other works [19–21], a closed-loop system is used to control the length

of the extrudate. Controlling the length of the extrudate may result in fewer scrapped parts, minimizing material usage. Reducing the extra flash at the bottom of the mold reduces cooling time. Therefore, the overall cycle time is reduced when material usage is decreased. Ultimately, using a closed-loop system in the EBM process to reject unexpected disturbances and machine drift should result in lower material usage, shorter production time, and final products with better quality.

1.3.2 Closed-loop control

In this thesis, an in-cycle controller is introduced for EBM. Figure 1.7 shows the cross section of a slit die extruder configuration. The polymer enters through an inlet into a barrel. The walls of the barrel are fixed while the die walls move towards and away from each other symmetrically to change the die gap. The molten polymer is squeezed out of the die and forms a sheet shaped extrudate. The origin of the coordinate system is at the die exit, establishing x as the distance away from the die. After applying die gap programming, measurements of a thickness sensor located at a fixed point L below the die are stored as a reference signal after a satisfactory cycle. An in-cycle controller is proposed to maintain the extrudate thickness close to the reference signal and eliminate machine drift. The input of the controlled model is the die gap and the output is the thickness of the extrudate measured by the sensor. For instance, if a new material is introduced, the sensor will measure the thickness of the extrudate. The measured signal is compared to the reference signal in real time, and if a difference between the two signals is computed, the controller will compensate for the error by modifying the die gap immediately in the current extrusion cycle.

1.4 Control design

Figure 1.8 shows the extrusion process and closed-loop system configuration. A suitable model of the dynamical evolution of the extrudate thickness is required for the control design. Sensors based

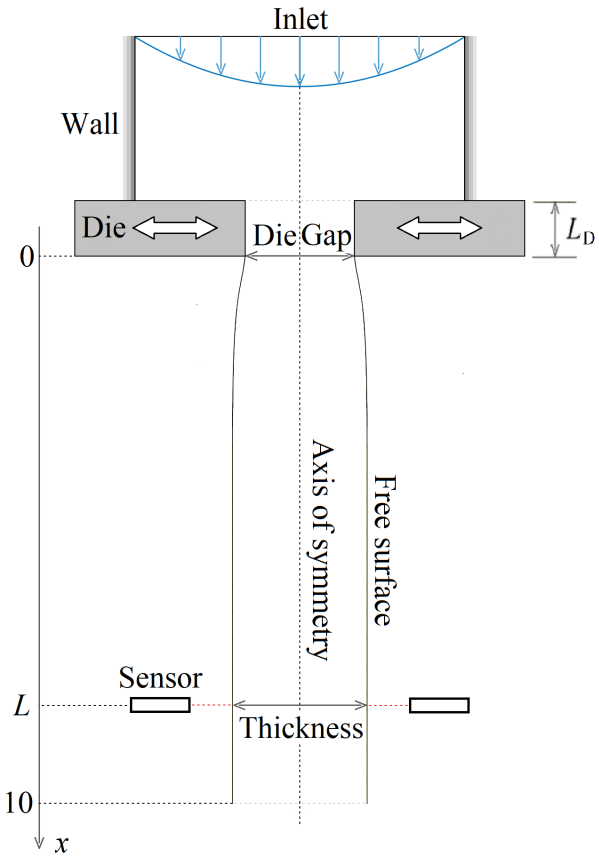

Figure 1.7: Extruder configuration

on laser or mm-wave radar technology can be placed at a fixed point on one side or two sides along the extrudate below the die. The thickness of the extrudate is measured by the sensors in real time. If a drift happens in the machine and is captured by the sensors, a difference between the desired thickness and disturbed thickness is computed. Afterwards, the controller sends the signal to the actuator to adjust the die gap automatically in order to compensate for the drift.

1.4.1 Modeling

Modeling and simulation of the extrusion process is challenging due to complex fluid behavior that is dependent on various factors [22, 23]. Typically, the extrusion process is modeled and simulated

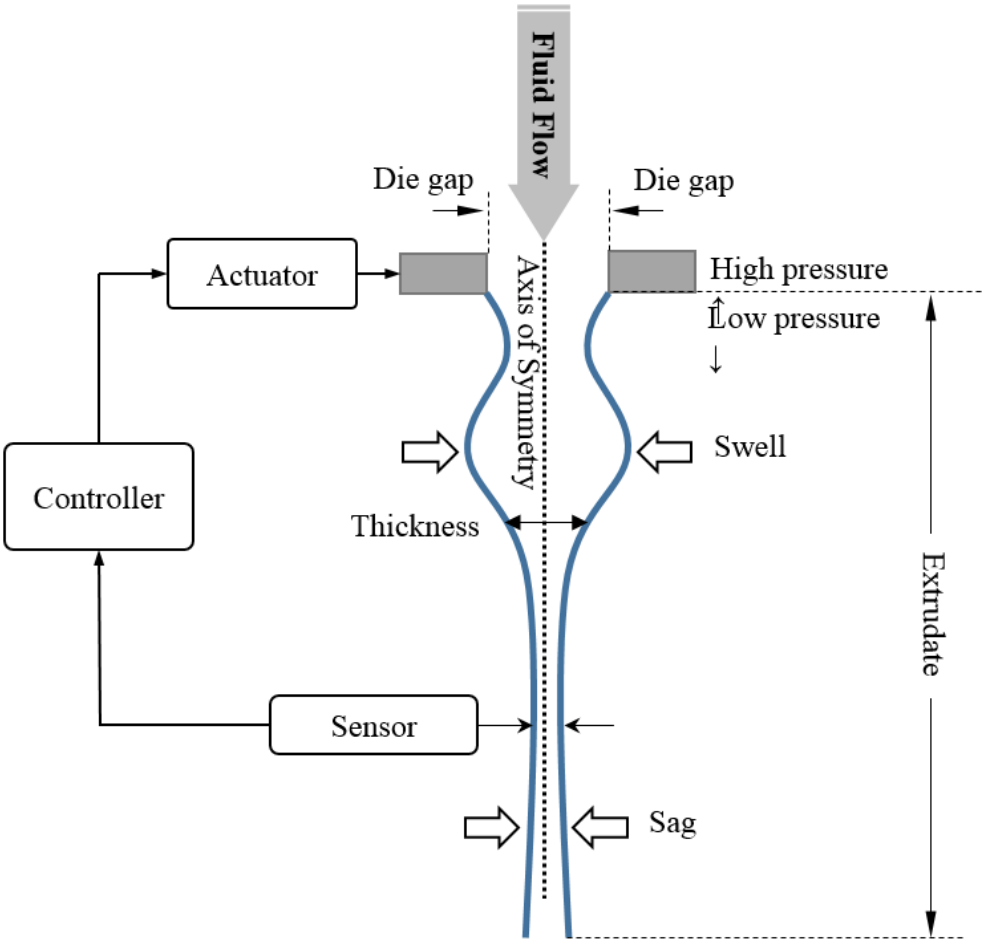

Figure 1.8: Overall closed-loop system configuration

for constant die gap using physics based Finite Element Method (FEM) [24–28]. The proposed controller regulates the extrudate thickness by changing the die gap online. Given that the input is the die gap, a time dependent model with a varying die gap is required to model the extrusion process. Models simulating varying die gap are rare in the literature [29–31]. Moreover, good control oriented models are characterized by being simple enough to design controllers, having short computational time to run online, and having the ability to be identified from the process using simple tests. In [29], FEM is used to simulate the extrusion process with varying die gap.

FEM models are constituted of high-order nonlinear equations that are complex and have high computational cost. Therefore, FEM models are not suitable on practical in automatic control design. In [30], a simple model with constant delay is proposed to model the extrusion process. The delay term plays an important role in the overall structure of the model. The constant delay may be under-predicted or over-predicted for different locations along the extrudate. In order to model material transports phenomena better, a novel extrusion model with input-dependent time varying delay is proposed in [31] and used in this work as a reference model. The model is computationally cheap, suitable for controller design, and useful for different types of configurations. The proposed model in [31] has a transport partial differential equation/ nonlinear ordinary differential equation (PDE/nonlinear ODE) cascade structure that is used in this thesis in the controller design.

1.4.2 Smith predictor

The closed-loop system aims to maintain a desired extrudate thickness and eliminate machine drift. The proposed model in [31] includes an input-dependent delay. Delayed systems' stability has been studied extensively over the years [32, 33]. Time delay in the controlled plant necessitates the use of appropriate classes of controllers to result in a stable system [34, 35]. Typically, model predictive systems are used in the literature to deal with systems having long time delays. Moreover, predictive feedback controllers are developed in [36–40] to compensate for the input dependent delays in transport systems. These controllers deal with the PDE/nonlinear ODE cascade systems and are aimed at improving the performance of systems in the presence of disturbances. In addition, the internal model principle based on a Smith predictor technique is introduced in [41,42] to compensate for a time delay of stable systems having long dead times. A predictive model is used in the Smith predictor configuration to separate the delay term from the real plant in order to facilitate the controller design. Moreover, the Smith predictor technique is modified in [43–46] to

improve the tracking problem and to reject the disturbances. Using the Smith predictor technique in order to compensate for the time delay requires a satisfactory predictive model. Any modeling error may result in poor performance. Therefore, the modeling error is considered in the controller design to ensure the desired performance and stability of the process [47–50].

1.4.3 H_∞ control

H_∞ control theory is used in a wide variety of systems such as systems having a long dead time. This type of controller deals with the effect of a delay which impacts performance of the closed-loop system [51–55]. A noticeable analogy exists between the controller design approach presented here and the techniques used in robust control problems [56–59] and constrained control problems [60, 61]. Moreover, the H_∞ optimal control technique is utilized in process control in order to mitigate the effect of disturbances, overshoot and steady state error [62–66]. In this work, the H_∞ optimal controller is proposed and used in a Smith predictor configuration to regulate the extrudate thickness in the presence of disturbances or machine drifts.

1.4.4 Robust H_∞ control

A feasibility analysis of using the closed-loop system was performed in order to regulate the extrudate thickness in the presence of a disturbance [17, 18]. The controller is a simple adaptive controller that does not consider uncertainties in the system. An H_∞ optimal controller is proposed in the Smith predictor configuration to maintain the desired extrudate profile when the die gap is disturbed by a constant disturbance in the input later on in this thesis. The resin uncertainty, sensor noise, and modeling error are not considered in the controller design. Referring to Figure 1.8, the extrudate model is composed of a delay, a nonlinear static function, and a linear time-invariant (LTI) system with memory. The transport delay is the time needed for the material to travel from

the die exit ($x = 0$) to the location of the sensor. Thus, the transport delay is dependent on the input and on the location x along the extrudate. Given that the input to the model is the die gap, uncertain parameters such as input disturbances and material properties may cause the uncertainty in the input. Therefore, the uncertain input results in an uncertain time delay system. Therefore, a robust controller is designed in the Smith predictor configuration in order to compensate for the uncertain time delay system. Robust controllers are designed in [70–74] for uncertain time delay systems in which parameter uncertainty is time-varying and norm bounded. Also, the controller performance is affected by the size of the delay. The robust H_∞ controller can overcome the larger delay uncertainty at locations further away from the the die compared to the conventional controllers.

1.5 Thesis contributions

Problem statement and scope

As mentioned above, the main difficulties in extrusion blow molding arises from machine drift, disturbances and uncertainties during extrusion, molding, and cooling stages, and a limited control over the final products. These issues may result in more defective parts. Researchers have discussed these issues and proposed automatic controllers to overcome these problems in different industrial applications such as thermoforming [44, 75–78]. On the other hand, most of the work done previously in EBM is related to optimization problems in which the desired thickness profile can be obtained iteratively in the next cycles [11, 12]. The optimization process is a cycle-to-cycle controller. The sensor measures the thickness of the manufactured part. Afterwards, the obtained thickness is compared to the desired thickness. Accordingly, the controller computes the desired setpoints for the die gap from the thickness error. The drawback of the cycle-to-cycle control is a lack of ability to compensate for the drift during the current extrusion cycle.

On the other hand, there are few works related to the in-cycle control in the literature related to EBM. The online monitoring of the parison thickness in real time (current cycle) is discussed briefly in [17, 18] to improve EBM. For instance, if a new material is introduced or machine drift is observed during the current cycle, the sensor will measure the thickness in real time. Then, the controller will compensate for the drift by changing the die gap immediately. In order to design an in-cycle controller for EBM, a mathematical model is required in which the dynamical model of extrudate can be obtained. The input of the dynamical model is the die gap and the output is the thickness. There are limited references in the literature discussing the dynamical model for extrudate thickness when the die gap is changed from one set point to the other.

In order to obtain the mathematical model, the UBC team built an experimental setup consisting of a slit die extruder with variable die gap for which the results are published in [30]. Our team at McGill collaborated with the UBC team to collect the experimental data using their setup. Collecting the data was not successful using their setup due to device failure and difficulties in measurements. Therefore, our team proposed a FEM model replicating the mathematical model of extrudate for the extrusion process with varying die gap in [29]. This model is not suitable for the controller design due to its high order and complexity. Therefore, the FEM model is used as a reference model to obtain the lower order model suitable for control design.
In this thesis, we aim to tackle the issues associated with in-cycle control of twin sheet extrudates which is related to the NGFS machine. The contribution can be summarized as follows.

1.5.1 Modeling

The FEM model in [29] consists of a large number of nonlinear ordinary differential equations. The FEM model is developed by Raffi Toukhtarian in [29]. The suitable model for the control

design must be simple in addition to having low computational cost to be able to run in real time. The parameter identification method is used to obtain the model from the FEM model. The low order model was proposed by Raffi Toukhtarian, Mostafa Darabi, and Benoit Boulet in [31]. Raffi Toukhtarian was the primary author of the article and is responsible for writing the manuscript. The model consists of the nonlinear static function, the non-minimum phase linear time-invariant system and the delay. Mostafa Darabi helped the primary author in developing the non-minimum phase linear time-invariant system and simulation. Benoit Boulet provided supervision and editorial input in preparation of the manuscript. Looking at the FEM model, it is possible to determine different components of the higher order model. The step input is used to obtain the lower order model from the FEM model. The proposed suitable model for control design [31] has transport PDE/nonlinear ODE cascade structure. Moreover, the proposed model is composed of delay, nonlinear static function and transient blocks. The parameters of the model are identified based on the minimization of the error between the FEM simulator and the step input response of the proposed model. The proposed model has advantages over the FEM model such as, being suitable for the control design, computationally less expensive, and consuming less time to run in real time. Moreover, using the proposed model, the same identification procedure is possible to simulate a wide range of setups and fluid types. In addition, using the FEM model, another lower order model is proposed to be used specifically for the control design in this work. The new model has a different block structure compared to the model in [31]. The model in [31] has a delay block first, then a nonlinear static function, and the last block is the transient model. On the other hand, the new model has the nonlinear static function as the first block, then the transient model, and the delay is the last block. The reason for creating the new model is to use the model in model predictive control techniques.

1.5.2 Control design

As mentioned above, the low-order model proposed for the control design is composed of delay, nonlinear static function, and transient blocks. The input of the model is the die gap and the output is the extrudate thickness. The delay term of the model is input-dependent, and is obtained by a transport partial differential equation.

1.5.3 H_∞ controller

Mostafa Darabi is the primary author in developing the controller based on the H_∞ optimal technique which is addressed in Chapter 3. In addition, Mostafa Darabi developed the new model according to the main model in [31] to be used in the Smith Predictor configuration. Raffi Toukhtarian contributed in Chapter 3 by helping to develop the low order model for the controller design which is addressed in [31]. Benoit Boulet contributed in Chapter 3 by reviewing the overall controller design and editorial input for writing this chapter. The model has an input-dependent delay which may cause instability in an closed-loop system. Moreover, the transient block of the model is a linear time-invariant system that has non-minimum phase dynamics. The delay also may cause non-minimum phase dynamics due to zeros in the right half plane due ti higher order of Padé approximation [96]. Moreover, the input disturbance may disturb the delay because of its dependency on the input. Therefore, the controller must be good enough to compensate for the delay and the non-minimum phase dynamic, in addition to disturbances. In this work, an H_∞ controller is proposed in the Smith predictor configuration to maintain the extrudate thickness in the presence of the disturbances and machine drifts. Moreover, the constant input disturbance is added to the input to assess the controller. Finally, the delay term can be compensated by the configuration of the Smith predictor and the transient dynamics can be covered by the H_∞ controller.

1.5.4 Robust H_∞ controller

Mostafa Darabi is the primary author in developing the controller based on the robust H_∞ optimal technique which is addressed in Chapter 4. In addition, Mostafa Darabi conducted the literature review and developed the uncertainty model. Raffi Toukhtarian contributed in Chapter 4 by helping to develop the low order model for the controller design which is addressed in [31]. Benoit Boulet contributed in Chapter 4 by reviewing the overall controller design and editorial input for writing this chapter. The novel model is proposed in this work to be used in the Smith predictor configuration as a predictive model. The model that is obtained from the FEM model in [31] is assumed as a real plant model in the Smith predictor configuration. On the other hand, the predictive model is generated by the blocks swap of the original model. The blocks swap causes time delay uncertainty. In addition, the disturbance on the input also may cause more delay uncertainty due to input-dependent delay structure. Therefore, a robust H_∞ controller is proposed in the Smith predictor configuration to overcome and compensate for uncertainties.

Sensor placement

Mostafa Darabi was responsible for testing different types of sensors which are aimed to be applied in the extrusion blow molding machine. Different types of sensors, such as laser and ultrasonics, are studied in this work to be deployed on a real machine. The experimental open-loop systems are studied by using these sensors but the sensors are not implemented in the closed-loop system yet. But theoretically, the open-loop system, open-loop system with disturbance, and closed-loop system responses are compared to each other by calculating the summation of the error between the desired extrudate thickness and the measured ones. Accordingly, an optimal location is determined for the sensor to be placed in the real machine.

1.5.5 Related publications

This doctoral research has resulted in three manuscripts, a list of which is provided here:

1- Darabi, M., Toukhtarian, R., Alizadeh, H. V., Boulet, B. Closed-loop thickness control and sensor placement in extrusion blow molding. Paper Accepted for publication in International Journal of Automation and Control, October 2020

Mostafa Darabi is the primary author of the above manuscript in proposing the new controller design for the extrusion process. In addition, the literature review is done by the author and the new model is developed to be used in the Smith Predictor configuration. Raffi Toukhtarian helped in writing the modeling section of the manuscript. Benoit Boulet provided editorial input to review the manuscript in terms of technical part as well as the overall writing.

2- M. Darabi, R. Toukhtarian, B. Boulet, Robust H_∞ controller synthesis for extrusion blow molding process, It is in progress of submission.

Mostafa Darabi is the primary author of the above manuscript in proposing the new controller design for the extrusion process. In addition, the literature review is done by the author and the new model is developed to be used in the Smith Predictor configuration. Also the author compared the results in this manuscript to those of the previous manuscript in terms of the performance and reliability. Raffi Toukhtarian contributed the low order model proposed in [31] to be used as the main model of the controller in this manuscript. Benoit Boulet provided editorial input to review the manuscript in terms of technical part as well as the overall writing.

3- R. Toukhtarian,M. Darabi, S. Hatzikiriakos, H. Atsbha, B. Boulet, Parameter Identification of Transport PDE/Nonlinear ODE Cascade Model for Polymer Extrusion with Varying Die Gap, accepted for publication in Canadian Journal of Chemical Engineering

The primary author Raffi Toukhtarian is responsible for writing and developing the technical parts of the manuscript. The model consists of the nonlinear static function, the non-minimum

phase linear time-invariant system and the delay. Mostafa Darabi helped the primary author in developing the non-minimum phase linear time-invariant system and simulation. Benoit Boulet provided supervision and editorial input in preparation of the manuscript. All authors contributed by giving technical inputs and reviewing the manuscript.

1.5.6 Patent

This doctoral research has resulted in the filing of a United States Patent (USPTO):

- United States patent application No. US2020/0353663A1, Method and System for regulating an extrusion process, Nov 2020.

1.6 Thesis organization

This thesis is organized in five chapters. Chapter 2 provides the modeling section of the extrusion process. In addition, different types of the sensors are studied in Chapter 2 for EBM application. Chapter 3 introduces the feasibility of using the closed-loop system in EBM. In addition, the H_∞ controller is designed to eliminate the disturbances and machine drifts in order to maintain the extrudate thickness profile. Sensor placement in the actual machine is also discussed in this chapter. In Chapter 4, an uncertainty analysis is done for the extrusion process. Moreover, a robust H_∞ controller is designed to compensate for the disturbances and model uncertainties. Finally, the main conclusions of this research are reviewed and some research directions for future work are discussed in Chapter 5.

Chapter 2

EBM process modeling and monitoring

Extrudate thickness model

A Finite Element Method (FEM) simulator is developed in [29] to simulate the extrudate thickness behavior during the extrusion process. A time dependent simulator using the dimension-less Navier Stokes equations is proposed. The FEM simulator simulates gravity-free isothermal incompressible Newtonian fluids by solving the Navier-Stokes equations using Arbitrary Eulerian Lagrangian (ALE) based FEM. The FEM simulator of a viscoelastic fluid flow is too complex and is not suitable for controller design. The Navier-Stokes equations are discretized according to a mesh that is made up of Taylor-Hood $P1 - P2$ iso-parameteric triangular elements. The mesh includes 977 nodes from which 276 are corner nodes. Velocity in the x-direction, velocity in the y-direction, node x-position and node y-position are calculated at all the nodes, while the pressure is only calculated at the corner nodes. The discretized governing equations to find the solution, result in very high-order nonlinear Ordinary Differential Equations (ODEs). Moreover, using the FEM simulator may take several hours to produce results. Therefore, the FEM model is used in this work as a reference model to derive the control oriented model which is used for controller

design later on in Chapters 3 and 4.

Figure 2.1 depicts the cross section of the slit die extruder. The origin ($x = 0$) of the system is at the die exit and x is the distance away from the die. Moreover, the Reynolds number of 2.5 and Mesh 2 of [29] is used to define the parameters of the lower order model. The molten polymer enters into the die through the inlet. The die walls can move towards and away from each other to vary the die gap. The fluid inside the die is at high pressure during the extrusion stage. Therefore, the molten fluid is squeezed out of the die, forming the suspended sheet shaped extrudate. The die gap variation is studied in this work to obtain its effects on extrudate thickness during the transition from one value to the other. The bulging and necking effects may appear along the extrudate following the die gap change. The bulging and necking effects change according to different factors such as die length, die gap change, and duration of die gap change.

2.1 Low-order extrusion model

The proposed model in [31] is designed to replicate the main features of the step response of a reference FEM model in [29]. The step response of the reference model developed in [29] is used to identify the parameters of the control oriented model. As shown in Table 2.1, the model parameters are dimensionless to obtain the non-dimensionalized Navier Stokes equations. Therefore, lengths are divided by the Die length L_D, velocities by the maximum velocity at the inlet V_s, and time t by $T_s = {}^{L_D}/_{v_s}$. Figure 2.2 shows different input signals $u_1(t)$, $u_2(t)$, and $u_3(t)$ representing the die gap variation with respect to time. The values of $u_1(t)$, $u_2(t)$ and $u_3(t)$ change from 1.8 to 2.2, 2.3 to 2.7 and 2.8 to 3.2, respectively, during a period $\Delta T = 1$. As mentioned above, all the parameters in this work are dimensionless but in a real machine the die gap opening is dependent on the thickness of the extrudate and typically on the order of a few millimetres (mm). The die gap increases with a constant second derivative of value a for the first half of ΔT and then increases with a constant

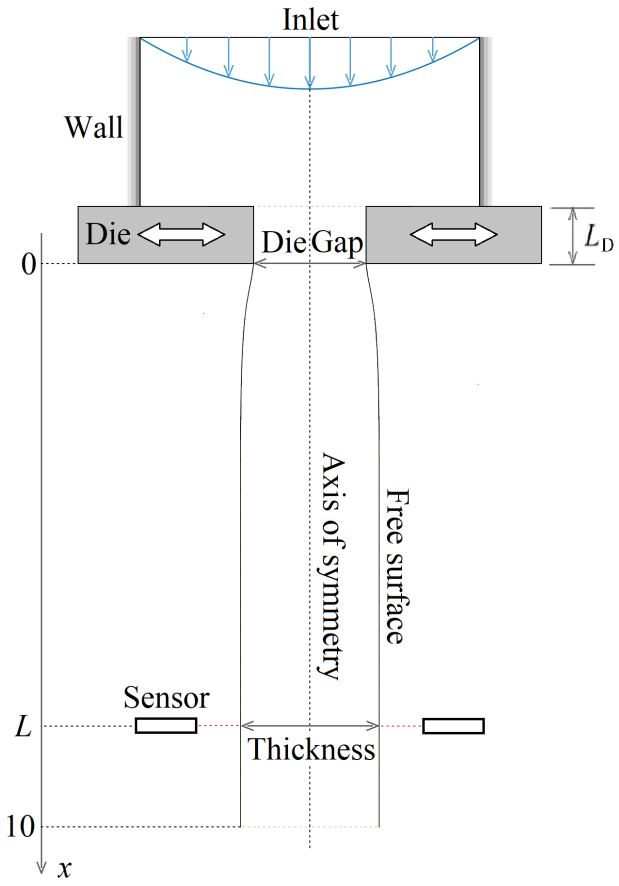

Figure 2.1: Extruder configuration

second derivative of value $-a$ during the second half.

Figure 2.3 shows the extrudate shape at $t = 0$, $t = 2$, $t = 3$, $t = 4$, and $t = 5$ for inputs u_1, u_2, and u_3. The considered extrudate is from $x = 0$ to $x = 10$. It is assumed that u keeps its initial value for a long period of time before $t = 0$. Therefore, the steady-state extrudate shape is shown in Figure 2.3 at $t = 0$. Die swell can be observed where the extrudate thickness values are larger than the die gap. Moreover, the extrudates develop a neck like shape when the die gap increases suddenly. When the die gap is increased, the thickness decreases before it increases resulting in a neck like shape. The opposite is true when the die gap is decreased resulting in a bulge on the

Table 2.1: Dimensionless parameters.

Parameter	Reference value	Normalized value
length ($l^\star$)	L_D	$l = \frac{l^\star}{L_D}$
velocity ($v^\star$)	V_s	$v = \frac{v^\star}{V_s}$
time ($t^\star$)	$T_s = \frac{L_D}{V_S}$	$t = \frac{t^\star}{T_s}$

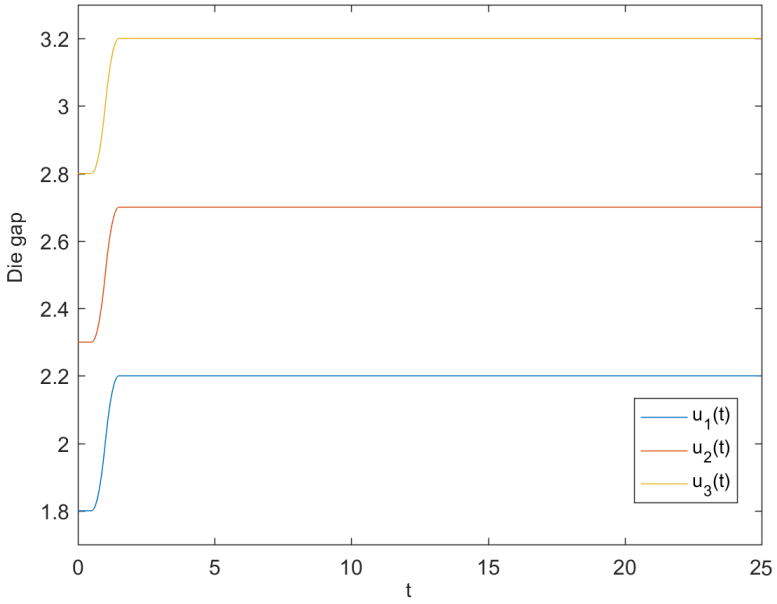

Figure 2.2: Die gap opening versus time

extrudate. Bulging and necking phenomena are mainly due to the transient change in volumetric flow rate at the die exit when the die gap is decreased or increased. Even though the volumetric flow rate is constant at the inlet, the volumetric flow rate changes at the die exit due to the change of volume between the die walls. The bulging and necking phenomena were first described in [29]. In Figure 2.3, the neck shape travels downward fastest for $u_1(t)$ and slowest for $u_3(t)$ because the material velocity is higher for smaller die gaps.

Figure 2.4 shows the extrudate thickness $y(t)$ at $x = 1$, $x = 5$, and $x = 9$ when inputs $u_1(t)$,

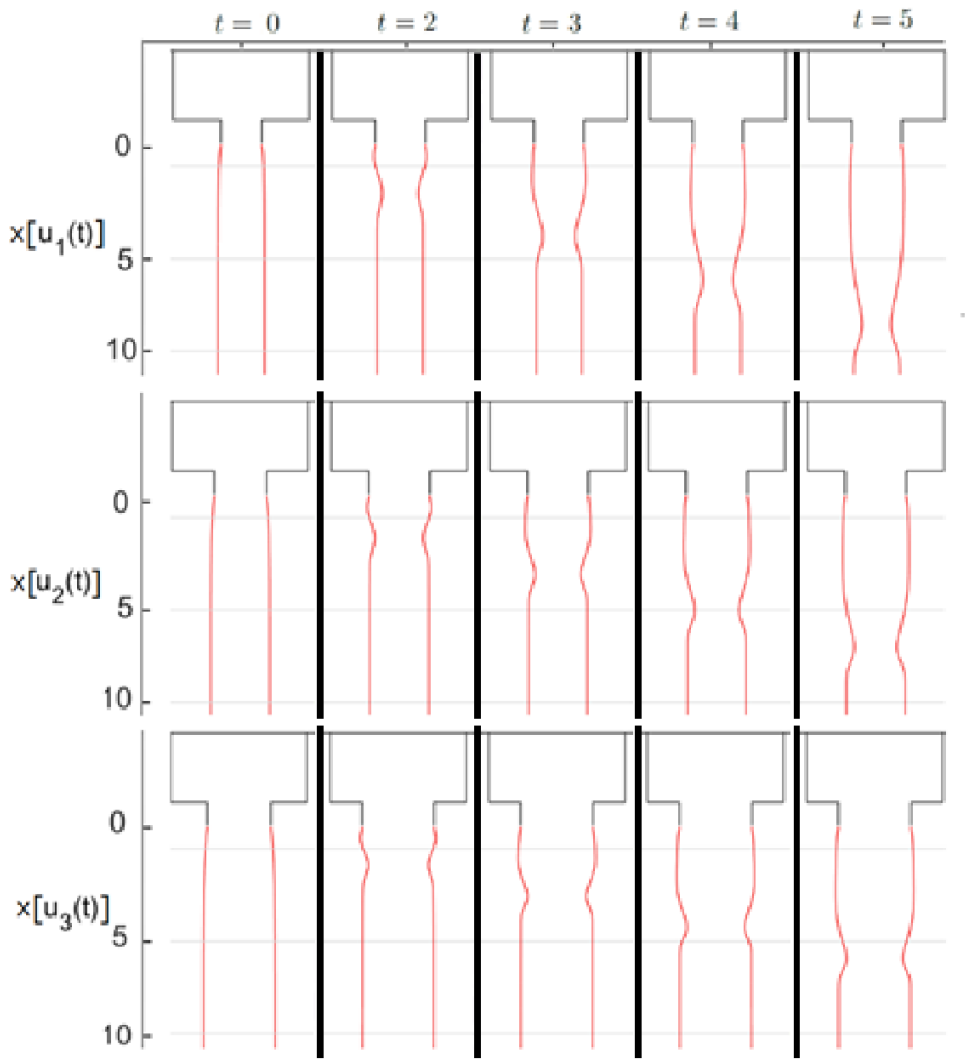

Figure 2.3: Thickness change of the extrudate along normalized distance x at different time steps t

$u_2(t)$, and $u_3(t)$ are applied. The $x = 1$, $x = 5$, and $x = 9$ locations are pointed out by gray lines in Figure 2.3. The signals at different values of x share common characteristics. The signals show

delay with respect to $u(t)$ especially for larger values of x. The transport delay is the time needed for the material to travel from the die gap to the intended location. Given that the flow rate at the inlet is constant, smaller die gaps cause faster material transport resulting in less delay. Therefore, the transport delay is dependent on the input from the instant that the material leaves the die until it reaches the intended location. Moreover, the signals undergo a small notch before settling to their final value.

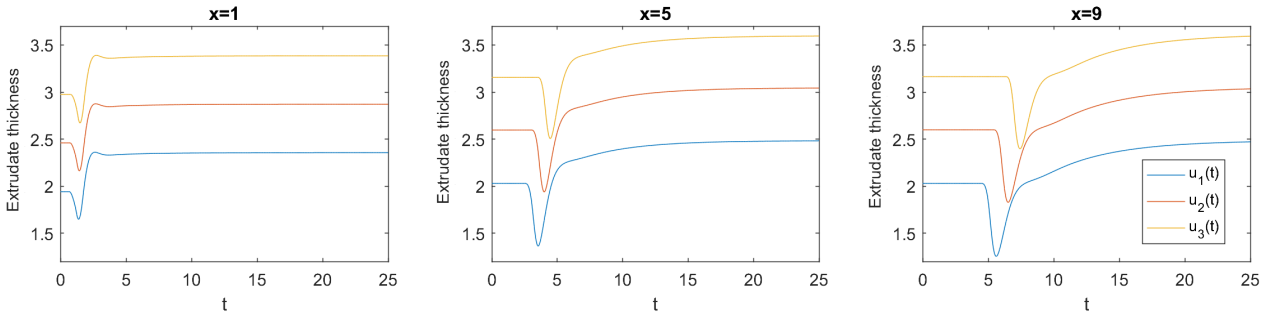

Figure 2.4: Extrudate thickness at $x = 1$, $x = 5$, and $x = 9$ for $u_1(t)$, $u_2(t)$, and $u_3(t)$, respectively

2.1.1 Die gap programming

Die gap programming is used to tune the setpoints in order to control the extrudate thickness and the final product in EBM. Die gap programming is considered as an open-loop optimization task. In this section, the example described in [31] is reconsidered. Extrusion time is divided into 8 equal intervals in which the die gap is set to a constant value. Usually, most of the stretching during molding occurs in the middle of the extrudate. Therefore, the middle of the extrudate is chosen to be thicker. On the other hand, the molds clamp at the top and the bottom of the extrudate, thus, the top and bottom are chosen to be thinner. The die gap programming is done by trial and error in order to form the desired extrudate shape at $t = 8$. Figure 2.5 shows the die gap versus time for

one complete cycle and is used as a input $u(t)$ for the simulation results later on in this work.

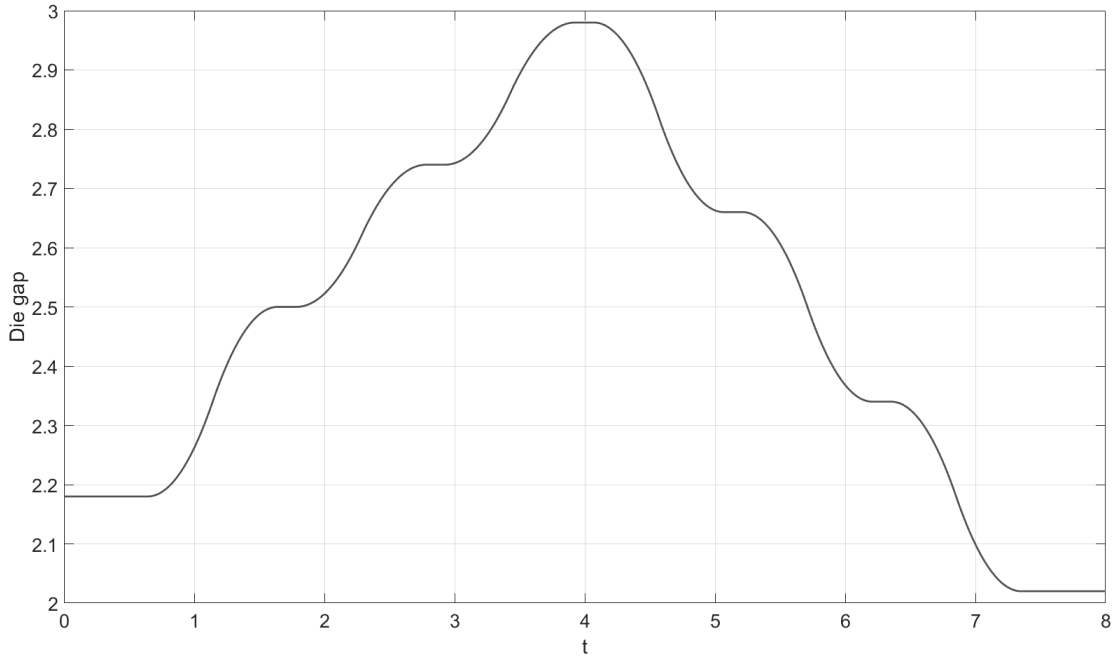

Figure 2.5: Die opening versus time

2.1.2 Model structure

Low order linear transfer functions with delay are used in [44, 79, 80] to model a wide range of processes due to their simplicity and practicality. In addition, Hammerstein models are used as nonlinear black box models in various applications where the parameters are identified from experimental results [81–84]. The proposed model uses a Hammerstein model with delay to replicate the extrudate thickness at a certain distance from the die [31]. The model is composed of a delay $\theta(x,u)$, a nonlinear static function $f_s(x,u)$ and a linear time-invariant system $H(s,x)$ shown in Figure 2.6.

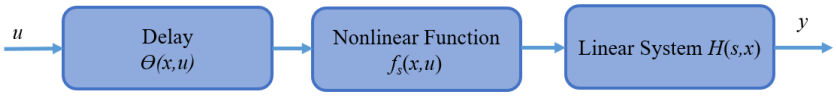

Figure 2.6: Block diagram of the control oriented model

Transport delay

During extrusion, the observed delay is due to different factors. The material transport delay is due to the time needed for the material to travel from the die to the measured location. During extrusion process, particles on the extrudate do not have uniform velocity. Therefore, the extrudate changes shape as it is being extruded. In this work, it is assumed that the delay is entirely due to material transport. To simulate the model, the delayed input $u_d(t,x)$ is computed for different values of x and t using the transport equation in (2.1),

$$\frac{\partial u_d(t,x)}{\partial t} = -v(t,x)\frac{\partial u_d(t,x)}{\partial x}, \tag{2.1}$$

where $v(t,x)$ is the particle velocity. The boundary condition at $x = 0$ is $u_d(t,0) = u(t)$. It is assumed that the initial value of u has remained constant for a long time before $t = 0$. Therefore, the initial condition is $u_d(0,x) = u(0)$. The particle velocity v is dependent on x and t in (2.2),

$$v(t,x) = \beta f_v(x)\frac{Q_0 - L_D\frac{du(t)}{d(t)}}{u(t)} \tag{2.2}$$

where function $f_v(x)$ is chosen to be a second-order polynomial. At $x = 0$, $f_v(0) = f_{v0}$ where $f_{v0} > 1$. $f_v(x)$ decreases until it reaches x_0 where $f_v(x_0) = 1$ and $\partial f_v(x_0)/\partial x$ is set to 0. Q_0 is the volumetric flow rate at the inlet, and L_D is the length of the die. In addition, the velocity is multiplied by coefficient β to better fit the slope of the delay with respect to x. The delay and its

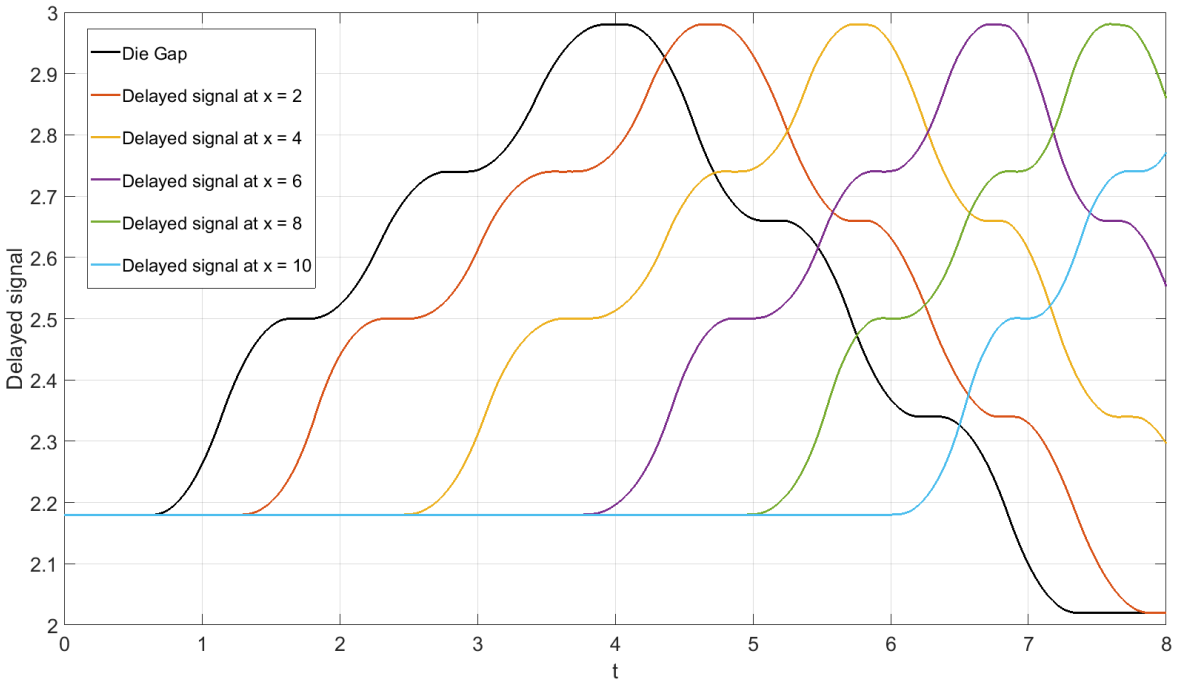

Figure 2.7: Delayed input signals at $x = 2, 4, 6, 8$, and 10

parameters are further discussed in [31]. Figure 2.7 shows delayed input signals for $x = 2, 4, 6, 8$, and 10. The signal which is shown in black is the die gap programming. According to the Figure 2.7, it is shown that position $x = 10$ has the largest delay compared to the other points below the die. Therefore, the delay is increased for the points further away from the die which can be justified by transport equation (2.2) as well.

Nonlinear static function

The delayed signal $u_d(t, x)$ in (2.1) is the input to the Hammerstein model composed of two cascaded elements, $f_s(x, u)$ and $H(s, x)$. The first element is a static nonlinear function which yields the steady-state thickness for a constant die gap u and location x away from the die. If a constant die gap is applied for a sufficiently long time, the extrudate will attain a steady shape. The steady

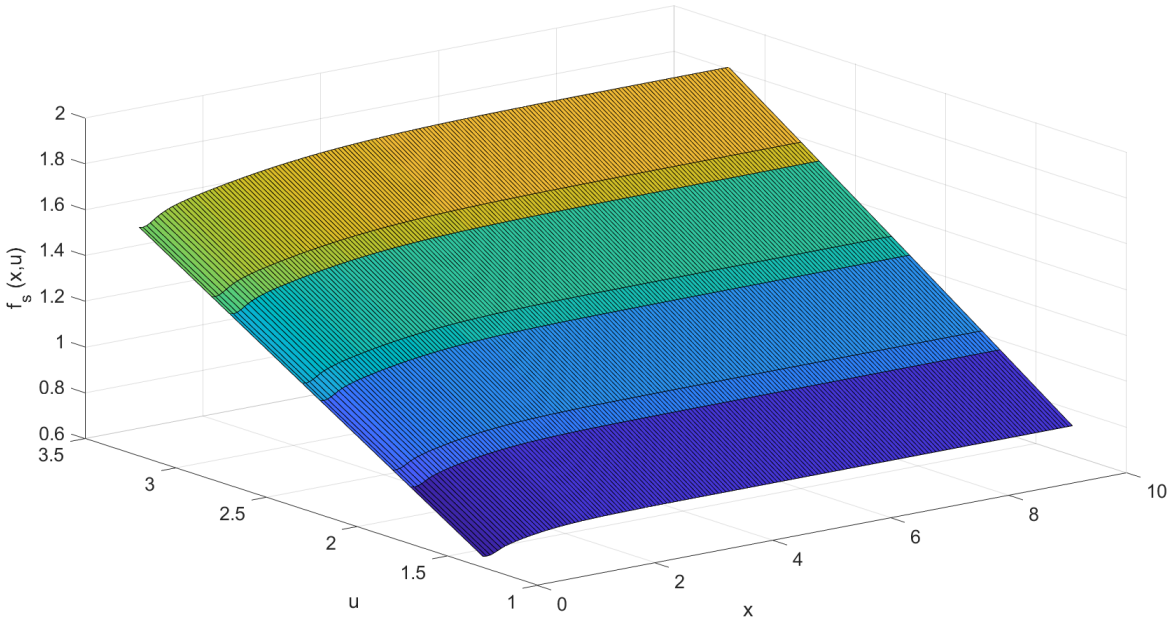

Figure 2.8: Steady state thickness with respect to x and u

extrudate shape is depicted in Figure 2.3 at $t = 0$. The function $f_s(x, u)$ is an interpolation function created by using the steady thickness at the combination of $u = 1.8, 2.2, 2.3, 2.7, 2.8, 3.2$ (6 points) and, $x = 0, 0.0625, 0.125, ..., 10$; (161 points). The function is obtained using curve fitting in [88].

Figure 2.8 shows the nonlinear static function $f_s(x, u)$. This function is proposed by using 6 thickness values. The x axis is divided into 161 points to obtain $f_s(x, u)$. The large number is defined to monitor the parameter variation of the linear time-invariant (LTI) system with respect to x that is explained in the next section.

Non-minimum phase LTI system

The element $H(s, x)$ in Figure 2.6 is a linear time-invariant system that has non-minimum phase dynamics and a unity dc gain. The linear system replicates the transient change of the thickness

from one steady value to the next. The non-minimum phase dynamics recreate the necking and bulging effects mentioned before. Given that the linear system has unity dc gain, the steady-state value of the extrudate is determined by $f_s(x, u)$. Moreover, the linear model is a 4th-order system obtained by a parameter identification algorithm. The algorithm is based on minimizing the integral of the step response error between the low order model in [31] and the FEM model in [29]. Step response tests are widely used to identify low order systems with delay [85–87]. Figure 2.9 shows the extrudate thickness at $x = 2, 4, 6, 8,$ and 10. All the thickness signals below the die have a common behavior while exiting the die. The delay is longer for the points further away from the die. Moreover, the signals show the non-minimum phase behavior as mentioned above. Ultimately, the signals undergo minima due to the the necking effect shown in Figure 2.3 and reach the steady state at the end.

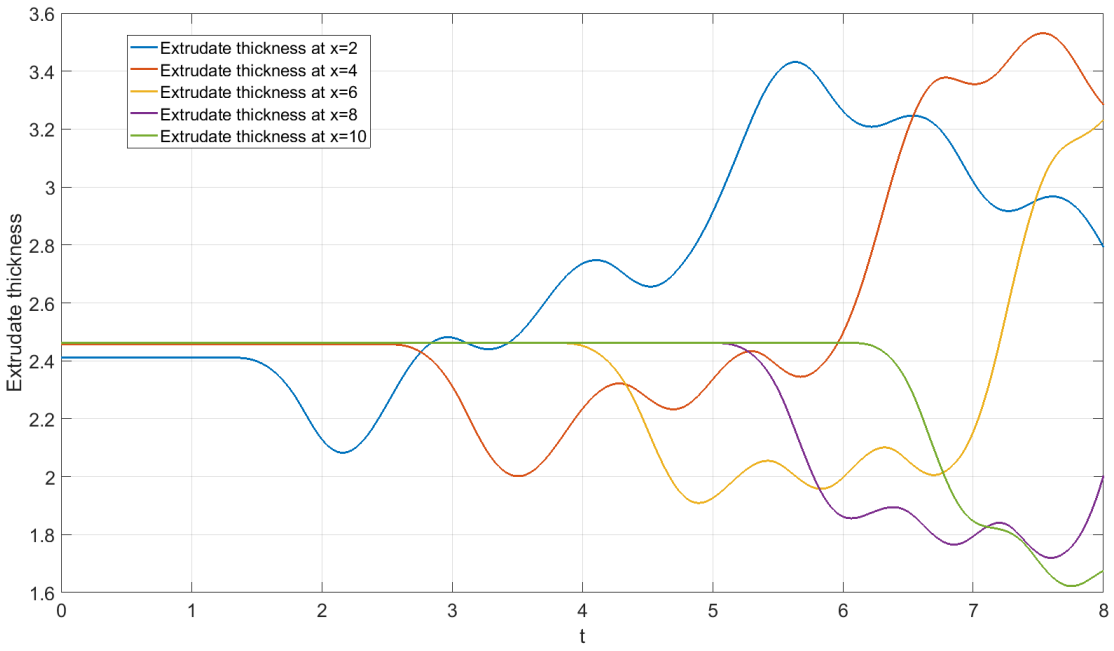

Figure 2.9: Extrudate thickness at $x = 2, 4, 6, 8,$ and 10

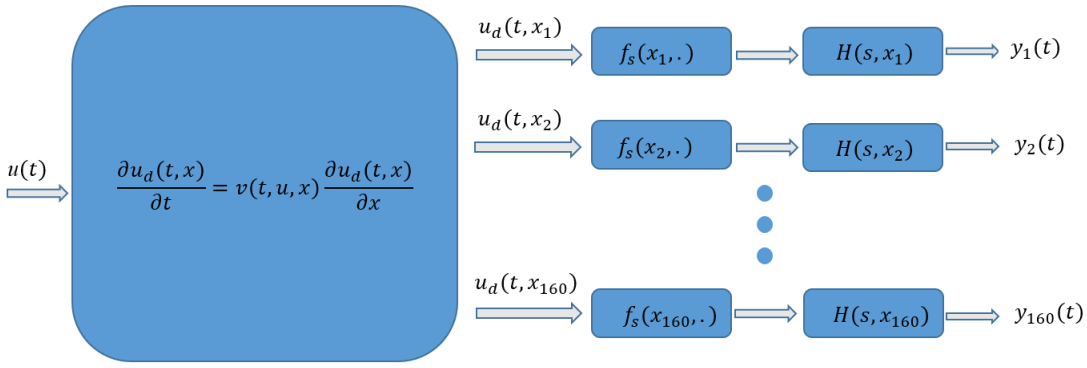

Figure 2.10: Overall block diagram for extrudate segments

Overall system

To simulate the overall shape of the extrudate, the thickness must be modeled for different values x_i of x. In this work, 160 Hammerstein blocks are used to simulate the thickness at different locations away from the die. Figure 2.10 shows the block diagram of the overall model. As mentioned before, the model is constituted by delay, nonlinear static function, and transient blocks. The transport equation outputs the delayed input for different values of x. $u_d(t,x_i)$ is the input for the Hammerstein models. The output thicknesses at x_1, x_2,... and x_{160} are denoted by $y_1(t), y_2(t)$, ..., and $y_{160}(t)$.

2.2 Monitoring and sensors

Each product has a particular geometry that needs input parameters to be fed to the machine. The thickness distribution along the extrudate is crucial to produce a final part with desired specifications. The extrusion process is strongly affected by the sag and swell phenomena described above. In order to produce consistent parts with acceptable features, it is necessary to monitor the thickness of the extrudate during extrusion. A proper sensor is selected in this work based on the

measurement precision, harsh environment, repeatability of the process, and fast sampling rate. The monitoring process could be described as in-cycle or cycle-to-cycle. In the in-cycle process, the measurement is done during the current cycle in real time. Therefore, if any drift is observed, the compensation can occur during the current cycle. On the other hand, the process measurement is done at the end of the cycle in cycle-to-cycle process. Therefore, the correction would happen for the next cycles if needed. Accordingly, based on the application, different types of sensors can be considered for the monitoring process.

Thickness sensors can be divided into different classes. Non-contact, with contact, one-side, or two-side sensors, are used in industry to measure the thickness. For the in-cycle process, it is hard to reach inside the mold. Therefore, the sensors need to be of the non-contact type to measure the extrudate thickness before entering the mold. The non-contact sensors measure dimensions without touching the surface. In this case, production processes can be monitored continuously, ensuring quality and reducing rejects. Such measurement systems are flexible and easy to integrate. Avoiding contact with the object helps in measuring the soft, sticky, hot, or other sensitive surfaces. Non-contact sensor for the in-cycle process can be found as optical micrometers, laser, Eddy current, capacitive, and radar sensors. On the other hand, for the cycle-to-cycle process, the measurement is done when the final part is ready. Therefore, it is easier to choose the right sensor for measurement. In this work, an ultrasonic sensor is picked to be tested for this application. The thickness of the piece is measured when the final part is ready. Afterward, if the measured thickness is varied from the reference, the controller correction happens for the next cycle. In addition, the one-side or two-side sensor is used for monitoring dependent on the extrudate shape in which the one-side sensor is preferred for the cylindrical-shaped extrudate while both types can be used for sheet-shaped extrudate.

2.2.1 In-cycle monitoring

A two-side laser sensor is considered in this work for in-cycle monitoring. The laser triangulation sensors can be divided into two types according to their performance and the purpose of application [89]. The two types are high-resolution lasers and proximity type laser triangulation sensors. The high-resolution laser typically is used in displacement and position monitoring applications. It provides high accuracy in addition to low-temperature drift. Moreover, this type of sensors is frequently used in process monitoring and closed-loop feedback control systems. On the other hand, the proximity sensor is less expensive compared to the high-resolution lasers. This sensor is generally used to detect the presence of a part, or in counting applications.

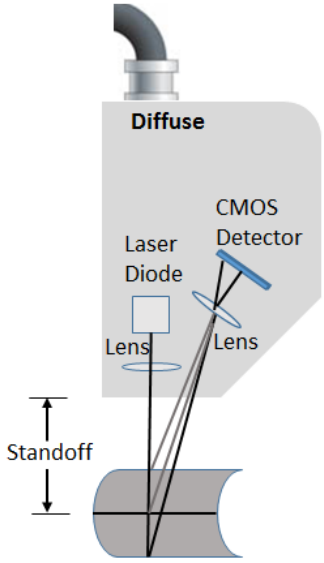

Figure 2.11: Laser triangulation principle

Figure 2.11 shows the laser triangulation principle. Laser triangulation sensors contain a solid-state laser light source and a position-sensitive detectors (PSD) or CMOS/CCD detector. A laser beam is projected on the part that is being measured, which is the extrudate in this work. A portion of the beam is reflected through focusing optics onto a detector. As the extrudate is being

extruded, the laser beam proportionally moves on the detector. In addition, PSD type sensors are more susceptible to false reflections from changing surface conditions, which can reduce their accuracy. On the other hand, CCD and CMOS systems are typically more accurate over a wider variety of surfaces. In such systems, unwanted reflections from changing optical properties of the extrudate that is measured can easily be ignored during signal processing. Therefore, this allows them to be used during the extrusion process. The advantage of the non-contact laser sensor is that the extrudate being measured is not damaged during the monitoring process. Moreover, it can measure the high-frequency motions of the object. The measurement range is also large enough to allow them to be used in different applications. On the other hand, the drawback is that the environmental conditions are important to obtain highly accurate measurements. Since the laser system is an optical type sensor, it is important to keep the optical path clean and free from dirt and foreign materials. Moreover, due to the sensitivity of the electronic components, the operating temperature range is limited, and it is not recommended to use this sensor for the high-temperature environment without extra cooling devices.

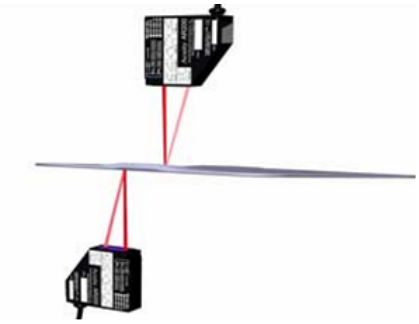

Figure 2.12: Two sided laser sensor

A one-side laser sensor for thickness measurement is possible if one side of the material can be held constant against a fixed reference plane. However, a two-side laser sensor is preferred for thickness measurement. The two-side laser sensor is used to measure the wood thickness,

quality control of concrete block manufacturing, a separation distance between rollers, and brake rotor thickness as shown in Figure 2.12. In this work, the two-side laser sensor is used in an experimental setup to measure the thickness of the extrudate when is extruded. The operating environment temperature is up to 50°C. Moreover, the measurement range is between 75mm to 130mm. Figure 2.13 depicts the experimental setup that is developed to measure the thickness of the extrudate.

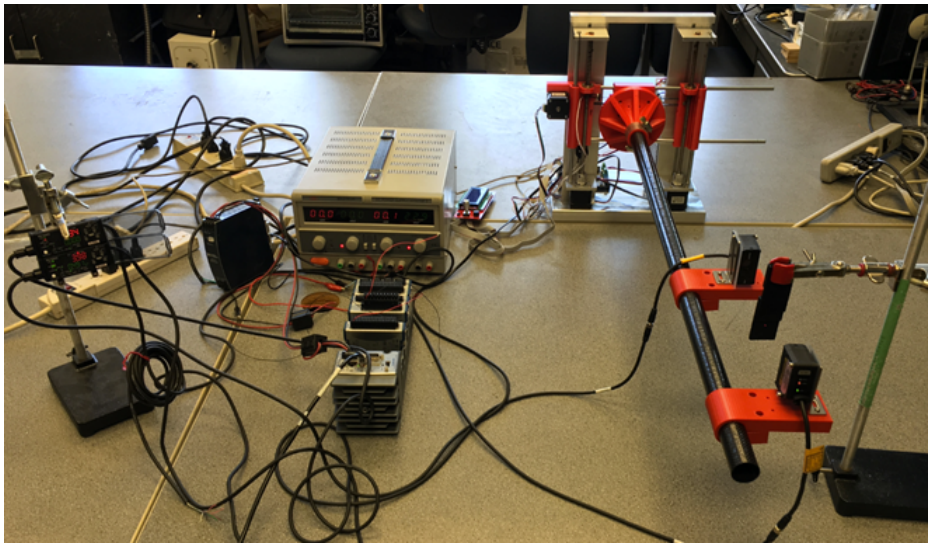

Figure 2.13: Experimental setup for laser sensor

The two sensor heads are attached to the fixture which is shown in red. A robotic arm is built to move the sensor up and down to measure the thickness of the extrudate surface. Moreover, a data logging instrument is used to collect the thickness data in real-time. In order to measure the original part, an extrudate piece is obtained to be used in this experiment. The length of the extrudate is 7.5cm, and is divided into five different points, i.e., 1.5cm from each other. Before using the laser sensor, the thickness of the five points is measured by micrometer which are 4mm, 8mm, 12mm, 4mm, and 8mm, respectively. Afterwards, the robotic arm moves the sensors up and down for ten times to obtain ten measurements for different instances.

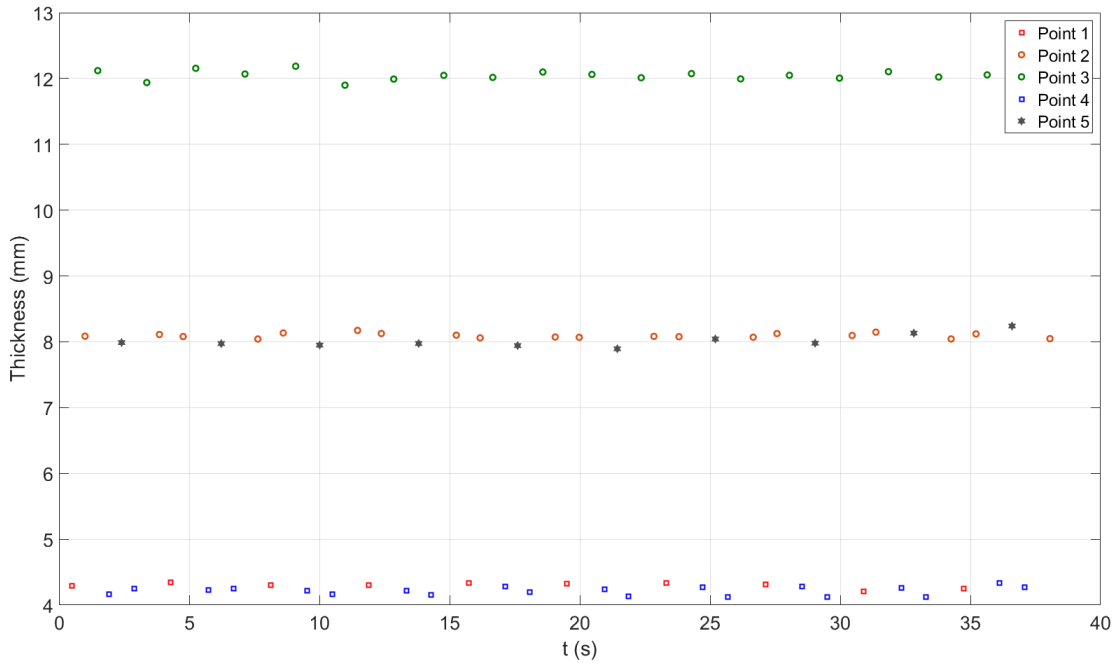

Figure 2.14: Data logging for five points along the extrudate

Figure 2.14 shown the data collected by laser sensors for five different points along the extrudate. Moreover, Table 2.2 illustrates the accuracy of the data collected by sensors. The actual thickness data measured by the micrometer is written in the second column. The third column shows the data measured by the laser sensors. The laser accuracy is obtained in the last column, which is more than 92%. The point #1 is the first point measured along the extrudate. Due to beam vibration caused by the robotic arm at the starting point, the accuracy is lower than the other points. Therefore, the laser sensor is a reliable measurement device to be used in this application.

2.2.2 Cycle-to-cycle monitoring

Sound energy can be generated over the extensive frequency range. A human can hear audible sound limited to 20kHz. Ultrasound is sound energy at a higher frequency which is not sensed by

Table 2.2: Data logging analysis of laser sensor

Points	Actual measured value	Sensor measured value	Accuracy
1	4mm	4.3011mm	>92%
2	8mm	8.0928mm	>98%
3	12mm	12.0401mm	>99%
4	4mm	4.2149mm	>94%
5	8mm	8.0115mm	>99%

the human ear. The sound energy generated by ultrasound in the range of 50kHz to 100MHz can travel through the air, water, or steel. Figure 2.15 shows the principle of sound energy distribution through materials. The transducer contains a piezoelectric element which is excited by a short electrical impulse to generate ultrasonic waves [90]. The sound waves travel through the test object until they encounter a wall or other surface. Afterward, the reflected waves travel back to the transducer. Ultimately, the transducer converts the sound energy to electrical energy. There are two types of sensors used to measure the thickness, immersion, and dual element transducers. Immersion transducers use water to couple sound energy into the test object. Moreover, they are suitable for on-line measurement of moving products. On the other hand, the dual-element transducers are used to measure rough surfaces. They have separate transmitting and receiving elements which are incorporated by a delay line.

In this work, an immersion ultrasonic thickness gauge is used to measure the thickness of the final part. The small probe, which is called ultrasonic transducer sends a sound pulse through the test object and then reflect from the inside surface. Due to the reflection of the sound waves through different boundaries, the measurement is typically done by a one-side transducer in pulse/echo mode. The sound velocity in the test object is an essential part of the thickness calculation in (2.3), where T is the thickness and t is the time of the waves to travel back and forth through the materials. Different materials transmit sound waves at different velocities, faster in more robust

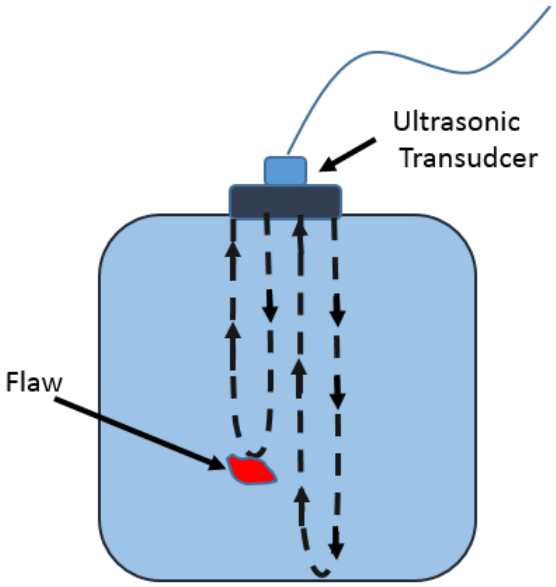

Figure 2.15: Ultrasound principle

materials, and slower in smooth materials.

$$T = v \times \frac{t}{2} \tag{2.3}$$

Moreover, the sound velocity can be changed by temperature. Therefore, it is always necessary to calibrate an ultrasonic thickness gauge to the speed of sound for the material undergoing measurements. On the other hand, the drawback of the ultrasonic transducer is that the high-frequency sound waves do not travel well through the air. So, it is necessary to use couplant between the sensor and the test object so that, the sound waves can be transmitted well through the materials.

Two ultrasonic immersion sensors are used for cycle-to-cycle monitoring in this work. To have a reliable experiment, the two immersion sensors are installed in the cooling fixture at the production plant to measure the thickness of the fuel tank when the part is submerged into the water bath as shown in Figure 2.16. The final part is immersed in the water bath after the molding

stage for 35 seconds to be cooled by water. The reference thickness values of the fuel tank for both sensor positions were provided as 5.09mm, and 7.56mm, respectively. The thickness at the locations of sensors #1 and #2 is recorded for eight different parts over a time of 20 seconds after the piece is submerged in the water bath completely. Figure 2.17 shows the thickness of the eight different parts obtained by using the ultrasonic sensor at position #2. The average thickness value, which was acquired by the sensor for eight different parts is 7.33mm.

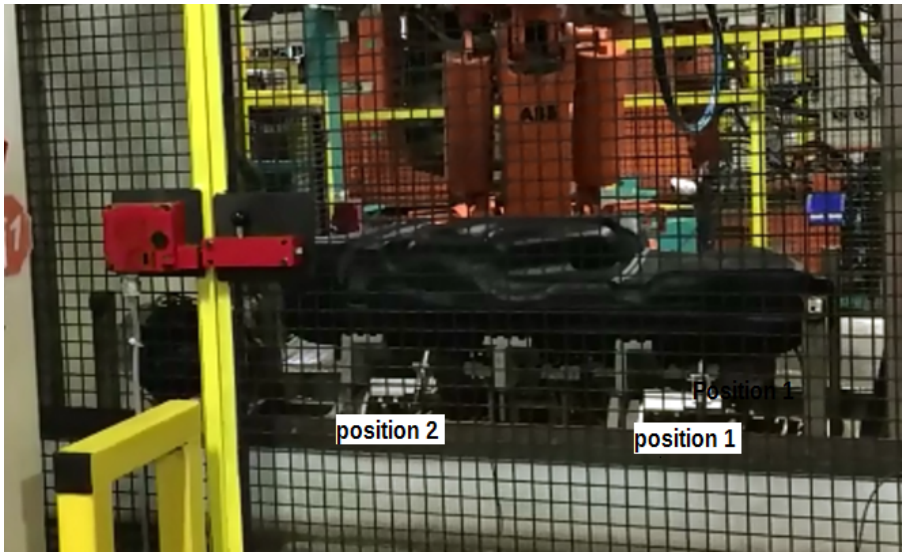

Figure 2.16: Ultrasonic sensors installed at Kautex inc. plant

In addition, one of the eight parts measured in the water bath is taken out to be measured with a micrometer. Figure 2.18 shows two pieces which are cut from the original part. The thickness of these two pieces is measured by the micrometer. Moreover, a conventional ultrasonic sensor with couplant is used to measure the thickness of the pieces. Table (2.3) shows the analysis of data collected by immersion transducer in the water bath, micrometer, and conventional ultrasonic sensor out of the water bath. The micrometer reading is considered as a reference value. It is shown that the ultrasonic transducer installed in the cooling stage measured the thickness with accuracy of more than 95%.

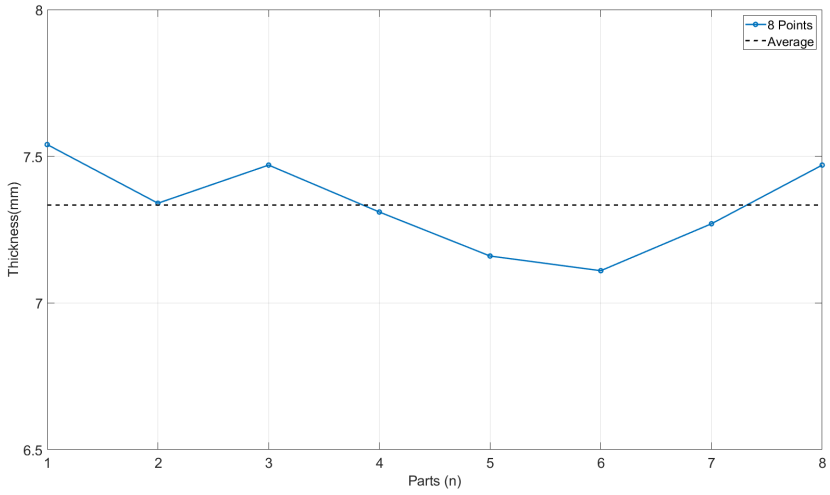

Figure 2.17: Thickness measure by ultrasonic sensor for 8 different parts and their average

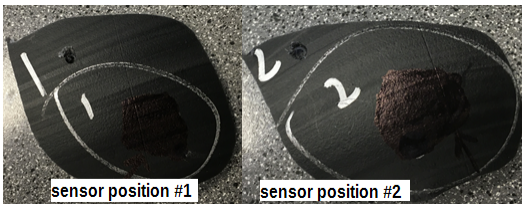

Figure 2.18: Part pieces for validation

On the other hand, it should be noted that the water is turbulent in the water bath. Also, the final part is shrinking due to temperature change from high to low. Therefore, the immersion transducer is applicable to the cooling stage of a cycle-to-cycle monitoring process.

Table 2.3: Data logging analysis of ultrasonic sensor

Readings	Sensor #1	Sensor #2	Accuracy
Immersion transducer	5.45mm	7.33mm	>95%
Conventional transducer	5.30mm	7.28mm	>97%
Micrometer	5.20mm	7.10mm	Ref

Chapter 3

Closed-loop thickness control

3.1 Introduction

A low-order model of the extrudate thickness is explained in the previous chapter and used in this section to reproduce the main aspects of the step response of a reference FEM model [29]. The model could also come from data obtained by experiments run on a machine. The step response is used to identify the parameters of the model that is suitable for the control purpose. As shown in Table 2.1, the model parameters are dimensionless, lengths are divided by the Die length L_D, velocities by the maximum velocity at the inlet v_s, and time t by $t_s = {}^{L_D}/_{v_s}$. The input $u(t)$ is varied from 2 to 3 as shown in Figure 2.5. Moreover, the proposed model in [31] uses a Hammerstein model that is composed of a low order linear transfer function and nonlinear static function with a delay to replicate the extrudate thickness shown in Figure 2.1 at a certain distance from the die.

Disturbances and machine drifts can cause damaged parts and require the machine operator to retune the machine. The objective of this work is to reduce the effects of disturbances and drifts in the EBM process by using automatic feedback. Thickness variations from a desired signal are measured by a sensor at a fixed location from the die. The controller automatically changes the

die gap to minimize the variations. For instance, the die geometry, misaligned die slabs, or worn die could vary the die opening from its desired value. Therefore, the disturbance is modeled by a constant value added to the input $u(t)$ where the die opening is the input of the low-order model. The controller is designed to ensure a stable closed-loop system and to compensate for the added disturbance. The controlled plant has an input-dependent delay cascaded with a Hammerstein model as mentioned before.

3.2 Controller design

In order to produce the parts within acceptable specifications, it is necessary to reduce the effect of the disturbances and the drifts during the extrusion process. The closed-loop system aims to keep the repeatability of cycles in producing a consistent extrudate during every cycle. To do so, an H_∞ controller in a Smith predictor configuration is used to meet the objectives.

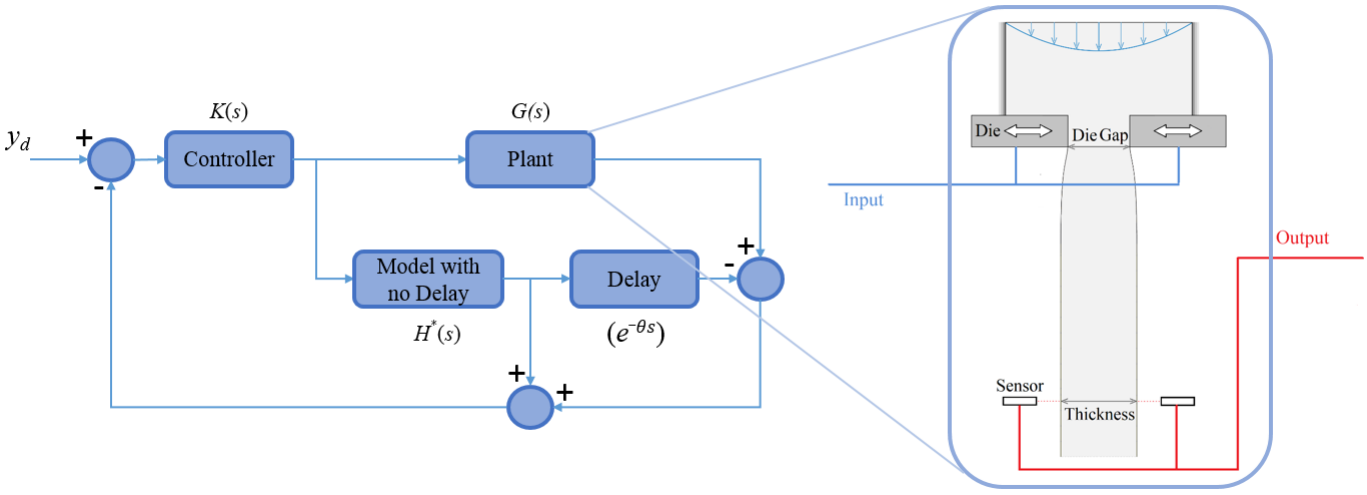

Figure 3.1: Smith predictor control block diagram

3.2.1 Smith predictor technique

As mentioned before, the Smith predictor configuration is used to deal with systems containing time delays [41]. Figure 3.1 shows a conventional block diagram of a Smith predictor where $G(s)$ is the controlled plant and is given by

$$G(s) \simeq H(s)e^{-\theta s}. \tag{3.1}$$

The plant is split into two parts: the delay-free model $H(s)$, and the time delay term $e^{-\theta s}$. Using the Smith predictor configuration, the controller is designed according to the delay-free system $H(s)$ and the delay is compensated for by the configuration. Moreover, this technique belongs to the class of Internal Model Control [98, 99] that requires a good model to ensure a desired performance. The predictive model is given by

$$G^*(s) = H^*(s)e^{-\theta^* s}. \tag{3.2}$$

Assuming that the modeling error is equal to zero, i.e., $G(s) = G^*(s)$, the closed-loop transfer function T_{yy_d} is given by

$$T_{yy_d} = \frac{y}{y_d} = \frac{KH^* e^{-\theta^* s}}{1 + KH^*}. \tag{3.3}$$

On the other hand, the transfer function of conventional unity feedback is given by

$$T_{yy_d} = \frac{y}{y_d} = \frac{KH^* e^{-\theta^* s}}{1 + KH^* e^{-\theta^* s}}. \tag{3.4}$$

Comparing (3.3) to (3.4) shows that the time delay term $e^{-\theta^* s}$ is eliminated from the characteristic equation in (3.3) using the Smith predictor configuration if perfect modeling is assumed. Eliminating the delay term in the denominator facilitates controller design using the Smith predictor over conventional feedback design.

3.2.2 Predictive model

In order to use the Smith predictor configuration in the controller design, the delay block should be placed after the transient block. Figure 3.2 shows the real plant model versus the predictive model. As mentioned before, the model of the real plant includes time delay and Hammerstein blocks. The difference between the real plant model and the predictive model is in the arrangement of blocks. In the real plant, the delayed input is the input of the Hammerstein block [31]. The delay term in the predictive model is placed after the Hammerstein block making the model suitable for the Smith predictor configuration. In Figure 3.2, u_d is the desired input, y_1' is the output of the nonlinear static function, y_2' is the output of Hammerstein model, y_d and y_d' are the outputs of the real plant model and predictive model, respectively.

Even though the predictive model and the real plant are not identical, the blocks swap is justified in this work. Given the input $u(t)$ (see Figure 2.5), Figure 3.3 depicts the extrudate thickness for the original plant versus the predictive model at $x = 2.5$. The signals show additional delay with respect to $u(t)$ especially for larger values of x that is explained in the next chapter. Therefore, the blocks swap causes variation between the two plants that should be considered in the controller design.

In order to simulate the overall system, the delay must be obtained for different values of x and

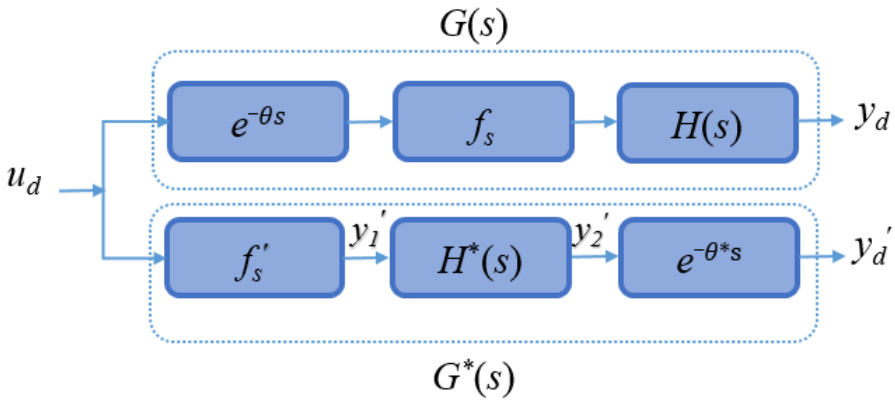

Figure 3.2: Real plant model (top branch) versus the predictive model (bottom branch)

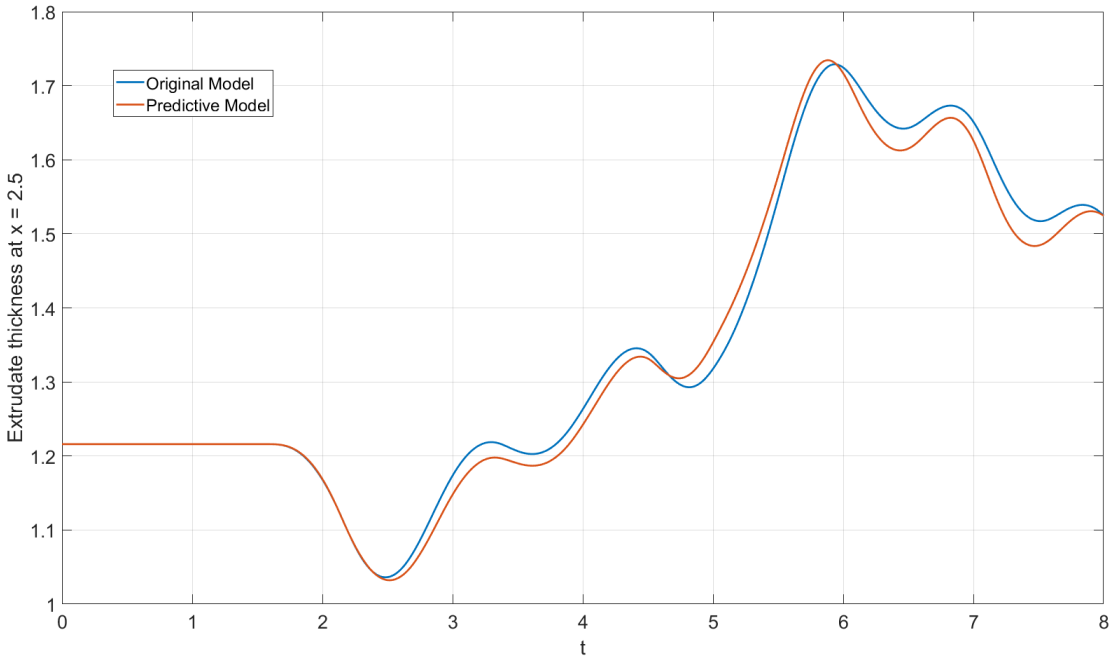

Figure 3.3: Extrudate thickness of original plant versus predictive model at x = 2.5

t. To do so, the transport equation should be solved numerically. The transport equation is recalled again in (3.5)

$$\frac{\partial u_d(t,x)}{\partial t} = -v_f(x,t)\frac{\partial u_d(t,x)}{\partial x} \tag{3.5}$$

The boundary condition at $x = 0$ is $u_d(t,0) = u(t)$. The initial value of u is considered to be a constant value for a long period before $t = 0$. Therefore, the initial condition is $u_d(0,x) = u(0)$. In order to solve (3.5), the equation is discretized with respect to space and time. The solution is obtained at spatially equidistant points 0.003125 (dx) away from each other and the time step is 0.0025. The extrudate length is equal to 10. Therefore, 3200 points are defined along the extrudate based on the solution found at 0.003125 away from each other. In order to discretize the right side of the transport equation spatially, the Crank-Nicolson Finite Difference Method (FDM) [91, 92] is used and described in (3.6).

$$\begin{cases} x_1 :\rightarrow \frac{\partial u_1}{\partial t} = -v_f(x,t)\frac{u_2-u_0}{2dx} \\ x_2 :\rightarrow \frac{\partial u_2}{\partial t} = -v_f(x,t)\frac{u_3-u_1}{2dx} \\ \vdots \\ x_{3199} : \frac{\partial u_{3199}}{\partial t} = -v_f(x,t)\frac{u_{3200}-u_{3198}}{2dx} \\ x_{3200} :\rightarrow \frac{\partial u_{3200}}{\partial t} = -v_f(x,t)\frac{2u_{3200}-2u_{3199}}{2dx} \end{cases} \tag{3.6}$$

The overall model structure is shown in Figure 2.10 in Section 2.1.2. The extrudate length is divided into equal distances and 160 points are picked as a sampling point to form the overall structure. Therefore, for every 20 consecutive points along the extrudate, one system is created, leading to 160 ($i \in$[1,. . . ,160]) systems in total as shown in Figure 2.10. As mentioned above, the

overall system is constituted of 160 individual systems. The Backward Finite Difference Method [93, 94] is used to solve the transport equation for the last system ($i = 160$) as written in (3.6). The numerical method is used to transform the partial differential equation (3.6) into a difference equation to simplify the controller design for simulation results. To do so, at time t, the extrudate is discretized spatially to obtain the spatial difference system in which the independent variable is space rather than time t. Moreover, the state vector $w[n]$ in (3.7) is considered to represent the difference equation in (3.6) such that $n \in$[1,2,. . . ,3200], is the index of x_n,

$$\begin{cases} w[n+1] = Aw[n] + Bu[n] \\ y[n] = Cw[n] + Du[n] \end{cases} \tag{3.7}$$

where, the matrices A, B and C of the difference equation are given in (3.8) and D is equal to 0.

$$A = \begin{pmatrix} 0 & -1 & 0 & 0 & \dots & \dots & 0 \\ 1 & 0 & -1 & 0 & \dots & \dots & 0 \\ 0 & 1 & 0 & -1 & 0 & \dots & \vdots \\ \vdots & 0 & \ddots & \ddots & \ddots & \dots & \vdots \\ \vdots & \vdots & \ddots & \ddots & \ddots & \ddots & \vdots \\ 0 & \dots & \dots & \dots & 1 & 0 & -1 \\ 0 & \dots & \dots & \dots & \dots & 2 & -2 \end{pmatrix}_{3200\times3200} \quad B = \begin{pmatrix} 1 \\ 0 \\ 0 \\ \vdots \\ \vdots \\ \vdots \\ 0 \end{pmatrix}_{3200\times1} \quad C = \begin{pmatrix} 0 & \dots & 1 & 0 & \dots & 0 \\ 0 & \vdots & \dots & 1 & 0 & 0 \\ 0 & \vdots & \ddots & 0 & \ddots & \vdots \\ 0 & \dots & \dots & \dots & \dots & 1 \end{pmatrix}_{160\times3200} \tag{3.8}$$

In addition, the particle velocity $v_f(x,t)$ is also dependent on space x and time t as recalled again

in (3.9).

$$v_f(t,x) = \beta f_v(x) \frac{Q_0 - L_D \frac{\partial u(t)}{\partial (t)}}{u(t)} \tag{3.9}$$

At $x = 0$, $f_v(0) = f_{v0}$ where $f_{v0} > 1$. $f_v(x)$ decreases until it reaches x_0 where $f_v(x_0) = 1$ and $\partial f_v(x0)/\partial x$ is set to 0. β, x_0, and f_{v0} are found by minimizing the delay error between the FEM model in [29], and low-order model obtained in [31]. The minimum error is obtained for $\beta = 1.12397437$, $x_0 = 2.5219$, and $f_{v0} = 3.158$, respectively. Moreover, $f_v(x)$ is defined as a second order polynomial in 3.10.

$$f_v(x) = 0.3393x^2 - 1.7114x + 3.158 \tag{3.10}$$

The transport equation outputs the delayed input for different values of x and different times t. $u_d(t, x_i)$ is the input of the Hammerstein model which is composed of a nonlinear static function followed by a linear time-invariant system. The nonlinear static function is obtained using the curve fitting in section 2.1.2. Moreover, the selected transfer function of the LTI system is a 4th order system given in (3.11). The coefficients n_j and m_j for different values of x are given in Tables 3.1, and 3.2.

$$sys_i = \frac{m_0^i s^3 + m_1^i s^2 + m_2^i s + m_3^i}{n_0^i s^4 + n_1^i s^3 + n_2^i s^2 + n_3^i s + n_4^i} \tag{3.11}$$

Finally, the output thickness at x_1, x_2,... and x_{160} are denoted by $y_1(t), y_2(t)$, ..., and $y_{160}(t)$.

Table 3.1: LTI systems coefficients ($e05 \rightarrow 10^5$).

n_j	$x = 0.5$	$x = 1$	$x = 2$	$x = 3.5$	$x = 5$	$x = 7$	$x = 9$	$x = 10$
n_0	1	1	1	1	1	1	1	1
n_1	1.116e05	8.936e04	7.618	6.701	6.14	5.531	4.732	4.425
n_2	9.068e05	4.442e05	22.39	17.15	14.33	11.76	9.025	8.029
n_3	3.776e06	1.14e06	28.51	18.54	14.03	10.69	7.592	6.415
n_4	9.333e05	3.021e05	6.623	3.908	2.694	1.851	1.235	1.015

Table 3.2: LTI systems coefficients ($e05 \rightarrow 10^5$).

m_j	$x = 0.5$	$x = 1$	$x = 2$	$x = 3.5$	$x = 5$	$x = 7$	$x = 9$	$x = 10$
m_0	−1.821e05	−1.352e05	−11.42	−10.96	−10.36	−9.598	−8.703	−8.315
m_1	−1.479e06	−6.686e05	−20.14	−19.76	−18.7	−16.46	−12.25	−10.64
m_2	3.022e06	7.156e05	11.92	2.384	−1.773	−4.516	−5.205	−4.822
m_3	9.333e05	3.021e05	6.623	3.908	2.694	1.851	1.235	1.015

3.2.3 H_∞ optimal control design

In this section, the controller design is discussed to compensate for unexpected disturbances and machine drift. To do so, some basics are introduced to explain the structure of the control design.

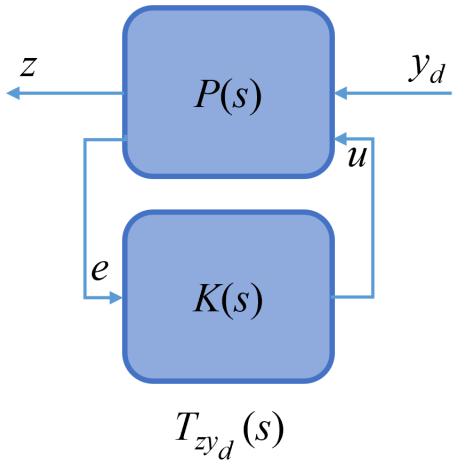

Figure 3.4: Linear fractional transformation (LFT) block diagram

Linear fractional transformation

A linear fractional transformation (LFT) is one way to represent the feedback systems. Typically, in the H_∞ control problem, the closed-loop system is introduced in the LFT format to simplify the controller design. Figure 3.4 shows the interconnection of the feedback system in the LFT format. The generalized plant $P(s)$ is described in (3.12). Signal z is composed of the output signal(s) to be minimized, e.g., $z = [e \quad u]^T$.

$$P(s) = \begin{pmatrix} P_{11}(s) & P_{12}(s) \\ P_{21}(s) & P_{22}(s) \end{pmatrix} \tag{3.12}$$

In Figure 3.4, T_{zy_d} is the closed-loop transfer function from y_d, the reference signal, to $e := y_d - y$, the error signal; y is the output signal, and u is the input signal. In this work, the lower LFT obtained in (3.13) gives an expression for the closed-loop transfer function from y_d to z.

$$F_L[P(s), K(s)] := P_{11}(s) + P_{12}(s)K(s)[I - P_{22}(s)K(s)]^{-1}P_{21}(s) \tag{3.13}$$

where the notation $F_L[P(s), K(s)]$ is another way of representing the closed-loop transfer function T_{zy_d}.

H_∞ technique

The intended die gap trajectory that outputs the desired extrudate thickness is found during die gap programming. The proposed controller is applied to maintain the desired thickness under unanticipated disturbances or machine drifts. If the thickness varies from its desired value, the controller compensates for the drift by changing the die gap. On the other hand, the controller takes no action in the absence of perturbations. The H_∞ technique can be used to design optimal

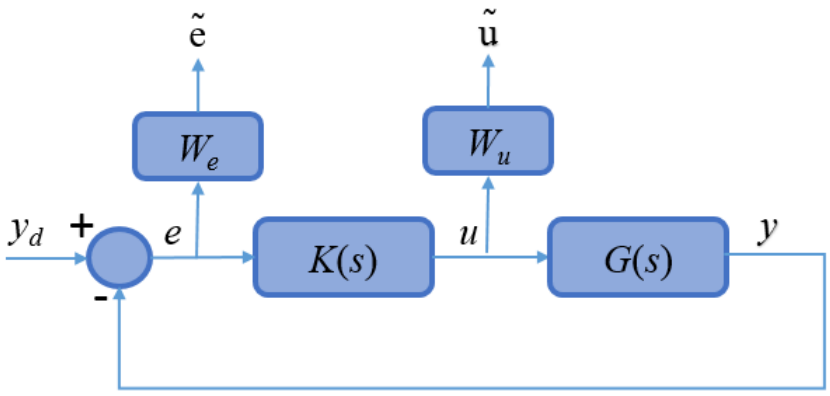

Figure 3.5: Conventional H_∞ block diagram

controllers that ensure stability and optimal performance. In order to minimize the error (e) in Figure 3.5, the H_∞-norm bound condition given by 3.14 must be satisfied for an appropriately small γ, ideally smaller than 1.

$$\| T z y_d \|_\infty < \gamma \tag{3.14}$$

T_{zy_d} is the closed-loop transfer function and γ is the upper bound on its norm. Parameter γ is obtained using a bisection method described in [67–69]. In order to improve the performance of the closed-loop system, γ needs to be minimized. Theoretically and numerically, it is a difficult task to reduce γ to obtain the optimum point. Therefore, a weighted error and a weighted input signals are considered in the closed-loop design. Moreover, W_e and W_u are the weighting functions that are used to constrain the error signal as well as the control signal, respectively. W_e is used in the controller design to reduce the sensitivity, generally at low frequencies. In addition, W_u is used to confirm that the control signal will not exceed its limits, in other words to constrain the control signal. Figure 3.5 shows the conventional H_∞ controller block diagram. The primary signals are the reference signal y_d , the error signal e, the weighted error signal $\tilde{e}$, the control signal u, the

weighted control signal $\tilde{u}$, and the output signal y. In addition, $G(s)$ is the actual plant and $K(s)$ is the controller.

In order to obtain the controller $K(s)$ using the H_∞ technique, the closed-loop system T_{zw} is considered in the Linear Fractional Transformation (LFT) format discussed above. System $P(s)$ is the generalized plant mapping $\begin{bmatrix} y_d \\ u \end{bmatrix}$ to $\begin{bmatrix} \tilde{e} \\ \tilde{u} \\ e \end{bmatrix}$ which is used to represent the part of the closed-loop system connected to the controller K and is given by (3.15).

$$P(s) = \begin{bmatrix} W_e & -W_e G \\ 0 & W_u \\ 1 & -G \end{bmatrix} \tag{3.15}$$

The transfer functions of $P(s)$ including weighting functions and actual plant must be stable to ensure the stability of the overall plant.

3.2.4 H_∞ Smith predictor controller synthesis

As explained in section 3.2.2, the model of the real plant includes time delay and Hammerstein blocks. The difference between the real plant model and the predictive model is in the arrangement of the blocks as shown in Figure 3.2. The signal u_d in Figure 3.2 is the desired input that is found by die gap programming in [31]. u_d must consistently produce a final product with the desired thickness in each cycle. To do so, an H_∞ optimal controller in a Smith predictor configuration as shown in Figure 3.6 is proposed to ensure that the desired thickness profile is obtained at every cycle. In Figure 3.6, $K(s)$ is the LTI regulator, f_s^{-1} is the inverse of the nonlinear static function, and d is the input disturbance. The input's operational region of the system is around u_d. The

signals y_d, y'_d and y'_2 are the desired outputs obtained by using the open-loop system mentioned above. On the other hand, the signals s_1, s_2 and s_3 are the outputs which are generated in real time during each cycle. In case s_1, s_2 and s_3 are equal to y_d, y'_d and y'_2 respectively, the error is equal to zero. Therefore, the reference signal is set to 0. In other word, the controller does not take any action in the cycle. On the other hand, if the sensor, which is placed below the die, shares any disturbance, then the controller compensates for this drift by changing the die gap. Thus, the controller will take action when the real plant is perturbed with respect to the predictive model, or when it is disturbed.

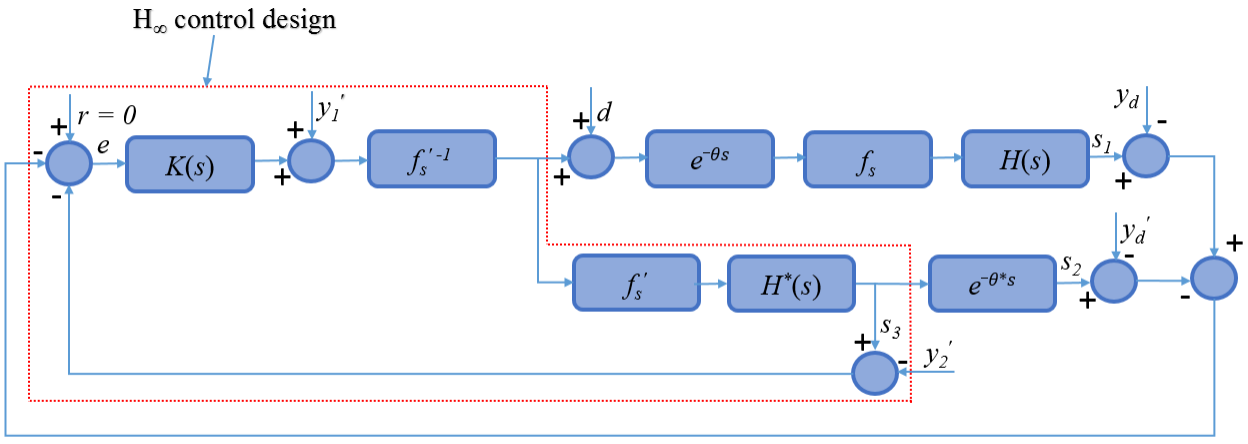

Figure 3.6: Block diagram of proposed H_∞ Smith predictor controller

3.3 Results & discussion

In this section, the mathematical model proposed in [31] and the one proposed in this work and described in Section 3.2.2 are used. The model parameters are shown in Table 3.3. A constant disturbance is added to the open-loop and closed-loop systems. The desired thickness profile of the extrudate at the end of the cycle obtained by input u_d is compared to the output of the closed-

loop and open-loop systems. The systems are compared to each other by calculating the summation of the absolute thickness difference of the extrudate at the considered 160 points. The results are simulated in Matlab and Simulink. As mentioned above, a Central Finite Difference Method is used to solve the equation in Matlab. Moreover, the Stiff/Trapezoidal solver is used to solve the equation in Simulink with variable time step.

Table 3.3: Simulation parameters.

Parameter	f_0	Q_0	L_D	β	x_0
value	3.158	4	1	1.1239	2.5219

3.3.1 Open-loop simulation

Die gap programming discussed in Chapter 2 is used to tune the setpoints in order to control the extrudate thickness and the final product in EBM. The die gap programming shown in Figure 2.5 is used as an input for the simulation of the open-loop and closed-loop systems. Figure 3.7a shows the desired extrudate shape due to u_d at $t = 8$. The extrudate thickness profile depicted in Figure 3.7a is considered as the reference shape which results in the desired final product. As mentioned before, EBM is susceptible to disturbances that may cause unacceptable extrudate shapes. In this work, disturbances and drifts are modeled by adding a constant value at the input. The input disturbance d is equal to 0.4 which is about 15% of the maximum die gap. Figure 3.7b shows the desired extrudate shape versus the extrudate shape with added input disturbance. As shown in Figure 3.7b, the disturbance can alter the extrudate shape which may result in undesired scrapped parts. Therefore, the extrudate shape must be consistent at every cycle in order to have a final product within desired specifications.

In order to obtain a consistent extrudate shape at the end of the cycle, a sensor is placed at

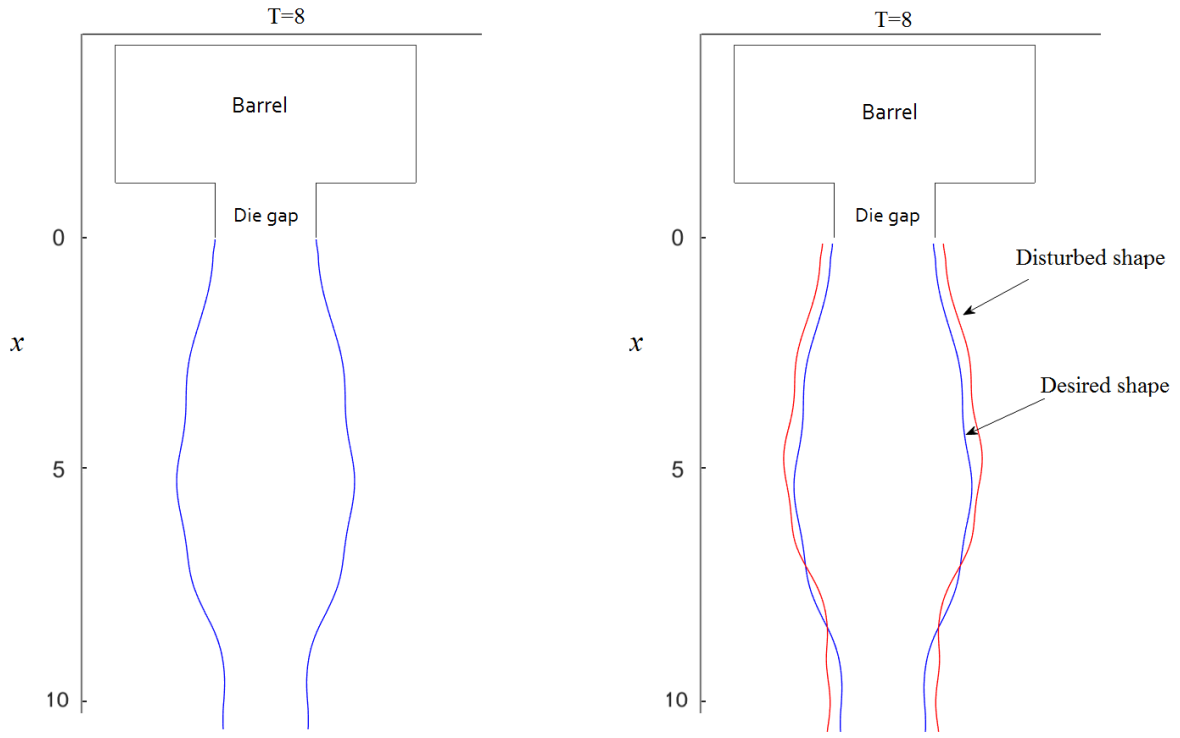

Figure 3.7: a) Desired extrudate shape, and b) Desired extrudate versus the disturbed extrudate

a fixed point down the die to monitor the thickness at that point online. In addition, a controller is proposed to immediately compensate for any drifts picked up by the sensor. Once the die gap programming is done, the signals for different values of x are measured and stored as a reference signal. The measured signal at the fixed point is compared to the reference signal to find the difference between two signals. In this work, it is later shown that making the thickness error small at a fixed point away from the die versus time ensures a consistent extrudate shape at the end of the cycle. The location of the sensor is a key feature that affects the performance of the controller. Therefore, controllers with sensors at different locations away from the die are considered and studied in later parts of the section. Figure 3.8 shows the desired extrudate thickness versus time at $x = 0.125, 0.5, 1, 1.25, 1.75, 2, 2.5$, and 3.5 that results in the final desired extrudate shape ($t = 8$). In Figure 3.8, the last points of the signals represent the formation of the final extrudate thicknesses

shown in Figure 3.7a.

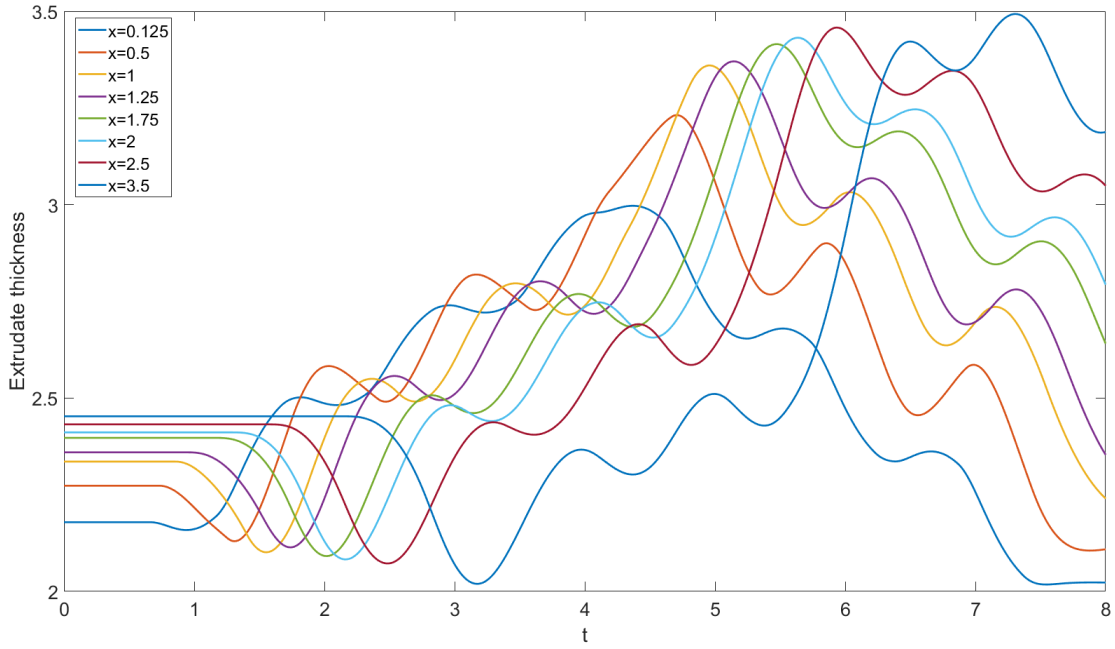

Figure 3.8: Desired extrudate thickness at different locations

3.3.2 Closed-loop simulation

The proposed H_∞ controller in the Smith predictor configuration in this work is designed to meet stability and performance requirements. The weighting functions W_e and W_u are chosen as follows:

$$W_e = \frac{0.0005}{s^2 + 0.021s + 0.00002} \tag{3.16}$$

$$W_u = 0.67 \tag{3.17}$$

These weighting functions are stable, minimum-phase systems, and satisfy the mixed sensitivity condition (3.18) introduced in [95].

$$\| F_L(P,K) \|_\infty < 1 \Rightarrow \quad \| W_e S \|_\infty < 1 \quad and \quad \| W_u T_{uy_d} \|_\infty < 1 \tag{3.18}$$

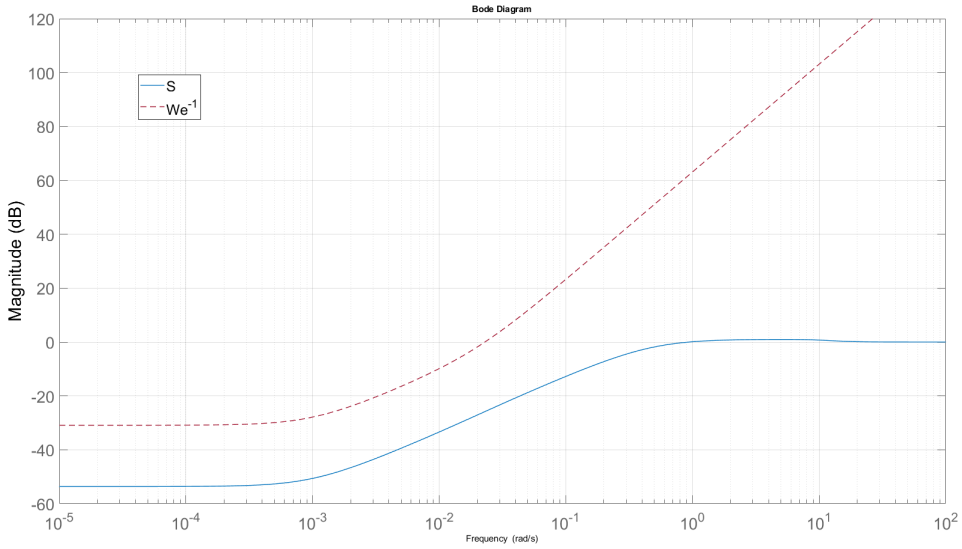

Figure 3.9: Sensitivity function S and W_e^{-1} versus frequency at $x = 0.125$

Where $F_L(P,K)$ is the closed-loop transfer function, P is the generalized plant in (3.15), and S is the sensitivity function ($S = {}^{1}/_{1+GK}$) mapping y_d to e. Figure 3.9 shows the sensitivity function (S) and inverse of error weight (W_e^{-1}) versus frequency at $x = 0.125$ that satisfies the condition in (3.18). Using the H_∞ optimal controller design technique, the minimal realization of $K(s)$ is a 6th order controller given in (3.19). The coefficients a_k and b_k for different values of x are given in Tables 3.4, 3.5, and 3.6. Moreover, the infinity norm of the closed-loop transfer function $\| T_{zy_d} \|_\infty$ and γ are equal to 0.6779 and 0.6781, respectively.

$$K(s) = \frac{b_0 s^5 + b_1 s^4 + b_2 s^3 + b_3 s^2 + 4.b_4 s + b_5}{a_0 s^6 + a_1 s^5 + a_2 s^4 + a_3 s^3 + a_4 s^2 + a_5 s + a_6} \tag{3.19}$$

Table 3.4: Controller coefficients.

a_k	$x = 0.125$	$x = 0.5$	$x = 1$	$x = 1.25$	$x = 1.75$	$x = 2$	$x = 2.5$
a_0	1	1	1	1	1	1	1
a_1	12.483×10^{-5}	1.116×10^{-5}	8.936×10^{-4}	11.02	8.45	8.235	7.89
a_2	4.229×10^{-6}	1.005×10^{-6}	5.602×10^{-5}	52.19	32.31	33.95	32.74
a_3	$3.83e07 \times 10^{-7}$	4.572×10^{-6}	1.717×10^{-6}	105.4	51.08	54.66	51.63
a_4	1.044×10^{-7}	1.273×10^{-6}	5.532×10^{-5}	33.12	15.36	17.65	17.51
a_5	2.031×10^{-5}	2.482×10^{-4}	1.09×10^{-4}	0.6517	0.3013	0.348	0.3463
a_6	192.7	23.55	10.35	0.0006186	0.000286	0.0003304	0.0003289

Table 3.5: Controller coefficients.

a_k	$x = 3.5$
a_0	1
a_1	8.409
a_2	47.24
a_3	82.05
a_4	32.93
a_5	0.6574
a_6	0.0006245

Table 3.6: Controller coefficients.

b_k	$x = 0.125$	$x = 0.5$	$x = 1$	$x = 1.25$	$x = 1.75$	$x = 2$	$x = 2.5$	$x = 3.5$
b_0	0.4854	0.3252	0.509	0.4211	0.3511	0.5996	0.6961	1.698
b_1	1.205×10^{-5}	3.628×10^{-4}	4.549×10^{-4}	4.465	2.844	4.583	5.011	11.42
b_2	1.927×10^{-6}	2.958×10^{-5}	2.272×10^{-5}	17.5	8.887	13.53	13.91	29.37
b_3	1.657×10^{-7}	1.235×10^{-6}	5.854×10^{-5}	30.49	12.13	17.42	16.68	32.14
b_4	4.463×10^{-6}	3.327×10^{-5}	1.673×10^{-5}	8.4	3.092	14.38	4.048	7.345
b_5	9.243×10^{-4}	7221	3593	0.1831	0.06405	0.09484	0.08254	0.1494

Different controllers are designed for different values of x. In other words, based on the sensor location, a different controller is designed accordingly. After die gap programming, the desired

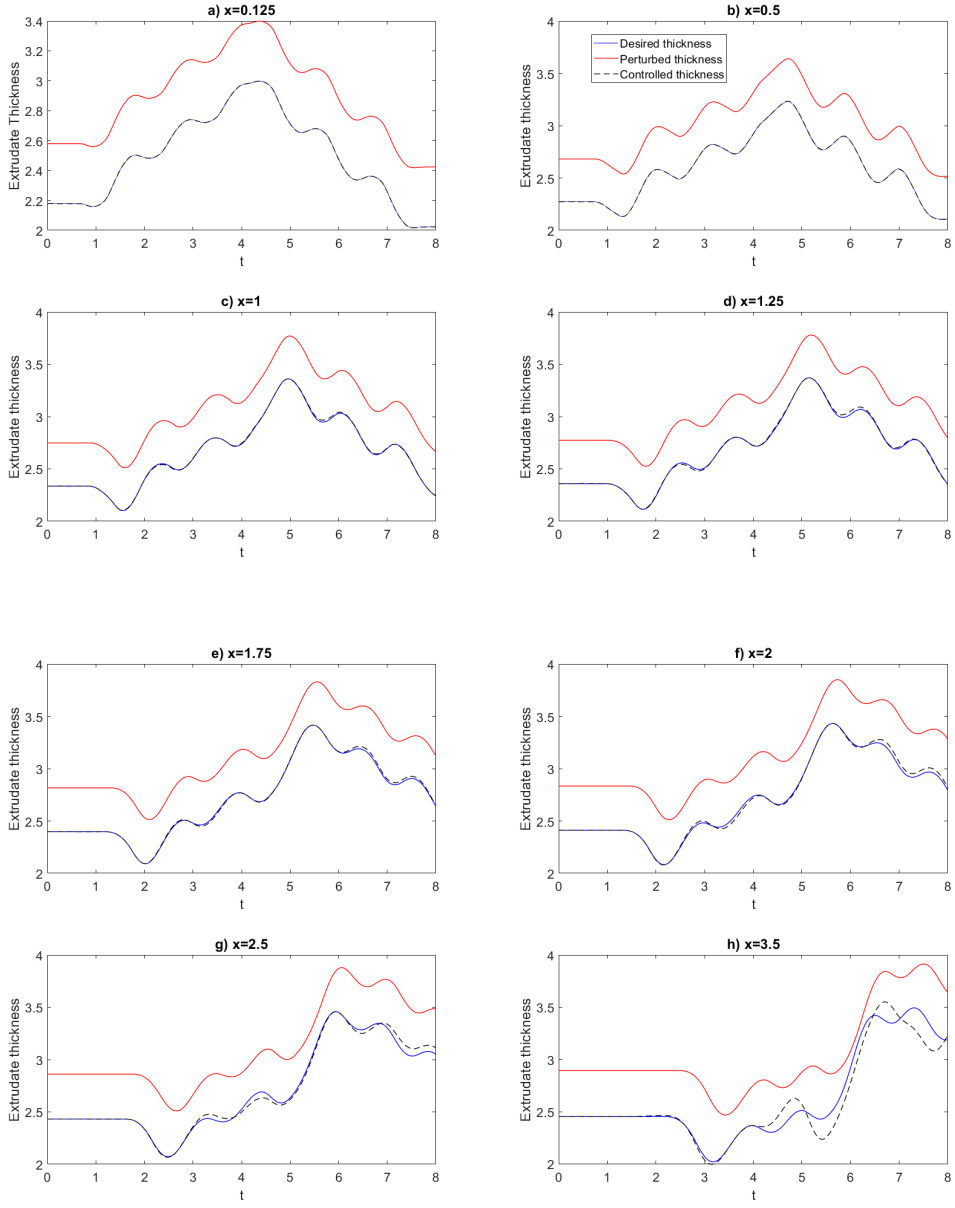

Figure 3.10: Comparison between thickness signals with and without disturbance for both open-loop and closed-loop systems

extrudate thickness profile is obtained. The readings of a sensor located at a fixed location from the die is considered to track the reference signal that needs to be obtained at every cycle. In Figure

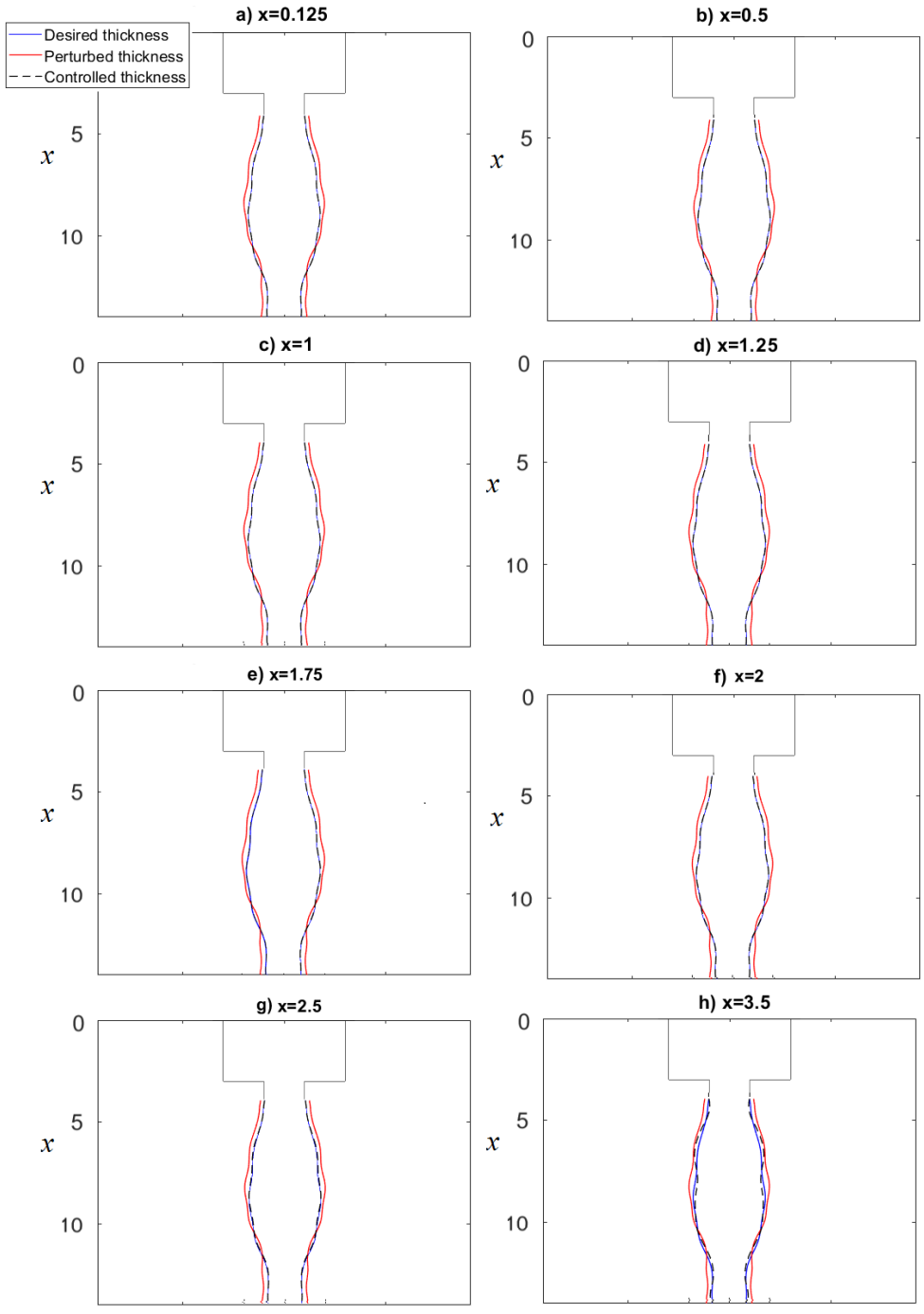

Figure 3.11: Comparison between overall extrudate shape with and without disturbance for both open-loop and closed-loop systems

3.10, the reference signal is shown in blue for $x = 0.125, 0.5, 1, 1.25, 1.75, 2, 2.5$, and 3.5 which is the same signal as shown in Figure 3.8. After adding the disturbance at the input, different thickness values are measured by the sensor. The disturbed signal is shown in red in Figure 3.10. The controller ensures that the desired signal is obtained even in the presence of a disturbance. The thickness measurements for the closed-loop systems are shown in black dashed-line in Figure 3.10. It can be observed that a controller with sensor placed closer to the die yields better performance.

Even though the controller maintains the thickness at one point, the overall thickness at the end of the cycle is also maintained, as shown in Figure 3.11. Moreover, Figure 3.11 shows the overall extrudate shapes when the sensor is placed at $x = 0.125, 0.5, 1, 1.25, 1.75, 2, 2.5$ and 3.5. The blue extrudate profile is the desired thickness, black profile shows the controlled extrudate in the presence of disturbance, and the red profile shows the uncontrolled profile with added disturbance.

3.3.3 Sensor location

Figure 3.12 shows the location of the sensor versus the error. The l_1-norm error is the absolute summation of the difference between the desired extrudate thickness and the controlled extrudate thickness at 160 points. It can be observed that the performance of the control system improves and the error decreases as the sensor is placed closer to the die. When the sensor is placed closer to the die, the material travels over shorter distances where measurements are made. Thus, the plant exhibits shorter delays. The decrease in error with the decrease of the distance between the die and the sensor may be true for input disturbances but cannot be generalized for other disturbance types. For example in the case of temperature change, larger machine drift values may be measured when the sensor is placed further away from the die. In general, the extrudate thickness tends to be close to the die gap for shorter distances from the die, making it harder to measure machine drifts.

Moreover, other factors such as the accuracy of the sensor may affect its optimal location. In addition, other practical constraints such as sensor-mold clearance and high ambient temperatures must be taken into consideration before choosing the location of the sensor.

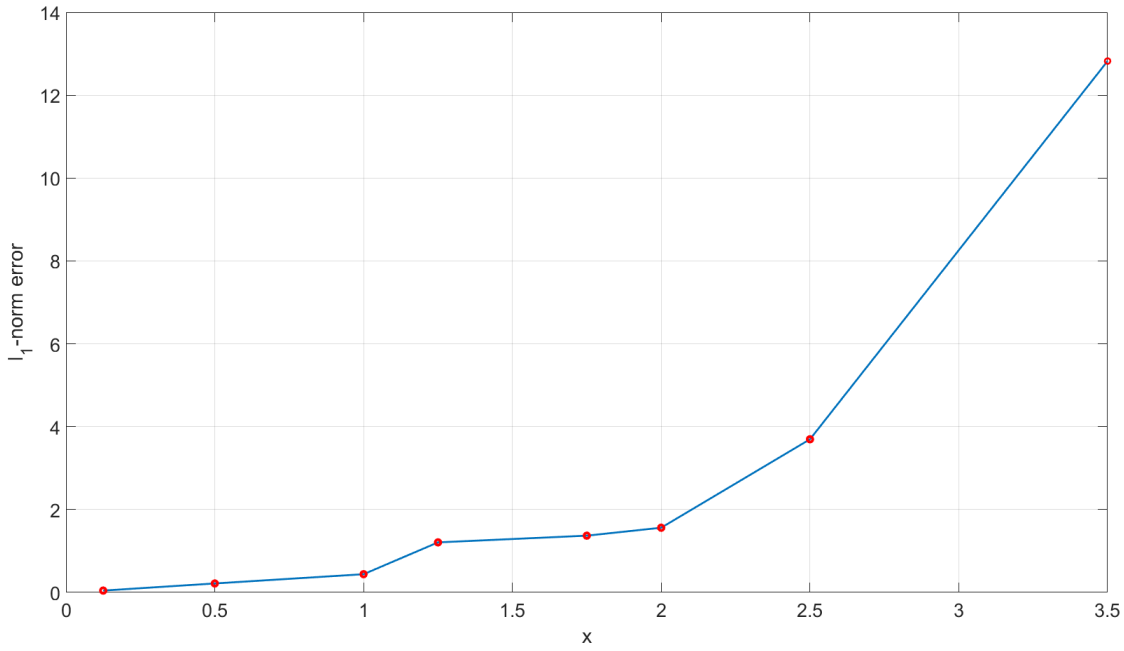

Figure 3.12: Sensor location versus l_1-norm of the error at 160 points

3.4 Conclusion

In this chapter, an optimal H_∞ controller in the Smith predictor configuration is introduced to regulate the extrudate thickness in the EBM process. A parameter identification based model from previous work is used to describe the dynamics of the extrudate during extrusion. This model is composed of a delay, a static nonlinear function and a linear system with memory modeled by a transfer function. In the closed-loop design, the Smith predictor technique is used to compensate for the delay term. An H_∞ optimal controller is designed according to the model's transfer func-

tion. The effects of the static nonlinear function are canceled out by incorporating its inverse in the control loop. Furthermore, the impact of the sensor location on the regulation performance is studied. Finally, the controller is designed to reject disturbances and to maintain the desired extrudate thickness profile which will improve the manufacturing quality and reduce the usage of raw materials.

Chapter 4

Robust closed-loop thickness control

4.1 Introduction

In Chapter 3, a feasibility analysis of using the closed-loop system is discussed in order to regulate the extrudate thickness in the presence of a disturbance. An H_∞ optimal controller is proposed in the Smith predictor configuration to maintain the desired extrudate profile when the die gap is disturbed by a constant disturbance. In this chapter, the delay uncertainty is addressed and considered in the controller design. Uncertainties such as sensor noise, modeling error, or resin variation are not considered in the controller design. As mentioned before, the delay term in the model is input-dependent. Particles observed by the sensor further away from the die show larger delay compared to the particles at the die exit or closer to the die and this delay depends on the material velocity which in turn depends on the die opening. Moreover, a constant disturbance is added to the input. Due to dependency of the delay on the input, the constant disturbance causes more uncertain delay. In addition, the blocks swap is proposed to create the predictive model for the Smith predictor configuration. The blocks swap differentiates the output of the original model and predictive one. Therefore, the difference also causes more uncertainty on delay that may result

in undesired extrudate thickness. Ultimately, the unacceptable extrudate thickness may also result in poor quality final parts.

In this chapter, a robust controller is designed in the Smith predictor configuration to compensate for the uncertain time delay system in addition to the added disturbance on the input. Robust controllers are designed and studied in [70–74] for uncertain time delay systems in which parameter uncertainty is time-varying and norm bounded. It has been noted that the controller performance is affected by the size of the delay. Uncertainties and machine drifts can cause unacceptable final parts and require the machine operator to retune the machine. The objective of this work is to reduce the effects of uncertainties and disturbances in the EBM process by using automatic feedback. Thickness variations from a desired signal are measured by a sensor at a fixed location from the die. The controller automatically changes the die gap to minimize the variations. Ultimately, a robust H_∞ technique is used to overcome the larger delay uncertainty at locations further away from the die compared to the conventional H_∞ controller in Chapter 3.

Modeling

A low-order model is developed in [31] to reproduce the main aspects of the step response of a reference FEM model [29] and could also come from a data obtained by experiment on a machine. The step response is used to identify the parameters of a model suitable for the control purpose. As shown in Table 2.1, the model parameters are dimensionless, lengths are divided by the Die length L_D, velocities by the maximum velocity at the inlet v_s, and time t by $t_s = {}^{L_D}/_{v_s}$. Moreover, the predictive model is proposed in Chapter 3 to be used in the Smith predictor configuration. The die gap programming in Figure 2.5 is the die opening versus time for one complete cycle and is used as a input $u(t)$ for the simulation results in this chapter.

4.2 Uncertainty analysis

The original model proposed in [31] and described in Chapter 2 is used in this work to represent a nominal model for the closed-loop system design. The plant model is a key feature in order to analyze uncertainties during the extrusion process. Figure 2.3 shows the bulging and necking effects on the extrudate. Bulging and necking effects are due to the change in the volumetric flow rate Q as described before. Given that the volumetric flow rate is constant at the inlet, the flow rate is changed at the die exit as a result of variations in the die gap. Therefore, uncertain volumetric flow rate or misaligned die walls result in an uncertain input $u(t)$. On the other hand, the transport delay shown in Figure 2.6 is the time needed for the material traveling from the die exit to the location of the sensor. Therefore, the transport delay is dependent on the input once the material leaves the die until it reaches the location of the sensor. Ultimately, an uncertain input causes uncertain transport delay which may result in unacceptable extrudate shape.

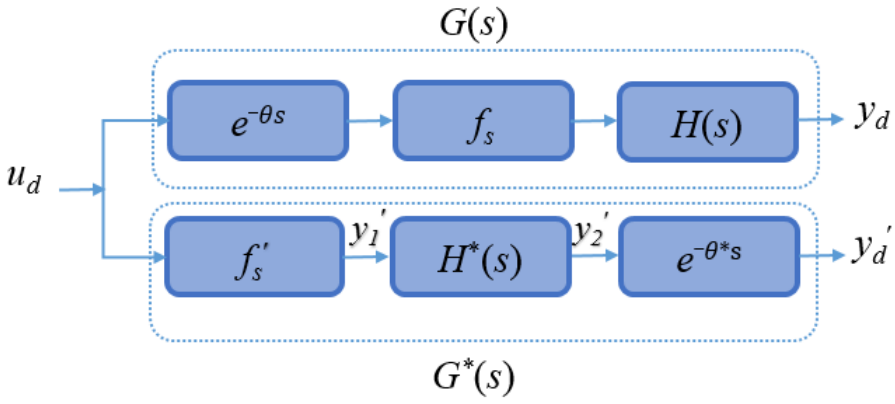

Figure 4.1: Real plant model (top branch) versus the predictive model (bottom branch)

In this work, a Smith predictor configuration [41] is used in the controller design to deal with the delay term that is modeled for the extrusion process in Chapter 2. In order to utilize this

technique, the delay term of the predictive model is placed after the Hammerstein block as shown in Figure 4.1 (same as Figure 3.2 reintroduced here for convenience). On the other hand, the delayed input is the input to the Hammerstein block in the original plant model. Figure 4.1 shows the original plant model versus the predictive model. u_d is the desired input, y_1' is the output of the nonlinear static function, y_2' is the output of Hammerstein model, y_d and y_d' are the outputs of the real plant model and predictive model, respectively. Since the predictive model and the original plant are not identical, the blocks swap causes delay uncertainty. Given the input $u(t)$, Figure 4.2 depicts the extrudate thickness for the original plant versus the predictive model at $x = 0.5, 1.25, 2.5$, and 3.5. The particle location closer to the die has less delay compared to the points further away from die. Therefore, the signals show additional delay with respect to $u(t)$ especially for larger values of x such as $x = 3.5$. Ultimately, the blocks swap causes more delay uncertainty for the points further away from the die which is considered in the controller design.

Uncertainty model

Mathematical models are developed to predict the behavior of the physical processes for different inputs. To do so, the approximation method is used to represent the physical process which results in model uncertainty. Therefore, the uncertainty needs to be modeled to be considered in the controller design. The time delay term is studied for different points along the extrudate. Moreover, even though the blocks swap results in some delay uncertainty, it is done to create the predictive model according to the control design requirement. Ultimately, an unstructured uncertainty is chosen to represent the dynamic perturbation of the original model in the frequency domain.

Considering different types of uncertainty models, the output multiplicative uncertainty model is used in this work to model the delay uncertainty. The output multiplicative uncertainty represents the uncertainty of the output of the system. The block diagram of the output multiplicative

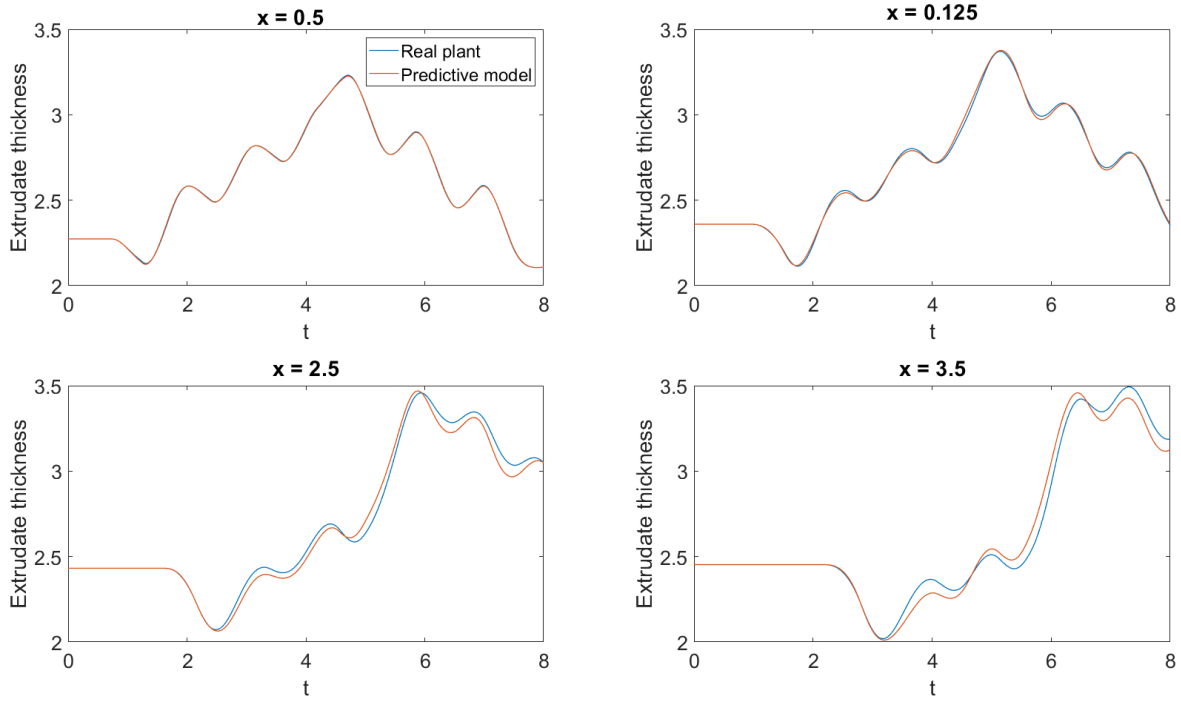

Figure 4.2: Extrudate thickness of real plant versus predictive model at $x = 0.5, 1.25, 2.5$, and 3.5

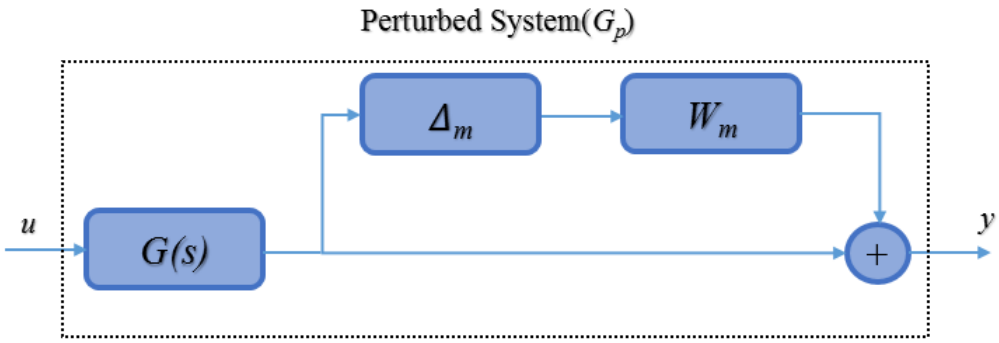

Figure 4.3: Output multiplicative uncertainty block diagram

uncertainty is shown in Figure 4.3, where $G(s)$ is the nominal system transfer function. In addition, $G_p(s)$ is the perturbed system transfer function as described in a mathematical expression of the output multiplicative uncertainty model in (4.1). Moreover, Δ_m represents an unknown normalized

stable LTI dynamics whereas W_m is the frequency variation of the output multiplicative uncertainty model corresponding to G, respectively.

$$G_p(s) = (1 + W_m(s)\Delta_m(s))G(s), \Delta_m \in H_\infty, \| \Delta_m \|_\infty < 1 \tag{4.1}$$

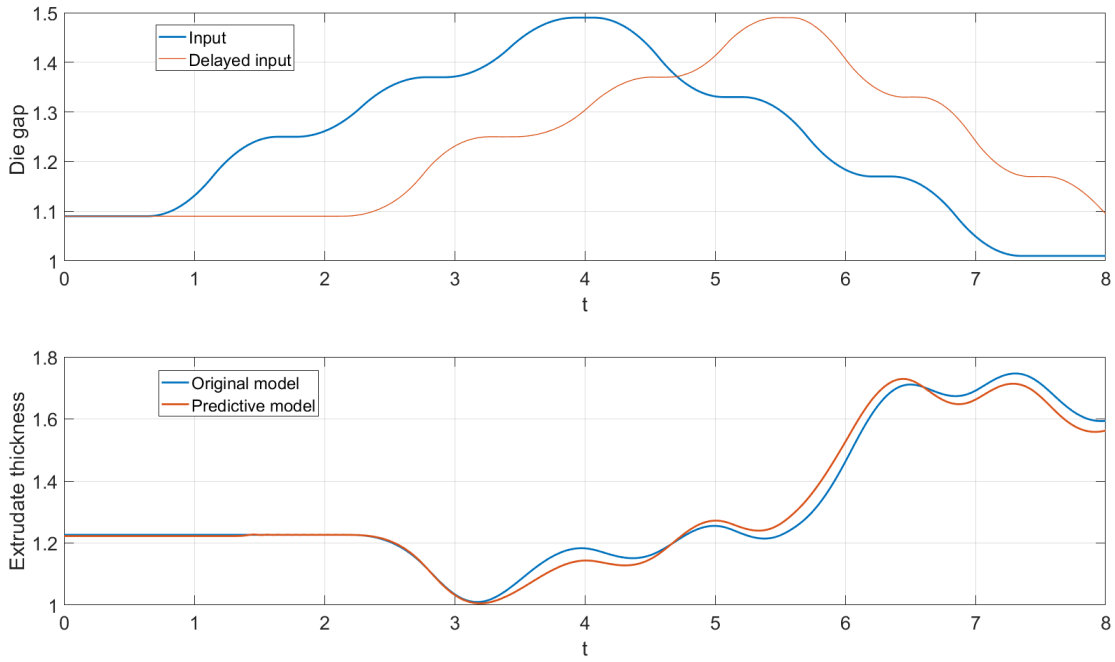

Figure 4.4: Top figure: Input signal versus the delayed input signal at $x = 3.5$, Bottom figure: Extrudate thickness for original model versus predictive model at $x = 3.5$

The nominal delay is obtained for different points along the extrudate by using the transport equation in 2.1. The computational method of the transport equation to obtain the delays for different particles at different locations is explained in Chapter 3. Subsequently when the delays are computed along the extrudate for the original model and the predictive model, the difference between the outputs of the original model y_d and the predictive model y'_d is computed, accordingly.

For instance, Figure 4.4 shows the input signal versus the delayed input signal at $x = 3.5$ in the upper box. Moreover, the extrudate thickness for the original model versus predictive model at $x = 3.5$ is shown in the lower box of Figure 4.4. The delay difference is computed to be about 1.35 when the sensor is located at $x = 3.5$. The delay difference may cause uncertainty specially for the points further away from the die which is justified by looking at the lower box of Figure 4.4. Therefore, the delay uncertainty must be considered in the controller design. To do so, the uncertain part of the delay is modeled in (4.2) by a first-order transfer function using a Padé approximation [96]

$$e^{-\tau s} \approx \frac{1 - \frac{\tau}{2}s}{1 + \frac{\tau}{2}s}, \tag{4.2}$$

where τ is the uncertain delay. Given the model assumption in (4.1), the small-gain theorem [97] states that the unity feedback closed-loop interconnection of the perturbed plant and the controller is stable if and only if the part of the closed-loop system connected to the uncertainty Δ_m, Tzy_d shown in Figure 4.5 has infinity norm less than one. The small gain theorem provides the necessary

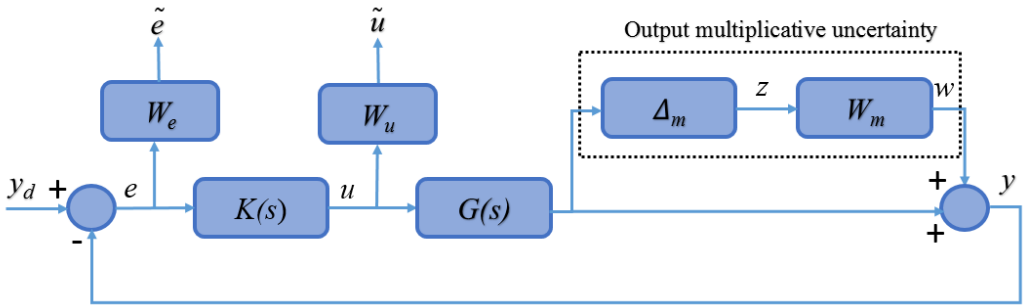

Figure 4.5: Unity feedback closed-loop interconnection T_{yy_d} of robust H_∞ controller

and sufficient conditions for the stability of the perturbed closed-loop system. Uncertainty analysis

is done for the uncertain part of the delay using the output multiplicative model considering all the delay variations. For instance, for the point $x = 3.5$, the amount of delay uncertainty is 15% which is calculated based on the difference of the outputs of the original model and the predictive one. W_m as written in (4.3) describes a transfer function whose magnitude covers the different relevant perturbations of the system $| \frac{G_p(j\omega)-G(j\omega)}{G(j\omega)} |$ in the frequency domain. Figure 4.6 shows the transfer function (dashed lines) and the plant perturbations. Ultimately, the coefficients m_i and n_i for the uncertainty weighting function are described in Table 4.1.

$$W_m = \frac{m_0 s^{13} + m_0 s^{12} + ... + m_{12} s + m_{13}}{n_0 s^{13} + n_0 s^{12} + ... + n_{12} s + n_{13}} \tag{4.3}$$

Table 4.1: Uncertainty weighting function coefficients.

m_i	value	n_i	value
m_0	1.001	n_0	1
m_1	19.87	n_1	19.33
m_2	180.3	n_2	171.7
m_3	987.1	n_3	924.8
m_4	3619	n_4	3351
m_5	9315	n_5	8564
m_6	1.716e04	n_6	1.574e04
m_7	2.266e04	n_7	2.085e04
m_8	2.115e04	n_8	1.962e04
m_9	1.358e04	n_9	1.277e04
m_{10}	5768	n_{10}	5514
m_{11}	1526	n_{11}	1482
m_{12}	225.2	n_{12}	222.1
m_{13}	14.07	n_{13}	14.06

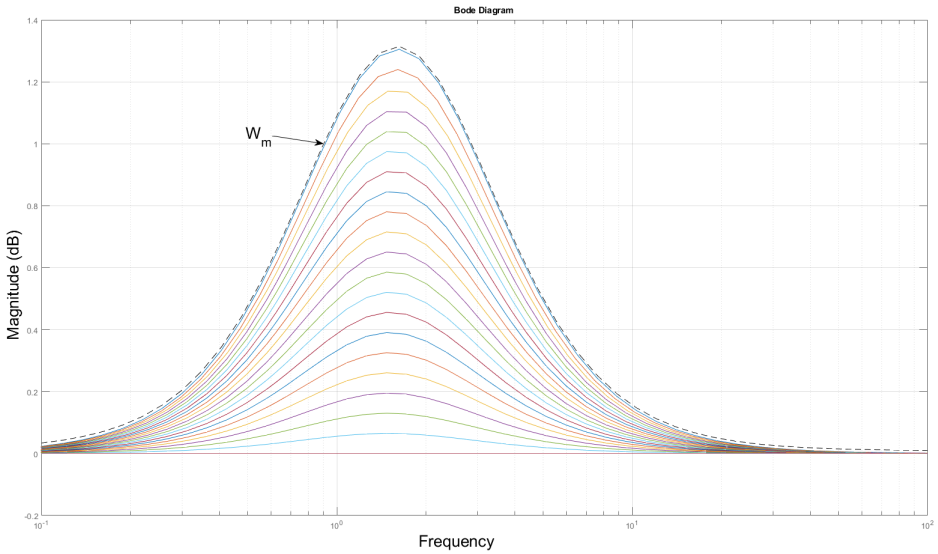

Figure 4.6: The weighting function (dashed lines) and the plant perturbations

4.3 Robust controller design

Parametric uncertainty in the extrusion process may result in unacceptable final parts and needs the machine operator to retune the setpoints. This task is time consuming and costly. Therefore, an automatic robust feedback controller is designed in this work in order to compensate for uncertainties and disturbances occurring during the extrusion process. Sensors based on laser or mm-wave radar technology can be placed at a fixed point at one side or two sides along the extrudate below the die. Afterwards, the thickness at that fixed point below the die is measured by the sensor and is compared to the reference signal. Basically, the controller will try to minimize the computed error between the measured and reference signals by changing the die gap automatically. In this work, the delay uncertainty is considered due to the blocks swap of the original plant model in order to create the predictive model as mentioned before. Moreover, the delay uncertainty is modeled by the first-order transfer function using the Padé approximation. In addition, a constant disturbance

is causing additional delay uncertainty added to the input to constrain the stability of the system in the presence of machine drift. Therefore, a robust H_∞ controller [100, 101] in the Smith predictor configuration is proposed to ensure the stability of the closed-loop system and to guarantee the desired closed-loop performance.

The Smith predictor configuration is proposed in [41] to deal with the systems containing time delays. For a fixed location x along the vertical extrusion axis, the model proposed in [31], after the blocks swap of Figure 4.1 can be divided into two parts, a Hammerstein model and a time delay term that is represented by (4.4):

$$system : \begin{cases} \eta = f_s(u) & (a) \\ G^\star(s) : \eta \mapsto y, \quad G^\star(s) = H^\star(s)e^{-\theta s} & (b) \end{cases} \tag{4.4}$$

where $G^\star(s)$ is the nominal predictive model, $f_s(u)$ is a nonlinear static function, $H^\star(s)$ is linear time-invariant system, and $e^{-\theta s}$ is a time delay term. Figure 3.1 shows the conventional block diagram of the Smith predictor configuration where the delay term is placed after the predictive model. $K(s)$ is the controller, $G(s)$ is the plant model, and $G^*(s)$ is the predictive model. After having canceled out the nonlinear static function by its inverse function placed after the controller, the predictive model can be represented by (4.5):

$$G^*(s) \quad = \quad H^*(s)e^{-\theta^* s}. \tag{4.5}$$

Assuming that the modeling error is close to zero ($G(s) \approx G^*(s)$), then the closed-loop transfer function is given by (4.6):

$$T_{yy_d} = \frac{y}{y_d} = \frac{KH^* e^{-\theta^* s}}{1 + KH^*}, \tag{4.6}$$

where the controller K is designed for the delay free system $H^*(s)$ using the Smith predictor configuration method. The main objective of the robust controller design is to maintain the desired

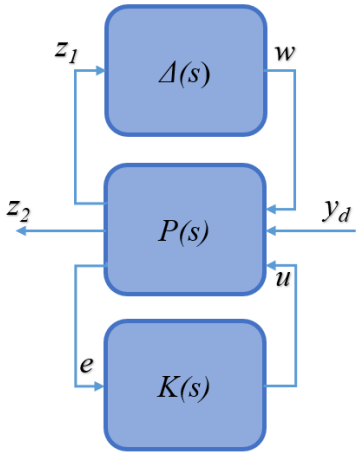

Figure 4.7: Linear fractional transformation (LFT) block diagram for robust H_∞ controller

extrudate thickness profile in the presence of disturbances and uncertainties. The controller is designed based on a robust H_∞ method. In order to define a mathematical expression of the controller $K(s)$, the closed-loop system can be written in a Linear Fractional Transformation (LFT) format explained in Chapter 3. Figure 4.7 shows the LFT block diagram where $\Delta(s)$ is an uncertainty block, $P(s)$ is a generalized plant model, and $K(s)$ is a robust controller. Typically, the generalized plant is used in the robust controller design to embed all the weighting functions that are found to improve the closed-loop performance and to shape the uncertainty. Therefore, $P(s) = \begin{bmatrix} w \\ y_d \\ u \end{bmatrix} \rightarrow \begin{bmatrix} z_1 \\ z_2 \\ e \end{bmatrix}$

is given by (4.7):

$$P(s) = \begin{bmatrix} 0 & 0 & G \\ -W_m W_e & W_e & -W_e G \\ -W_m & 1 & -G \end{bmatrix}, \tag{4.7}$$

where W_e is the weighting function applied on the error signal, W_u is the one applied on the control signal, and W_m is the one representing the output multiplicative uncertainty in (4.3). Weighting functions are implemented by transfer functions and used to constrain the performance as described in Chapter 3. Figure 4.5 shows the conventional robust H_∞ controller block diagram. The primary signals are the reference signal y_d , the error signal e, the weighted error signal $\tilde{e}$, the control signal u, the weighted control signal $\tilde{u}$, and the output signal y.

4.3.1 Robust H_∞ Smith predictor controller synthesis

As mentioned above, Figure 4.1 shows the original plant model versus the predictive model. In Figure 3.2, u_d is the desired input found by die gap programming in Chapter 2, y'_1 is the output of the nonlinear static function, y'_2 is the output of the Hammerstein model, y_d and y'_d are the desired outputs of the real plant model and predictive model respectively. Given u_d as an input, the thickness profile of the final part for all cycles must be consistently acceptable. Therefore, the robust H_∞ controller in a Smith predictor configuration shown in Figure 4.8 is proposed in this work in order to produce the final parts with desired specification during every cycles.

$T_{ey'_2}$ represents the closed-loop transfer function. Moreover, f'^{-1}_s is the inverse of the nonlinear static function that is placed after the controller to cancel out the effect of the nonlinear static function in the Hammerstein blocks. The operational region is around u_d in the open-loop system. If the outputs s_1, s_2 and s_3 are equal to y_d, y'_d and y'_2 respectively, the error e is equal to zero. Therefore, the reference signal is equal to zero in this so called regulator system.

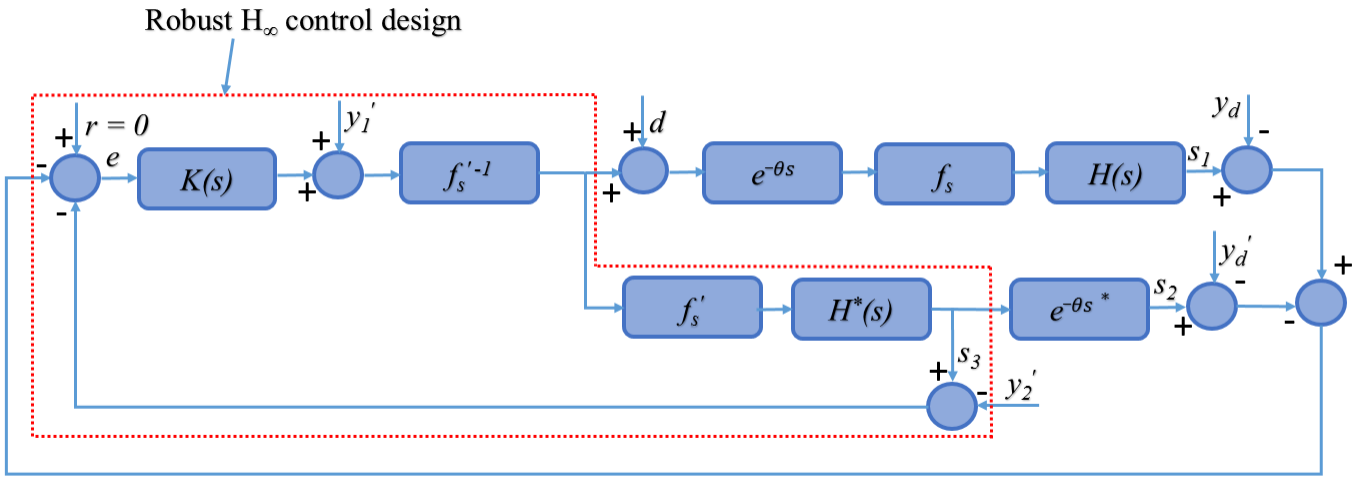

Figure 4.8: Proposed robust H_∞ Smith predictor controller

Furthermore, Figures 4.9a and 4.9b show the equivalent block diagrams of the proposed controller depicted in Figure 4.8 to understand the logic behind the design better. The uncertainty discussed in Section 4.2 is included in the controller design. The uncertainty is modeled in the LFT block diagram and it is shown in Figure 4.7 as well. In order to map the uncertainty in Figure 4.8, the equivalent of the proposed controller is shown in Figure 4.9a. The systems described in the generalized plant (4.7) must be stable in order to be used in the Smith predictor configuration. $H^{\star}(s)$ is a stable and non-minimum phase system but, it is inverted in the design of Figure 4.9a just to explain the conceptual theory behind the proposed controller in Figure 4.8 more clearly. Moreover, after canceling out the effect of the nonlinear static function by its inverse function, Figure. 4.9b shows the simplified block diagram of the proposed controller where $e^{-\theta^{\star}s}$ is the Padé approximation for the uncertain delay. Ultimately, the controller will take action when the thickness signal measured by the sensor is different from the reference signal. In other words, the controller will only compensate for disturbances occurring in the EBM process.

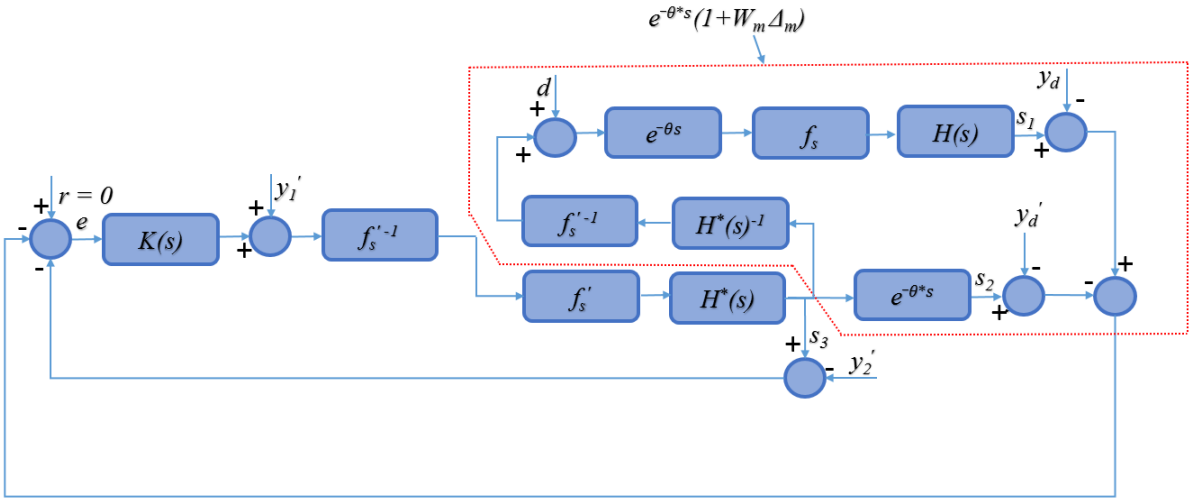

(a) Equivalent diagram of robust H_∞ Smith predictor controller

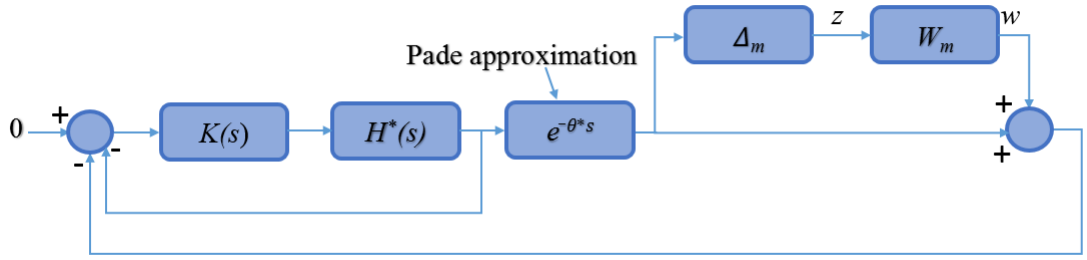

(b) Equivalent diagram of robust H_∞ Smith predictor controller

Figure 4.9: Proposed controller

4.4 Results and discussions

The low-order model proposed in [31] and mentioned in Chapter 2 is used in this section for the simulation results. The model parameters are shown in Table 4.2. The feasibility analysis of using the closed-loop system in EBM in order to overcome the disturbance is explained in Chapter 3. Moreover, an H_∞ controller is designed in the Smith predictor configuration to reject the added constant input disturbance. In addition, the closed-loop system with disturbance is compared to

the open-loop case and open-loop with disturbance. As a consequence, using the closed-loop system has advantage over the open-loop system in the presence of disturbance or machine drift. In this chapter, uncertainty analysis is done in section 4.2. As mentioned before, the blocks swap of the original plant model in order to propose the predictive model creates an uncertain time delay. According to the time delay difference generated between the real plant and predictive model, ±15% delay uncertainty is considered in the controller design. Moreover, in this section the simulation results using the robust controller are described and compared to the results obtained in Chapter 3.

Table 4.2: Simulation parameters.

Parameter value
$f_0 = 3.158$
Q_0=4
$L_D = 1$
$\beta = 1.12$
$x_0 = 2.5219$

The desired thickness profile of the extrudate at the end of the cycle is obtained by using input u_d found in section 2.1.1. A constant input d is added to the input in order to obtain the extrudate thickness profile at the end of the cycle in the presence of a disturbance. The extrudate thickness profile at the end of the cycle is obtained for the closed-loop system. The three systems are compared to each other by calculating the summation of the absolute thickness difference of the extrudate over the considered 160 points. The open-loop system is implemented in Matlab in order to generate the simulation results while the closed-loop system is simulated in Simulink. In order to simulate the delay term, the transport equation mentioned in (2.1) is discretized with respect to space and time. The solution is found at spatially equidistant points 0.003125 away from each other. The time step used is equal to 0.0025. Central-Finite-Difference Method is used to solve the equation in Matlab. Finally, the Stiff/Trapezoidal solver is used to solve the equation in Simulink

with variable time step.

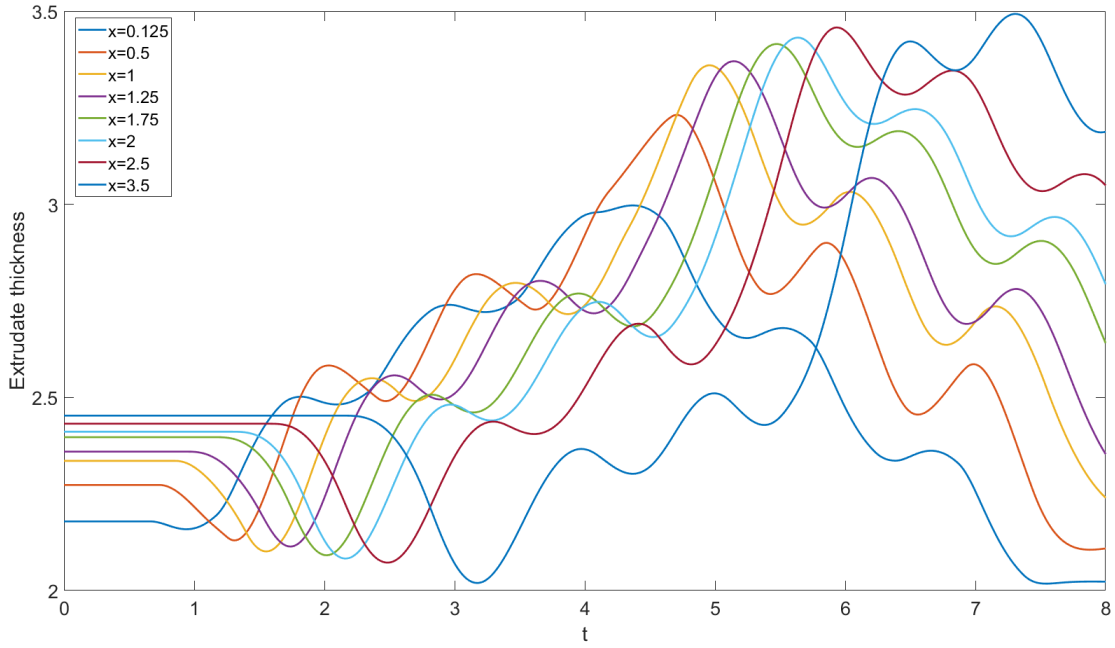

Figure 4.10: Desired extrudate thickness at different locations

4.4.1 Open-loop simulation

Figure 4.10 depicts the desired extrudate thickness versus time at $x = 0.125, 0.5, 1, 1.25, 1.75, 2, 2.5,$ and 3.5 below the die at $T = 8$ captured by the sensor. The 8 points in Figure 4.10 are considered as sampling points of the complete extrudate that includes 160 thickness points. The last values of the signals at $t = 8$ are picked in the simulation setup in order to form the overall extrudate shape. Therefore, Figure 4.11a shows the desired complete extrudate shape. On the other hand, Figure 4.11b shows the desired extrudate shape versus the disturbed one. Given the u in section 2.1.1 as an input, the blue profile is the desired extrudate shape. On the other hand, a constant input d equal to 0.4 is added to the input u in the simulation setup. Consequently, the red profile in Figure

4.11-b shows the extrudate profile which is disturbed by the constant value. The disturbance or uncertainty can change the extrudate shape which may result in an unacceptable part. Therefore, in order to have a final part with desired specifications, the extrudate shape must be consistent at every cycle. To do so, the sensor is placed at a fixed point below the die in order to measure the extrudate thickness in real time. Then, the measured signal is compared to the reference signal. If a difference is computed between the two signals, the controller will take action immediately to compensate for the error as shown later on in the next section.

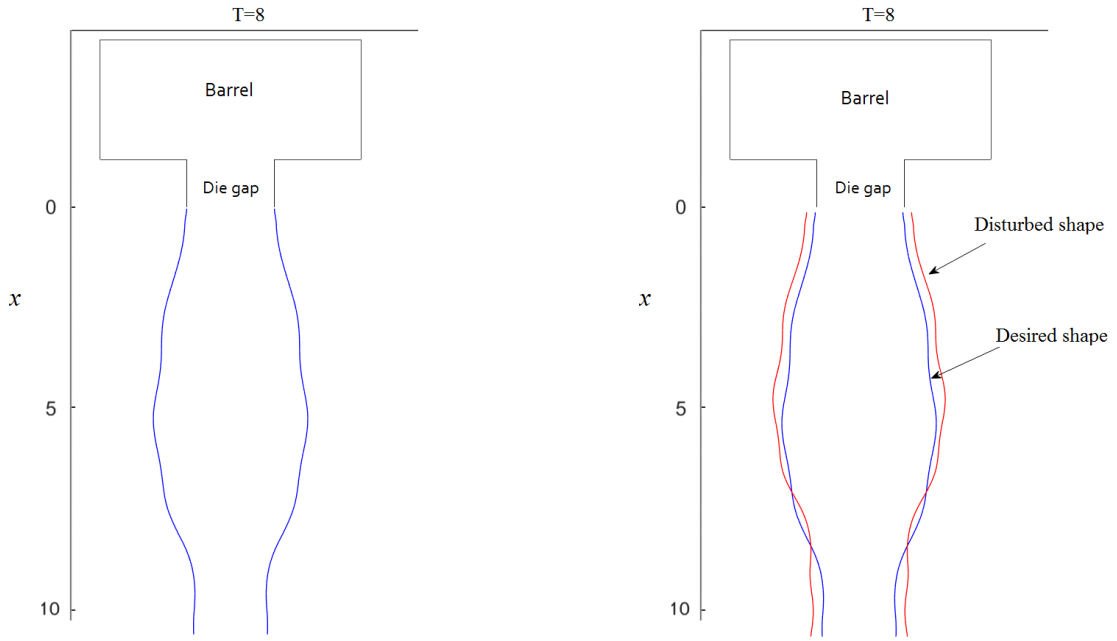

(a) Desired extrudate shape (b) Desired extrudate shape versus disturbed one

Figure 4.11: Extrudate shape at the end of the cycle (T=8)

4.4.2 Performance analysis

In this section, the operation of the proposed robust H_∞ controller is compared to the H_∞ controller described in Chapter 3. The performance of the two closed-loop systems are compared to

each other in the presence of a constant input disturbance and delay uncertainty. The weighting functions W_e and W_u are defined stable and minimum-phase systems in (4.8) and (4.9), respectively.

$$W_e = \frac{0.0005}{s^2 + 0.021s + 0.00002} \tag{4.8}$$

$$W_u = 0.67 \tag{4.9}$$

In order to achieve the performance requirements, the mixed sensitivity condition is described in (4.10)

$$\| F_L(P,K) \|_\infty < 1 \Rightarrow \quad \| W_e S \|_\infty < 1 \quad and \quad \| W_u T u y_d \|_\infty < 1 \tag{4.10}$$

where the S is the sensitivity function. The sensitivity function and the inverse of the error weighting function W_e^{-1} versus frequency at $x = 0.125$ is shown in Figure 4.12 where the stated condition in (4.10) is satisfied.

The controller $K(s)$ proposed in this work using the robust H_∞ method is a 15th-order transfer function. On the other hand, the controller $K(s)$ obtained in Chapter 3 is a 6th-order transfer function. In order to have a fair comparison between the two systems, a model order reduction technique [102, 103] is used to reduce the order of the controller. Therefore, the controller in this work $K(s)$ has been reduced to a 6th order transfer function that is represented by (4.11). The coefficients a_k and b_k for different values of x are given in Tables 4.3, 4.4, and 4.5. Moreover, the infinity norm of the closed-loop transfer function $\| T_{yy_d} \|_\infty$ and γ are equal to 1.7113 and 1.7115, respectively.

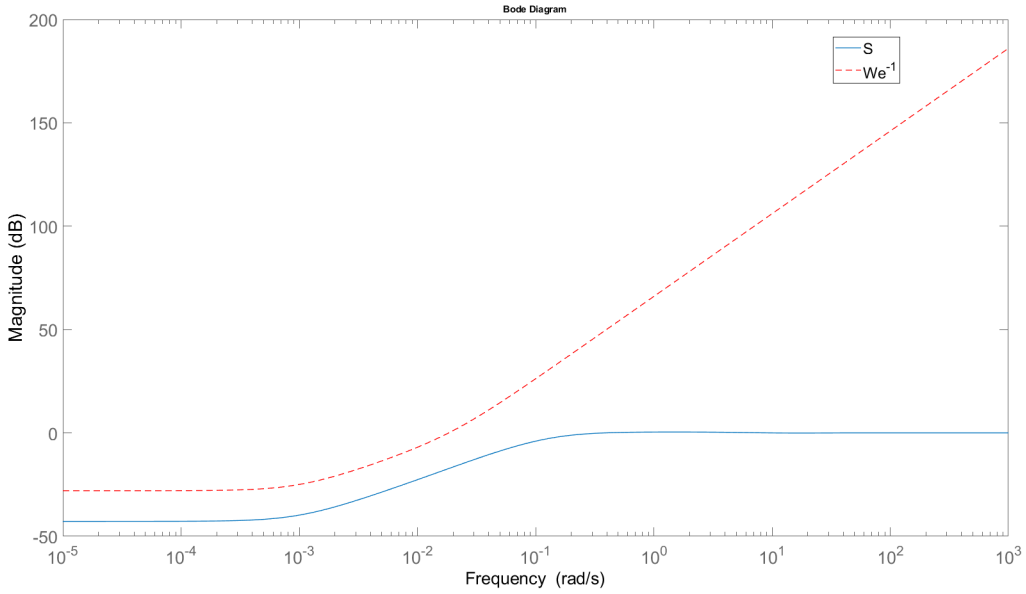

Figure 4.12: Sensitivity function S and W_e^{-1} versus frequency at $x = 0.125$

$$K(s) = \frac{b_0 s^5 + b_1 s^4 + b_2 s^3 + b_3 s^2 + 4.b_4 s + b_5}{a_0 s^6 + a_1 s^5 + a_2 s^4 + a_3 s^3 + a_4 s^2 + a_5 s + a_6} \tag{4.11}$$

4.4.3 Robust H_∞ controller

Different controllers are designed for different values of sensor location x. Once the desired die gap programming is obtained, the readings of a sensor located at a fixed location from the die is considered to be the reference signal that is applied at every cycle. Figure 4.13 shows the reference signal in blue, perturbed open-loop signal in red, and the closed-loop signal in black(dashed-line) at $x = 0.125, 0.5, 1, 1.25, 1.75, 2, 2.5,$ and 3.5. After adding the constant input disturbance, the disturbed signal which is shown in red is measured. The H_∞ controller is designed to compensate

Table 4.3: Robust controller coefficients ($e-05 \rightarrow 10^{-5}$).

a_k	$x = 0.125$	$x = 0.5$	$x = 1$	$x = 1.25$	$x = 1.75$	$x = 2$	$x = 2.5$
a_0	1	1	1	1	1	1	1
a_1	25.29	68.88	8.522	26.75	20.57	19.72	18.03
a_2	184.5	624.7	14.18	80.96	45.8	43.6	26.66
a_3	379.6	1363	4.202	81.73	32.91	32.84	8.454
a_4	96.67	346	0.086	20.34	7.039	7.358	0.1718
a_5	1.872	6.697	0.0001587	0.3939	0.1345	0.1412	0.0003058
a_6	0.00178	0.006601	7.9e-08	0.0003736	0.0001273	0.0001336	1.39e-07

Table 4.4: Robust controller coefficients ($e-05 \rightarrow 10^{-5}$).

a_k	$x = 3.5$
a_0	1
a_1	18.88
a_2	45.86
a_3	38.61
a_4	9.974
a_5	0.1936
a_6	0.0001836

Table 4.5: Robust controller coefficients ($e-05 \rightarrow 10^{-5}$).

b_k	$x = 0.125$	$x = 0.5$	$x = 1$	$x = 1.25$	$x = 1.75$	$x = 2$	$x = 2.5$	$x = 3.5$
b_0	0.1129	0.109	0.143	0.3214	0.4316	0.3494	0.4895	0.4479
b_1	2.056	6.531	0.82	2.685	2.565	2.025	2.228	2.553
b_2	19.91	48.22	2.132	9.226	6.748	5.195	4.426	5.871
b_3	47.72	181.7	0.6389	11.12	5.226	4.381	1.222	5.476
b_4	12.32	47.49	0.01319	2.739	1.068	0.9371	0.02495	1.191
b_5	0.2431	0.9322	1.253e-05	0.05369	0.0204	0.01817	2.378e-05	0.02316

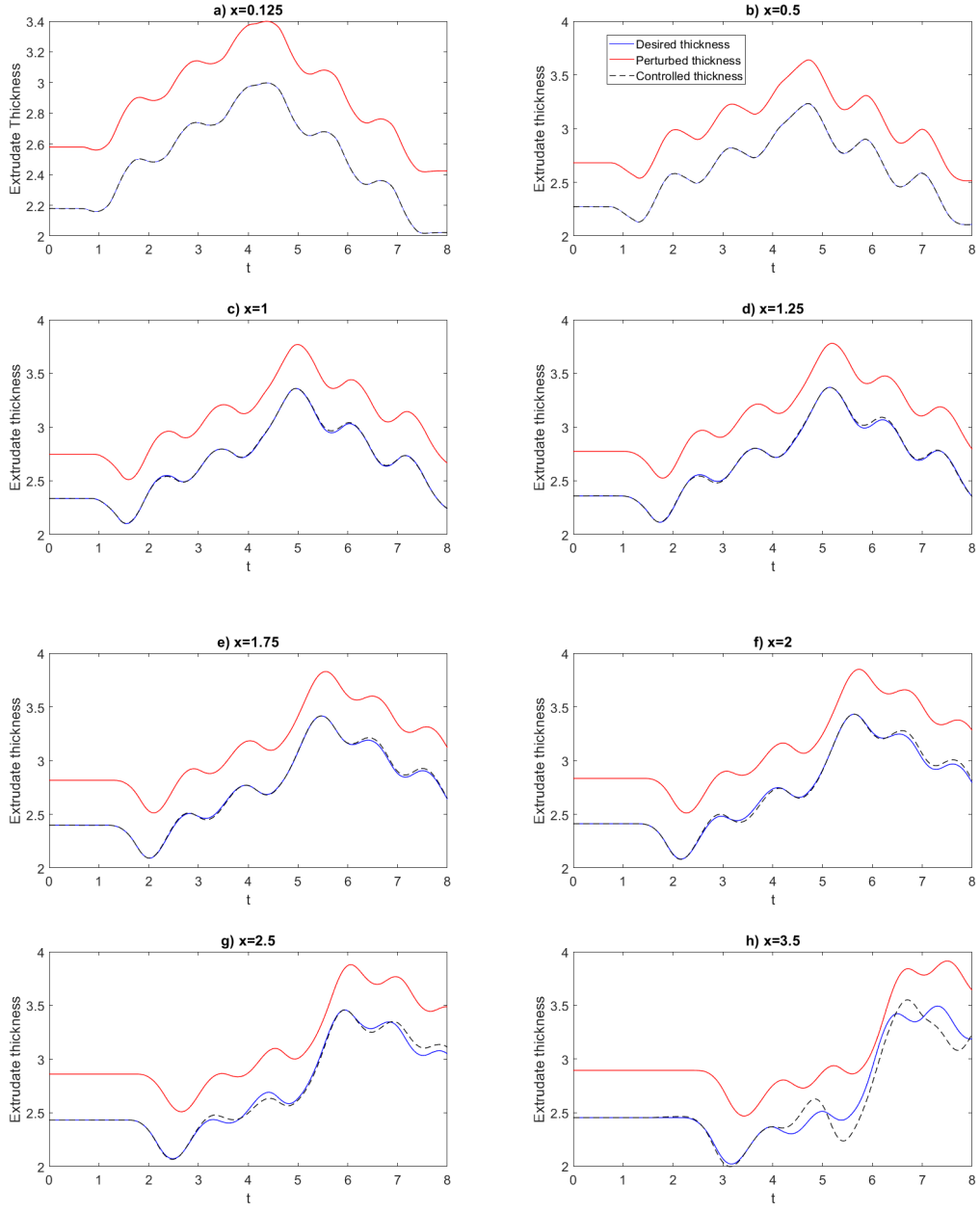

Figure 4.13: Desired, open-loop with disturbance, and closed-loop with disturbance thickness signals comparison of nominal H_∞ controller

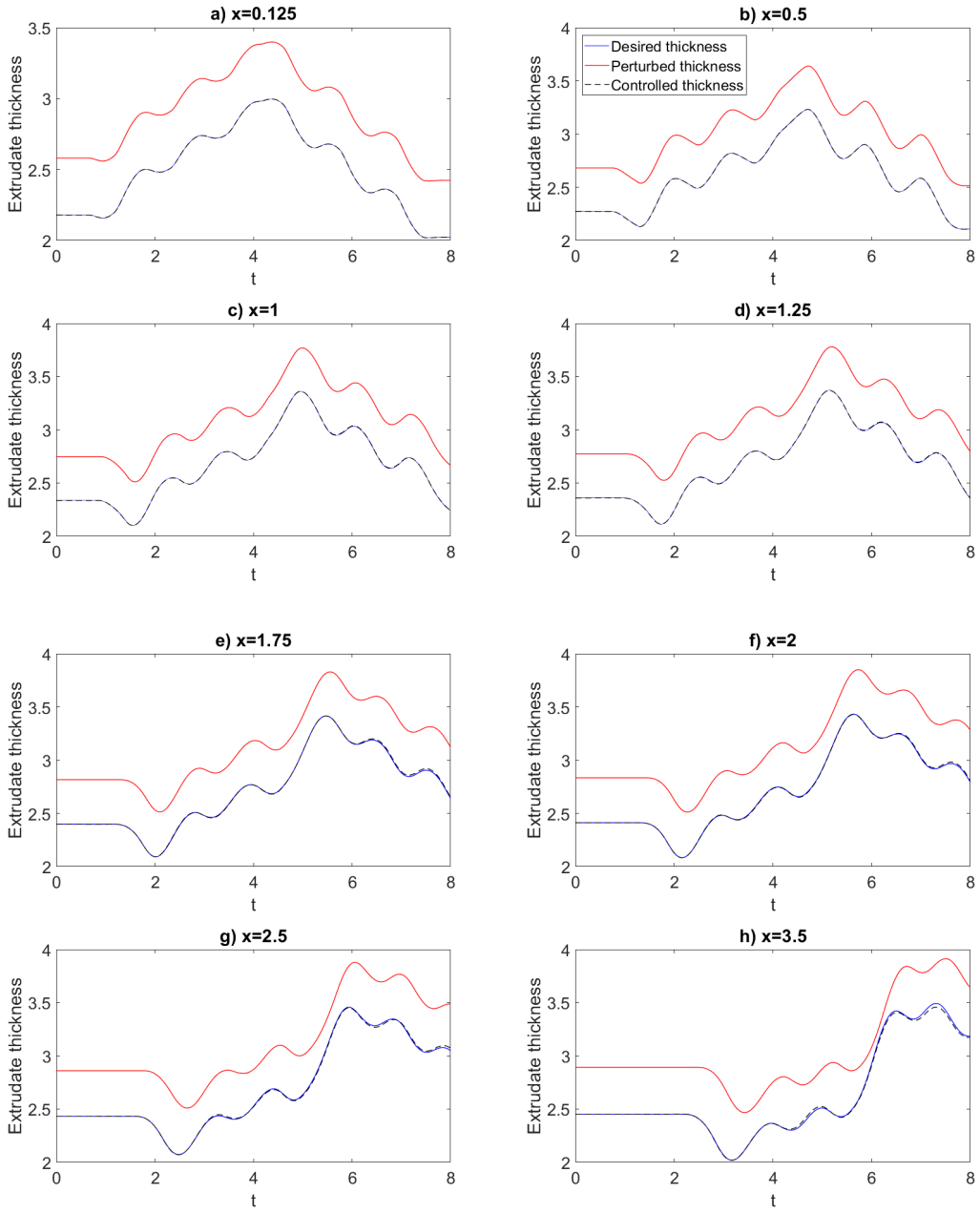

Figure 4.14: Desired, open-loop with disturbance, and closed-loop with disturbance thickness signals comparison of robust H_∞ controller

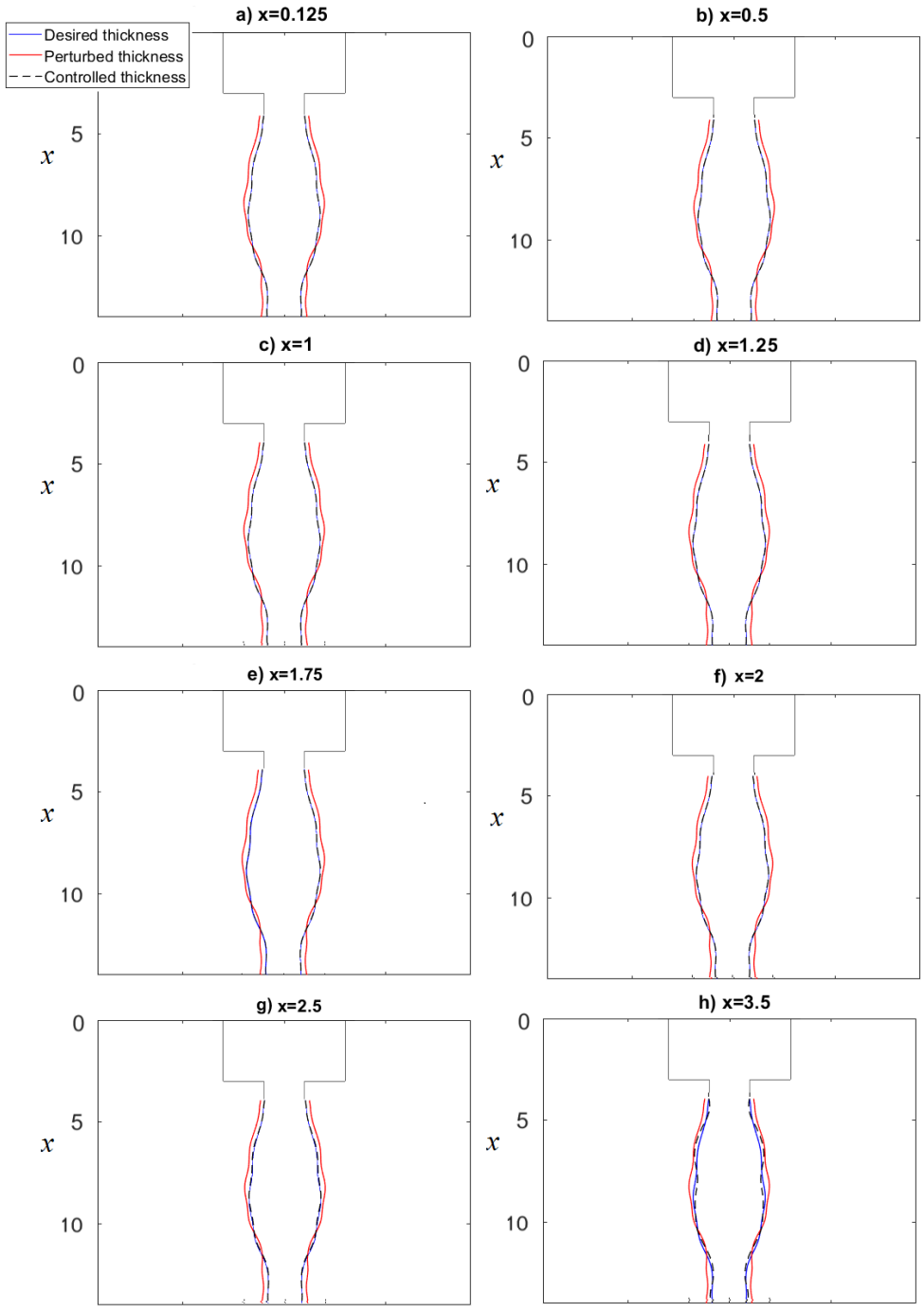

Figure 4.15: Desired, open-loop with disturbance, and closed-loop with disturbance comparison of complete extrudate for nominal H_∞ controller

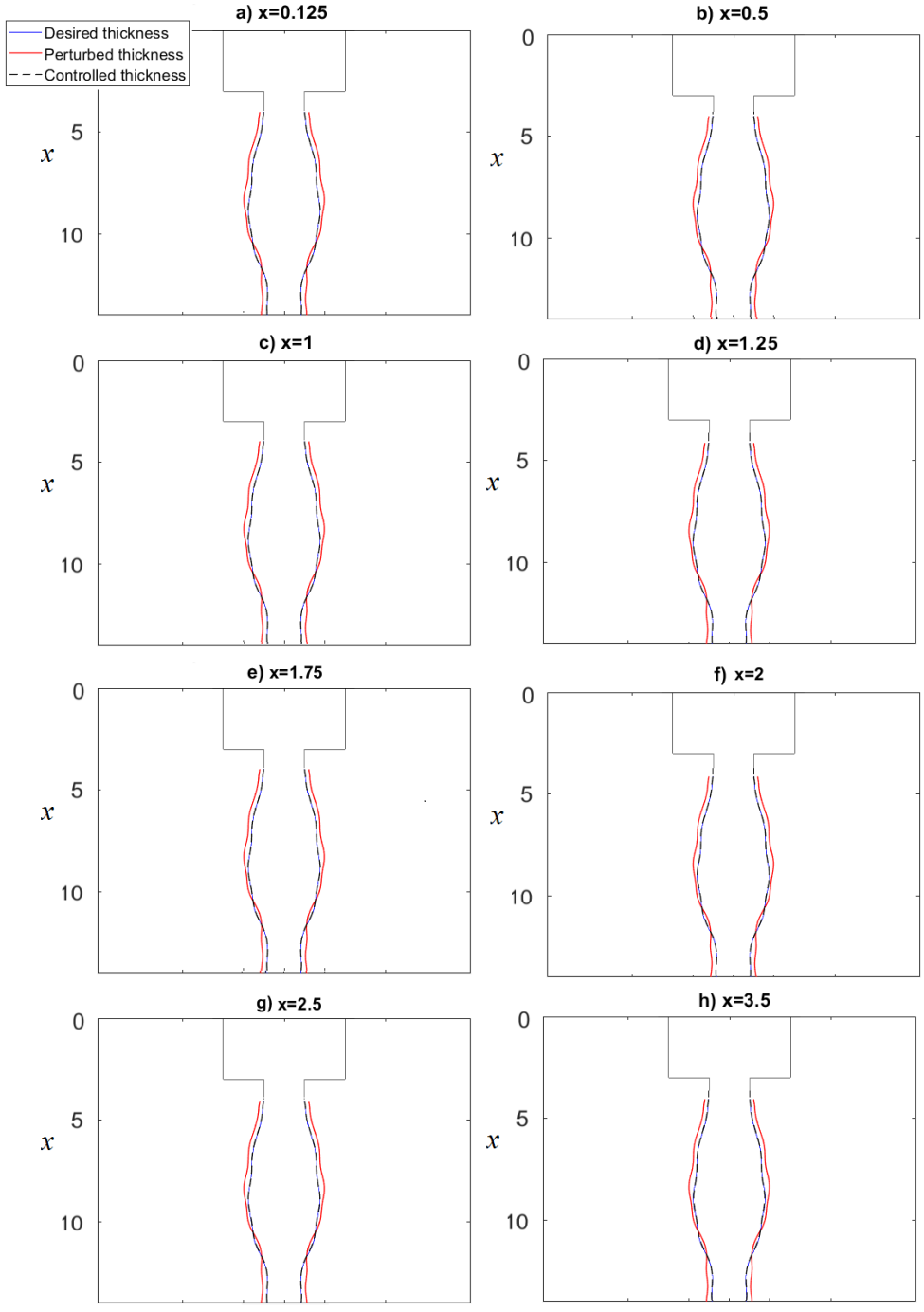

Figure 4.16: Desired, open-loop with disturbance, and closed-loop with disturbance comparison of complete extrudate for robust H_∞ controller

for the drift. The controlled signal with this controller is shown in black. In Figure 4.13, it is shown that by comparing the extrudate thickness of the open-loop systems and closed-loop system at the end of extrusion cycle, the performance is increased when the sensor is placed at locations closer to the die. This can be seen by comparing the variation in extrudate thickness in Figure 4.13a with 4.13h which increases dramatically from figure *a* to *h* as the distance from the die gap goes from $x = 0.125$ to $x = 3.5$.

On the other hand, Figure 4.14 depicts the reference signal in blue, perturbed open-loop signal in red, and the controlled signal in black(dashed-line) which is obtained by using the robust H_∞ controller at $x = 0.125, 0.5, 1, 1.25, 1.75, 2, 2.5$, and 3.5. It is shown that, for the sensor locations further away from the die, for instance $x = 2.5$, and 3.5, the robust H_∞ controller has better performance compared to the H_∞ controller where the closed-loop thickness signal tracks to the desired reference signal better. This also can be seen by comparing the variation in extrudate thickness in Figure 4.13h and Figure 4.14h in which the error between the closed-loop system and open-loop system decreases significantly for the system using the robust controller.

Even though the controller tracks the thickness at one location, the overall extrudate thickness is also obtained at the end of the cycle as shown in Figures 4.15-4.16. Figure 4.15 shows the overall extrudate shape that is controlled by using the nominal H_∞ controller while Figure 4.16 depicts the complete extrudate shape which is controlled by using the robust H_∞ controller at different values of $x = 0.125, 0.5, 1, 1.25, 1.75, 2, 2.5$, and 3.5. In other words, Figure 4.17 shows the performance of the closed-loop system using conventional H_∞ controller (Figure 4.17a) versus robust H_∞ controller (Figure 4.17b) at $x = 3.5$. For instance if the tolerance on the extrudate thickness is assumed to be 5%, using the robust H_∞ controller rejects the disturbance dramatically versus conventional H_∞ controller which results in better thickness of the desired thickness profile.

The two controlled systems are compared to each other by calculating the summation of the

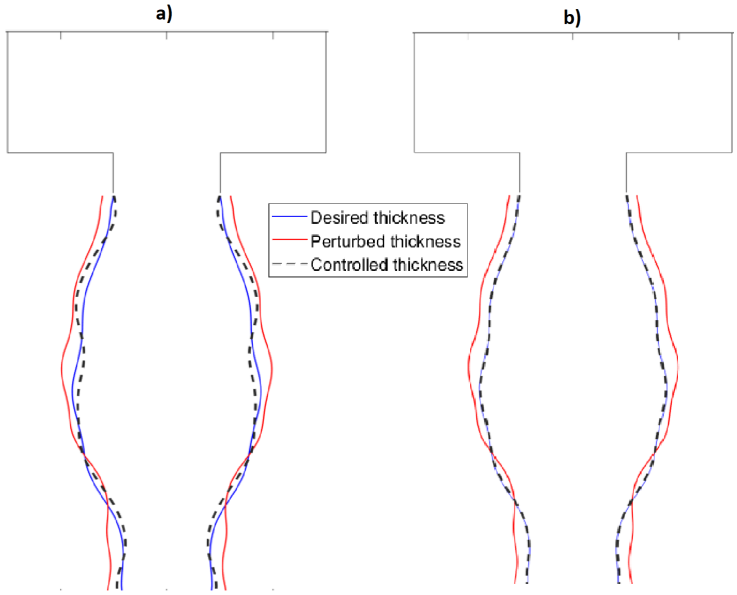

Figure 4.17: Performance of closed-loop system using (a) H_∞ controller versus closed-loop system using (b) robust H_∞ controller at $x = 3.5$

absolute thickness difference of the extrudate at the considered 160 points. Table 4.6 shows the l_1 norm of the error versus the location of the sensors at $x = 0.125, 0.5, 1, 1.25, 1.75, 2, 2.5$, and 3.5 for both systems. Moreover, the improvement of the control system using the robust H_∞ controller over the H_∞ controller is described in the last column of Table 4.6. For instance, at the furthest location from the die $x = 3.5$, the robust control shows more than 85% improvement compared to the nominal H_∞ controller. Therefore, the robust controller has better performance for the points further away from the die.

4.4.4 Sensor location

Finally, Figure 4.18 shows the location of the sensors versus the error for the nominal and robust controllers. The error is the absolute summation l_1 norm of the difference between the desired

Table 4.6: Performance analysis: l_1 norm of the end-of-cycle thickness error.

l_1 norm of error / Sensor location	H_∞ controller	Robust H_∞ controller	Improvement
x = 0.125	0.0446	0.0486	-0.09%
x = 0.5	0.2167	0.1159	46%
x = 1	0.4399	0.3532	19%
x = 1.25	1.2079	0.4430	63%
x = 1.75	1.37	0.9096	33%
x = 2	1.5617	0.9414	39%
x = 2.5	3.6963	1.5426	58%
x = 3.5	12.8238	1.8112	85%

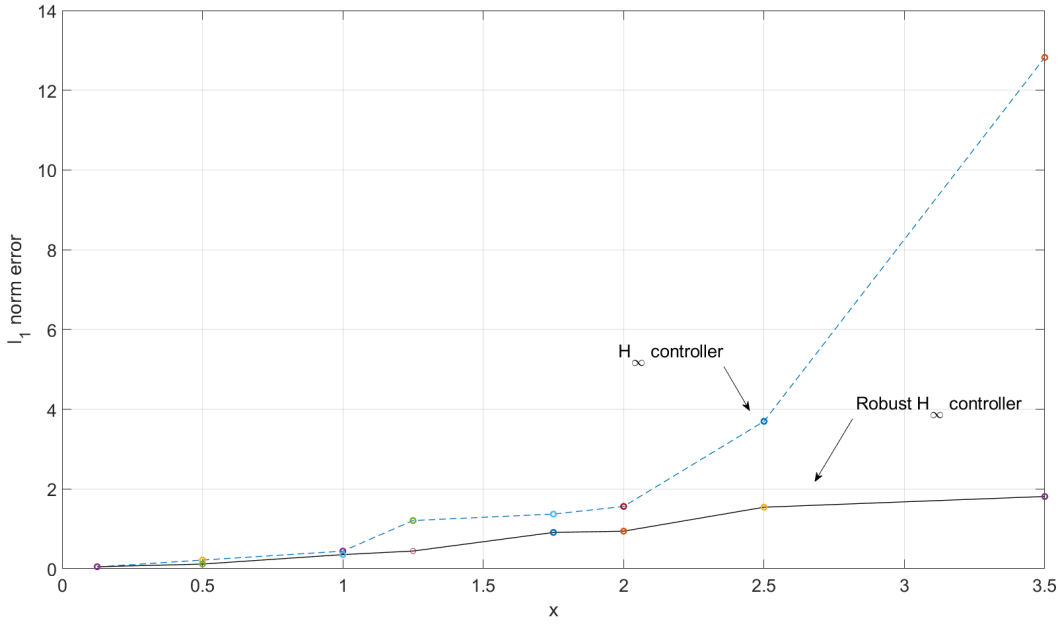

Figure 4.18: Sensor location versus l_1-norm of the error for closed-loop systems using an H_∞ controller and robust H_∞ controller

extrudate thickness and the controlled extrudate thickness at 160 points mentioned before. It can be observed that the performance of the control system improves and the error decreases as the sensor is placed closer to the die. The plant demonstrates shorter delay when the sensor is placed closer to the die due to the shorter travel distance for the material exiting the die. Moreover, the

robust H_∞ controller provides an advantage over the nominal H_∞ controller as the error is decreased significantly for the sensor locations further away from the die. Ultimately as discussed before, due to mechanical and physical constraints in the extrusion blow molding machine, the sensor can be placed further away from the die when the controller is robust.

4.5 Conclusion

In this chapter, a robust H_∞ controller in a Smith predictor configuration is proposed to regulate the extrudate thickness in the presence of disturbances and uncertainties. A low-order model of the extrusion process explained in Chapter 2 is used to replicate the dynamics of the extrudate during extrusion. The robust controller is designed in this work to maintain the thickness of the extrudate when the system is perturbed either by input disturbance or delay uncertainty. In addition, the performance of the robust H_∞ controller is compared to the performance of the nominal H_∞ controller in Chapter 3. The summation of the absolute values of the differences between the desired extrudate thickness and the controlled extrudate thickness is computed at 160 points. As a consequence, the overall performance of the extrusion process is improved using the robust H_∞ controller versus the nominal H_∞ controller, specially for the sensor locations further away from the die. Ultimately, the desired extrudate thickness profile can be maintained using the robust controller in the presence of uncertainties and disturbances which may improve the manufacturing quality and reduce the usage of raw materials.

Chapter 5

Conclusion

Mathematical models such as FEM, and experimental models are generally addressed in the literature for the extrusion process in blow molding machines with a constant die gap. On the other hand, the variation of the extrudate thickness during the extrusion process with varying die gap is rarely discussed in the previous works. Moreover, a low order model is proposed in previous work from the FEM simulator to reduce the simulation time and cost. This model is obtained by using the parameter identification method in which the parameters of the model is derived by minimizing the response between the low order model and the FEM one. This low order model is composed of delay, nonlinear static function and transient blocks. Moreover, the die gap programming is done to tune the setpoints for the new model to replicate the extrudate thickness obtained by FEM model.

The ability to obtain a desired thickness profile of the extrudate is challenging due to different factors that affect the extrusion process. The suspended extruded sheet may show swelling or sagging effects once it exits the die. The swelling effect causes the thickness of the extrudate to be larger than the die opening while the sagging effect causes the thickness to be smaller than the die

opening. Therefore, an uneven stretching during molding will cause non-uniform thickness along the extrudate especially for products with complex geometries. In order to reduce these effects in addition to machine drifts, the feasibility of using the in-cycle controller in EBM is studied in this work and different controllers are designed for this purpose, accordingly. A summary of the works done in this thesis is represented in this chapter as well as some recommendations for future work.

5.1 Summary

The works done in this thesis is part of a larger project that focuses on improving the overall EBM process. Chapter 1 starts with introducing the project overview and the reasons to design the closed-loop systems for the next generation of fuel systems. In the next section the EBM stages and NGFS are introduced to describe the formation of the extrudate. Afterwards, the EBM challenges and solutions to resolve these challenges are described. Moreover, the monitoring and control of EBM continues to elaborate the state of the technology, and the advantages of using a closed-loop system in EBM. Afterwards, the modeling techniques are studied which can be used to predict the extrudate thickness profile. Ultimately, different topologies of controllers are explained in order to reduce the effects of disturbances and machine drift.

In Chapter 2, a control oriented model is proposed based on the FEM model. The FEM model proposed in previous work is not suitable for control purposes. It is high order and hence computationally complex which results in a model that is not applicable for controller design. Moreover, the FEM model is time consuming and expensive. Therefore, the FEM model is used as a reference to generate the lower order model thanks to its higher accuracy. The lower order model is composed of the delay, nonlinear static function and transient blocks. The delay block shows additional delay with respect to the input. Moreover, the nonlinear static function depicts the steady state of the extrudate thickness. In addition, the die gap variation is modelled as a transient block

to obtain its effects on extrudate thickness during the transition from one value to the other. The bulging and necking effects appear on the extrudate during the die gap change. In order to capture these effects in real time, process monitoring and sensor selection are addressed in this chapter. The laser sensor is used to observe the extrudate thickness during its formation before the molding stage. This type of sensor can be implemented for in-cycle controller design later on. On the other hand, the ultrasonic sensor is used to monitor the thickness when the final part is ready in the cooling stage. Therefore, this type of sensor is generally used for cycle-to-cycle control in which the correction happens in the next cycle.

In Chapter 3, the lower order model explained in Chapter 2 is used as a reference model to propose a new model that is suitable for the controller design following the Smith predictor technique. The new model is also composed of the delay, nonlinear static function and transient blocks with different block orientations. The blocks swap is done for the new model to be used in the Smith predictor technique. The Smith predictor deals with the systems having large time delays. In order to use this technique, the part of the model included in the feedback should be delay free. Therefore, the delay block of the new model is placed after the transient block unlike the original model. Ultimately, the delay term is removed from the characteristic equation of the closed-loop system that results in straightforward controller design. Moreover, the sensor is placed below the die to observe the thickness of the extrudate during its formation. Afterwards, the measured thickness is compared to the reference value. Finally, the controller adjust the die when the thickness variation is computed to be bigger than 0. To do so, different controllers based on the H_∞ method are designed for different locations of x along the extrudate. In order to assess the controller performance, a constant disturbance is added to the input. The delay is computed for the different points below the die using the transport equation. The delay increases as the sensor is placed further away from the die. The delay is input-dependent and the added constant input disturbance

causes more complexity in controller design. In addition, the closed-loop, open-loop, and open-loop with disturbance systems are compared to each other by calculating the l_1 norm error of the extrudate thickness. Ultimately, the closed-loop system performs better in term of the amount of error compared to the open-loop system in case of disturbances and machine drift.

As mentioned in Chapter 3, the delay increases for the points further away from the die. In addition, the blocks swap of the original model causes additional uncertainty for the delay. Hence, an uncertainty analysis is done in Chapter 4 to obtain the amount of delay uncertainty. In order to apply the uncertainty in the controller design, the output multiplicative uncertainty technique is used to model the delay uncertainty. In addition, the robust H_∞ controller is designed for different locations of x, accordingly. In order to have a fair comparison of the closed-loop systems in Chapter 3 and 4, the constant disturbance is added to the input as well. The open-loop, the open-loop with disturbance, and the closed-loop systems using H_∞ and robust H_∞ controllers are compared to each other. The results obtained in Chapter 4 justify that the performance is improved significantly for the robust H_∞ controller compared to the nominal H_∞ controller especially for the points further away from the die. Moreover, sensor placement is studied in this chapter to find the best location for the sensor. Due to mechanical and physical constraints such as mold-sensor or die-sensor clearances, using the robust control helps to have more options for the sensor location. For instance, the sensor can be placed further away from the die where the robust controller shows acceptable results compared to the other systems.

5.2 Contributions to knowledge

Compared to traditional fuel tank systems, the NGFS (featuring slit dies) is an emerging technology that is better aligned with the ongoing efforts to combat climate change. There is a very limited number of studies in the scientific literature on twin-sheet extrusion, and even less so on

the development of in cycle control systems for this technology. Based on the results presented in chapter 3 and 4, the proposed control systems for the NGFS have a great potential to advance knowledge in the field of in cycle process control for fuel tank manufacturing in the automotive industry. Moreover, the next generation of fuel systems (NGFS) is a relatively new technology with the potential of reducing the environmental impact of leaks from fuel tanks. The proposed in-cycle controllers can greatly contribute to minimizing materials waste in EBM and the polymer processing technique used for the NGFS while reducing the production cost of fuel tanks. This is the first time that a complex optimal H_∞ controller method has been performed in the real-time control of the blow molding process. In addition, the delay uncertainty analysis studied in Chapter 4 is novel in the EBM process and can be compensated with the proposed Smith Predictor configuration technique joined with the robust H_∞ controller.

5.3 Future work

In this section, some recommendations are suggested to improve the overall performance of the EBM process in the future. For the modeling part, the sagging effect is not considered in developing the FEM model. The sagging effect is due to gravity which may cause the extrudate thickness to be smaller than the die opening. In addition, the FEM model is developed based on the Newtonian fluid in which the viscosity is assumed as a linear parameter. In future work, a non-Newtonian fluid can be considered in the simulation setup to improve the FEM model. On the other hand, with respect to the low order model for the control design, the parameters of the transient system are not defined. In other words, the relationship between the fluid type, temperature, viscosity, etc. with the parameters of the control oriented model are not discussed in this work. Taking into consideration these relationships could help to understand the effect of the parameters on the model better which may result in a more reliable controller.

As mentioned before, the low order model that is found by a parameter identification method is suitable for the controller design. In this work, the H_∞ and the robust H_∞ controllers are designed and compared to each other. The time delay term of the model is considered as a uncertain parameter. Using the Smith predictor, it is possible to compensate for the delay in the controller design. As mentioned above, the low order model can be developed to find the relationships between the parameters and physical phenomena which results in knowing the uncertainty sources better. Therefore, by knowing the source of uncertainties, the robust controller design may be improved to cover the other uncertain parameters, accordingly. Moreover, the delay term may be considered as a parameter which is varying over time. Therefore, the linear parameter varying technique in the control design may be another solution to approach such problems where the systems are having large varying delays.

In Chapter 2, the ultrasonic sensor is studied in the cooling stage which can be used for the quality control process. Having the low-order model and ultrasonic sensor, cycle-to-cycle controllers can be proposed to improve the quality of the products in the next cycles. For example, terminal iterative learning control (TILC) and space mapping techniques are studied in the literature which may be applicable for the cycle-to-cycle problem. With implementing such a sensor it is possible to optimize the die gap programming with few trials. Moreover, the laser sensor which is demonstrated in Chapter 2 can be used in the real EBM machine to collect the extrudate thickness data with respect to different inputs in various environmental conditions. The collected data can be used in machine learning applications to derive the process model. Furthermore, using the laser sensor and real time industrial processors, it may be possible to implement the closed-loop system on a real EBM machine to have consistent production with less wasted time and fewer scrapped parts.

Bibliography

[1] Dominick V Rosato, Andrew V Rosato, and David P Di Mattia. Blow molding handbook: technology, performance, markets, economics: the complete blow molding operation. Hanser Verlag, 2004.

[2] C. Elsasser, D. Eulitz and T. Kramer, “The Next Generation Fuel System,” Vehicle Technology Fuel Systems, 2010.

[3] Gligor ADRIAN, Elsasser CARSTEN, Eulitz DIRK, Hannah KEN , "A NEW MANUFACTURING PROCESS FOR PLASTIC FUEL TANKS NEXT GENERATION FUEL SYSTEM - NGFS", SCIENTIFIC BULLETIN, AUTOMOTIVE series, year XVI, no.20 (1)

[4] Han-Xiong Huang, Jiong-Cheng Li, and Cheng-Long Xiao. A proposed iteration optimization approach integrating backpropagation neural network with genetic algorithm. Expert Systems with Applications, 42(1):146–155, 2015.

[5] F Thibault, AM Yousefi, RW DiRaddo, and H Atsbha. Modeling of parison formation and process optimization for blow molded parts. In PPS-22 Conference, Yamagata, Japan, 2006.

[6] Azizeh-Mitra Yousefi and Haile Atsbha. Modeling of complex parison formation in extrusion blow molding: Effect of medium to large die heads and fuel tank geometry. Polymer Engineering and Science, 49(2):229–239, 2009.

[7] Jyh-Cheng Yu, Xiang-Xian Chen, Tsung-Ren Hung, and Francis Thibault. Optimization of extrusion blow molding processes using soft computing and taguchis method. Journal of Intelligent Manufacturing, 15(5):625–634, 2004.

[8] Jyh-Cheng Yu, Zhi-Fu Liang, and Tsung-Ren Hung. Evolutionary regional network modeling for efficient engineering optimization. In Evolutionary Computation (CEC),2014 IEEE Congress on, pages 1258–1264. IEEE, 2014.

[9] How to solve the blow molding problem, URL: https://www.lyondellbasell.com/globalassets/documents/polymers-technical-literature/how-to-solve-blow-molding-problems-6088.pdf?id=13947, Accessed on May 30 2019.

[10] J. R. Maurey, K. M. Flynn, and C. M. Guttman, "Certification of Standard Reference Material 1474a, A Polyethylene Resin", Polymers Division, Materials Science and Engineering Laboratory,National Institute of Standards and Technology.

[11] Thibault Francis, Malo Alain, Lanctot Benoit, and Diraddo Robert, "Preform shape and operating condition optimization for the stretch blow molding process", Polymer Engineering and Science, p289–301,v 47,2007.

[12] Yu, Jyh-Cheng, Chen, Xiang-Xian,Hung, Tsung-Ren, Thibault, and Francis,"Optimization of extrusion blow molding processes using soft computing and Taguchi's method",Journal of Intelligent Manufacturing,2004,625–634.

[13] Donald V. Rosato and Dominick V. "Blow molding handbook." Rosato, Carl Hanser Verlag, Munich, 1989.

[14] K. Kunisch, X. Marduel, Optimal control of non-isothermal viscoelastic fluid flow, Journal of Non-Newtonian Fluid Mechanics, Volume 88, Issue 3, 2000, Pages 261-301, ISSN 0377-0257.

[15] C.L. Cox, H. Lee, D.C. Szurley, Optimal control of non-isothermal viscous fluid flow, Mathematical and Computer Modelling, Volume 50, Issues 7–8, 2009, Pages 1142-1153, ISSN 0895-7177.

[16] Diraddo, R. W., and Andrés Garcia-Rejon. "On-line prediction of final part dimensions in blow molding: A neural network computing approach." Polymer Engineering & Science 33.11 (1993): 653-664.

[17] DiRaddo, R. W., W. I. Patterson, and M. R. Kamal. "Closed Loop Control of Parison Dimension Profiles in Extrusion Blow Molding." International Polymer Processing 6.3 (1991): 217-224.

[18] DiRaddo, R. W., and Andrés García-Rejón. "In-cycle Deterministic and Stochastic Dynamics of Extrusion Blow Molding." International Polymer Processing 7.3 (1992): 257-266.

[19] Schrand, H., Adaptive Control Loops Reduce Scrap, ANTEC (1989), p.952.

[20] Noguchi et al. "Parison length control method for blow molding machine." U.S. Patent No. 5,399,302. 21 Mar. 1995.

[21] Lee, N.C, Control Flash in Extrusion Blow Molding, Plastics Technology.

[22] Z. Kountouriotis, G. C. Georgiou, E. Mitsoulis, On the combined effects of slip, compressibility, and inertia on the newtonian extrudate-swell flow problem, Computers and Fluids 71 (2013) 297-305.

[23] A.-Y. Wong, J. Liang, Relationship between die swell ratio and melt flow index, Chemical Engineering Science 52 (18) (1997) 3219-3221.

[24] G. Russo, T. Phillips, Numerical simulation of steady planar die swell for a Newtonian fluid using the spectral element method, Computers & Fluids 39 (5) (2010) 780-792.

[25] S. Claus, C. Cantwell, T. Phillips, Spectral/hp element methods for plane newtonian extrudate swell, Computers & Fluids 116 (2015) 105-117.

[26] F. Habla, H. Marschall, O. Hinrichsen, L. Dietsche, H. Jasak, J. L. Favero, Numerical simulation of viscoelastic two-phase flows using openfoam, Chemical Engineering Science 66 (22) (2011) 5487-5496.

[27] V. K. Konaganti, M. Ansari, E. Mitsoulis, S. G. Hatzikiriakos, Extrudate swell of a high-density polyethylene melt: ii.modeling using integral and differential constitutive equations, Journal of Non-Newtonian Fluid Mechanics 225 (2015) 94-105.

[28] V. K. Konaganti, M. Ansari, E. Mitsoulis, S. G. Hatzikiriakos, The effect of damping function on extrudate swell, Journal of Non-Newtonian Fluid Mechanics 236 (2016) 73-82.

[29] Toukhtarian Raffi, Hatzikiriakos Savvas, Atsbha Haile, Boulet Benoit. (2018). Modeling polymer extrusion with varying die gap using Arbitrary Lagrangian Eulerian (ALE) method. Physics of Fluids. 30.

[30] V. Konaganti, E. Behzadfar, R. Kwak, E. Mitsoulis, S. Hatzikiriakos, Transient swell of a high density polyethylene using adjustable gap slit die, International Polymer Processing 32 (5) (2017) 574-581.

[31] R. Toukhtarian, M. Darabi, S. Hatzikiriakos, H. Atsbha, B. Boulet, Parameter Identification of Transport PDE/Nonlinear ODE Cascade Model for Polymer Extrusion with

Varying Die Gap, accepted for publication in Canadian Journal of Chemical Engineering, DOI:10.1002/cjce.23910.

[32] K. Gu and S.-I. Niculescu, “Survey on recent results in the stability and control of time-delay systems,” Transactions of the ASME, vol. 125, pp. 158–165, June 2003.

[33] K. Gu, Y. L. Kharitonov, and J. Chen, "Stability of TimeDelay Systems", Birkhliuser. Boston: Birkhliuser, 2003.

[34] Gu K, Niculescu S. Survey on Recent Results in the Stability and Control of Time-Delay Systems. ASME. J. Dyn. Sys., Meas., Control. 2003;125(2):158-165.

[35] Qing-Chang Zhong, control of dead-time systems based on a transformation, Automatica, Volume 39, Issue 2, 2003, Pages 361-366, ISSN 0005-1098.

[36] N. Bekiaris-Liberis and M. Krstic, "Compensation of Transport Actuator Dynamics With Input-Dependent Moving Controlled Boundary," in IEEE Transactions on Automatic Control, vol. 63, no. 11, pp. 3889-3896, Nov. 2018.

[37] M. Diagne, N. Bekiaris-Liberis, A. Otto and M. Krstic, "Control of transport PDE/nonlinear ODE cascades with state-dependent propagation speed," 2016 IEEE 55th Conference on Decision and Control (CDC), Las Vegas, NV, 2016, pp. 3125-3130.

[38] M. Diagne and M. Krstic, "State-dependent input delay-compensated Bang-Bang control: Application to 3D printing based on screw-extruder," 2015 American Control Conference (ACC), Chicago, IL, 2015, pp. 5653-5658.

[39] Mamadou Diagne, Nikolaos Bekiaris-Liberis, Miroslav Krstic, Compensation of input delay that depends on delayed input, Automatica,Volume 85,2017,Pages 362-373,ISSN 0005-1098.

[40] D. Bresch-Pietri, J. Chauvin, N. Petit, Invoking Halanay inequality to conclude on closed-loop stability of a process with input-varying delay1,IFAC Proceedings Volumes,Volume 45, Issue 14,2012,Pages 266-271,ISSN 1474-6670,ISBN 9783902823045.

[41] O. J. Smith, “A controller to overcome dead time,” ISA J., vol. 6, no.2, Feb. 1959, pp. 28-33.

[42] C. B. Brosilow. "The structure and design of Smith predictors from the viewpoint of inferential control." In Proceedings of Joint American Control Conference, Denver, Colorado, 1979.

[43] K. Watanabe and M. Ito, “A process-model control for linear systems with delay,” IEEE Transactions on Automatic Control, vol. AC-26, no. 6, Dec. 1981, pp. 1261-1266.

[44] Rahi Modirnia and Benoit Boulet. Application of the watanabe modified smith predictor control technique in thermoforming. In American Control Conference (ACC), 2012,pages 6448–6454. IEEE, 2012.

[45] Astrom, K. J., Hang, C. C., and Lim, B. C. (1994). A new Smith predictor for controlling a process with an integrator and long deadtime. IEEE Transactions on Automatic Control, 39(2), 343–345.

[46] W. D. Zhang, Y. X. Sun, and X. Xu, “Two degree-of-freedom Smith predictor for processes with time delay,” Automatica, vol. 34, no. 10, pp. 1279–1282, 1998.

[47] Rezaei, Sabereh and Shahrokhi, Mohammad, Robust controller design for discrete unstable non-minimum-phase delayed stochastic processes, International Journal of Control, Automation and Systems, Volume 11, Issue 2, Oct 2013, Pages 893–902.

[48] A. Nicoletti and A. Karimi, "H_∞ smith predictor design for time-delayed MIMO systems via convex optimization," 2014 IEEE Conference on Control Applications (CCA), Juan Les Antibes, 2014, pp. 1418-1424.

[49] Zhihua Qu, "Model reference robust control of weakly non-minimum phase systems," Proceedings of 32nd IEEE Conference on Decision and Control, San Antonio, TX, USA, 1993, pp. 996-1001 vol.2. doi: 10.1109/CDC.1993.325334.

[50] M. Roozbehani and C. R. Knospe, "Robust stability and H∞ performance analysis of interval-dependent time delay systems," Proceedings of the 2005, American Control Conference, 2005., Portland, OR, USA, 2005, pp. 4265-4270 vol. 6.

[51] Y. Feng and M. Yagoubi, "On state feedback h-infinity control for discrete time singular systems," IEEE Trans. Autom. Control, vol. 58, no. 10, pp. 2674–2679, Oct. 2013.

[52] D. Ding, Z. Wang, B. Shen, and H. Shu, " H ∞ state estimation for discrete time complex networks with randomly occurring sensor saturations and randomly varying sensor delays," IEEE Trans. Neural Netw. Learn. Syst., vol. 23, no. 5, pp. 725–736, May 2012.

[53] Z. Feng, J. Lam, and H. Gao, "Delay-dependent robust H ∞ controller synthesis for discrete singular delay systems," Int. J. Robust Nonlinear Control, vol. 21, no. 16, pp. 1880–1902, 2011.

[54] Z. Du, D. Yue and S. Hu, "H-Infinity Stabilization for Singular Networked Cascade Control Systems With State Delay and Disturbance," in IEEE Transactions on Industrial Informatics, vol. 10, no. 2, pp. 882-894, May 2014.

[55] Kamaldar, M., M. J. Mahjoob, M. Haeri Yazdi, H. Vahid-Alizadeh, and S. Ahmadizadeh. "A control synthesis for reducing lateral oscillations of a spherical robot." In 2011 IEEE International Conference on Mechatronics, pp. 546-551. IEEE, 2011.

[56] Alizadeh, H. Vahid, and Benoit Boulet. "Robust control of synchromesh friction in an electric vehicle's clutchless automated manual transmission." In 2014 IEEE Conference on Control Applications (CCA), pp. 611-616. IEEE, 2014.

[57] Tahmasebi, Rana, Hossein Vahid Alizadeh, Saman Rahimi, and Benoit Boulet. "Robust $_\infty$ force control of a solenoid actuator using experimental data and finite element method." In 2014 IEEE Conference on Control Applications (CCA), pp. 1172-1177. IEEE, 2014.

[58] Tahmasebi, Rana, Hossein Vahid Alizadeh, and Benoit Boulet. "Robust Gear Shifting Force Control of a Solenoid Actuator in an Automated Manual Transmission of an Electric Vehicle via μ-Synthesis." In 2015 IEEE Vehicle Power and Propulsion Conference (VPPC), pp. 1-6. IEEE, 2015.

[59] Kamaldar, M., Mohammad J. Mahjoob, and H. Vahid Alizadeh. "Robust speed control of a spherical robot using ARX uncertain modeling." In 2011 IEEE International Symposium on Robotic and Sensors Environments (ROSE), pp. 196-201. IEEE, 2011.

[60] Alizadeh, Hossein Vahid, Mohamed K. Helwa, and Benoit Boulet. "Modeling, analysis and constrained control of wet cone clutch systems: A synchromesh case study." Mechatronics 49 (2018): 92-104.

[61] Alizadeh, H. Vahid, Mohamed K. Helwa, and Benoit Boulet. "Constrained control of the synchromesh operating state in an electric vehicle's clutchless automated manual transmission." In 2014 IEEE Conference on Control Applications (CCA), pp. 623-628. IEEE, 2014.

[62] M. Chadli and M. Darouach, "Novel bounded real lemma for discrete-time descriptor systems: Application H $infty$ to control design," Automatica, vol. 48, no. 2, pp. 449–453, 2012.

[63] Jihai Jiang, Haichang Liu and O. Celestine, "Nonlinear H Infinity Control in Frequency Domain of Hydrostatic Transmission System with Secondary Regulation via GFRF," 2006 6th World Congress on Intelligent Control and Automation, Dalian, 2006, pp. 6416-6420.

[64] Q. Niu and Y. Liu, "H-infinity Control Theory in Vehicle Diesel Fuel Injection Pump Control System Design," 2010 International Conference on Machine Vision and Human-machine Interface, Kaifeng, 2010, pp. 98-100.

[65] L. Vu and D. Liberzon, "Supervisory Control of Uncertain Linear Time-Varying Systems," in IEEE Transactions on Automatic Control, vol. 56, no. 1, pp. 27-42, Jan. 2011.

[66] S. Boyd, V. Balakrishnan, P. Kabamba, A bisection method for computing the H_∞ norm of a transfer function and related problems, Math. Control Signals Systems 2 (1989) 207–219.

[67] Glover, K., and J.C. Doyle. "State-space formulae for all stabilizing controllers that satisfy an H_∞ norm bound and relations to risk sensitivity." Systems & Control Letters, Vol. 11, Number 8, 1988, pp. 167–172.

[68] Doyle, J.C., K. Glover, P. Khargonekar, and B. Francis. "State-space solutions to standard H_2 and H_∞ control problems." IEEE Transactions on Automatic Control, Vol 34, Number 8, August 1989, pp. 831–847.

[69] Safonov, M.G., D.J.N. Limebeer, and R.Y. Chiang. "Simplifying the H_∞ Theory via Loop Shifting, Matrix Pencil and Descriptor Concepts." Int. J. Contr., Vol. 50, Number 6, 1989, pp. 2467-2488.

[70] N.-. Su, H.-. Su and J. Chu, "Delay-dependent robust H/sub /spl infin// control for uncertain time-delay systems," in IEE Proceedings - Control Theory and Applications, vol. 150, no. 5, pp. 489-, 26 Sept. 2003.

[71] B. Zhang and S. Xu, "Delay-Dependent RobustH_∞Control for Uncertain Discrete-Time Fuzzy Systems With Time-Varying Delays," in IEEE Transactions on Fuzzy Systems, vol. 17, no. 4, pp. 809-823, Aug. 2009.

[72] Yun-Ping Huang and Kemin Zhou, "Robust stability of uncertain time-delay systems," in IEEE Transactions on Automatic Control, vol. 45, no. 11, pp. 2169-2173, Nov. 2000.

[73] J. S. Luo, P. P. J. Van Den Bosch, S. Weiland and A. Goldenberge, "Design of performance robustness for uncertain linear systems with state and control delays," in IEEE Transactions on Automatic Control, vol. 43, no. 11, pp. 1593-1596, Nov. 1998.

[74] Chong Lin, Qing-Guo Wang and Tong Heng Lee, "A less conservative robust stability test for linear uncertain time-delay systems," in IEEE Transactions on Automatic Control, vol. 51, no. 1, pp. 87-91, Jan. 2006.

[75] Guy Gauthier and Benoit Boulet. Robust design of terminal ilc with an internal model control using μ-analysis and a genetic algorithm approach. In American Control Conference (ACC), 2010, pages 2069–2075. IEEE, 2010.

[76] N Ghadipasha, JA Romagnoli, S Tronci, and R Baratti. A model-based approach for controlling particle size distribution in combined cooling-antisolvent crystallization processes. Chemical Engineering Science, 2018.

[77] WangyunWon, Kyungtae Park, and Jiyong Kim. Combined iterative learning and delta operator adaptive linear quadratic gaussian control of a commercial rapid thermal processing system. Chemical Engineering Science, 174:146–156, 2017.

[78] Manda Yang and Antonios Armaou. Revisiting apod accuracy for nonlinear control of transport reaction processes: A spatially discrete approach. Chemical Engineering Science, 181:146–158, 2018.

[79] T. Liu, Q.-G. Wang, H.-P. Huang, A tutorial review on process identification from step or relay feedback test, Journal of Process control 23(10)(2013) 1597-1623.

[80] S. Saxena, Y. V. Hote, Load frequency control in power systems via internal model control scheme and model-order reduction, IEEE Transactions on Power Systems 28 (3)(2013) 2749-2757.

[81] K. Narendra and P. Gallman, "An iterative method for the identification of nonlinear systems using a Hammerstein model," in IEEE Transactions on Automatic Control, vol. 11, no. 3, pp. 546-550, July 1966.

[82] Piroddi L, Farina M, Lovera M (2012) Black box model identification of non-linear input–output models: a Wiener–Hammerstein benchmark. Control Eng Pract 20(11):1109–1118.

[83] Takagi T, Sugeno M (1985) Fuzzy identification of systems and its applications to modeling and control. IEEE Trans Syst Man Cybern SMC 15:116–132.

[84] Hunter I W and Korenberg M J 1986 "The identification of nonlinear biological systems: Wiener and Hammerstein cascade models" Biol. Cybern. 55 135–44.

[85] T. Liu, F. Gao, Closed-loop step response identification of integrating and unstable processes, Chemical Engineering Science 65 (10) (2010) 2884-2895.

[86] G. Rangaiah, P. Krishnaswamy, Estimating second-order dead time parameters from under-damped process transients, Chemical Engineering Science 51 (7) (1996) 1149-1155.

[87] P. Balaguer, V. Alfaro, O. Arrieta, Second order inverse response process identification from transient step response, ISA transactions 50 (2) (2011)231-238.

[88] V. K. Konaganti, E. Behzadfar, R. Kwak, E. Mitsoulis, S. Hatzikiriakos,Transient swell of a high density polyethylene using adjustable gap slit die,International Polymer Processing 32 (5) (2017) 574(581).

[89] MTI Instruments, A worldwide provider of precision measurement solutions, https://www.mtiinstruments.com/.

[90] Olympus Scientific Solutions https://www.olympus-ims.com/en/ndt-tutorials/thickness-gage/introduction/operation/.

[91] Crank, J.; Nicolson, P. (1947). "A practical method for numerical evaluation of solutions of partial differential equations of the heat conduction type". Proc. Camb. Phil. Soc. 43 (1): 50–67.

[92] Thomas, J. W. (1995). Numerical Partial Differential Equations: Finite Difference Methods. Texts in Applied Mathematics. 22. Berlin, New York: Springer-Verlag. ISBN 978-0-387-97999-1.

[93] Paul Wilmott; Sam Howison; Jeff Dewynne (1995). The Mathematics of Financial Derivatives: A Student Introduction. Cambridge University Press. p. 137. ISBN 978-0-521-49789-3.

[94] Jordán, op. cit., p. 1 and Milne-Thomson, p. xxi. Milne-Thomson, Louis Melville (2000): The Calculus of Finite Differences (Chelsea Pub Co, 2000) ISBN 978-0821821077.

[95] Bibel, John E., and D. Stephen Malyevac. Guidelines for the selection of weighting functions for H-infinity control. No. NSWCDD/MP-92/43. NAVAL SURFACE WARFARE CENTER DAHLGREN DIV VA, 1992.

[96] C. R. Knospe and M. Roozbehani, "Stability of linear systems with interval time delays excluding zero," in IEEE Transactions on Automatic Control, vol. 51, no. 8, pp. 1271-1288, Aug. 2006.

[97] K. Zhou, J. C. Doyle, Essentials of robust control, vol. 104. Upper Saddle River, NJ: Prentice hall, 1998.

[98] B. A. Francis and W. M. Wonham, "The internal model principle of control theory", Automatica 12 (1976) 457–465.

[99] Roger C. Conant and W. Ross Ashby, "Every good regulator of a system must be a model of that system", International Journal of Systems Science vol 1 (1970), 89–97.

[100] L. Xie and E. de Souza Carlos, "Robust H/sub infinity / control for linear systems with norm-bounded time-varying uncertainty," in IEEE Transactions on Automatic Control, vol. 37, no. 8, pp. 1188-1191, Aug. 1992.

[101] H. Kokame, H. Kobayashi and T. Mori, "Robust H/sub /spl infin// performance for linear delay-differential systems with time-varying uncertainties," in IEEE Transactions on Automatic Control, vol. 43, no. 2, pp. 223-226, Feb. 1998.

[102] P. Feldmann, "Model order reduction techniques for linear systems with large numbers of terminals," Proceedings Design, Automation and Test in Europe Conference and Exhibition, Paris, France, 2004, pp. 944-947 Vol.2. doi: 10.1109/DATE.2004.1269013.

[103] C. J. Ramlal, S. Ibrir, A. Singh and S. Rocke, "A Comparison of Model-Order Reduction Techniques for Multiphase Transmission Line Systems," 2016 8th International Conference on Computational Intelligence and Communication Networks (CICN), Tehri, 2016, pp. 459-465. doi: 10.1109/CICN.2016.95